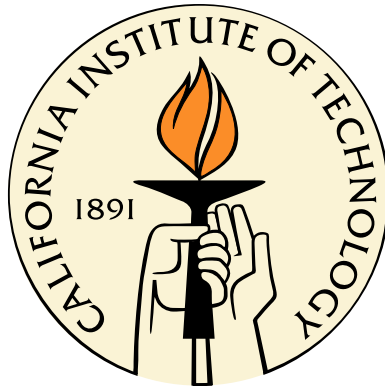


# Non-Abelian Quantum Hall States and Fractional Statistics

Thesis by  
Waheb Bishara

In Partial Fulfillment of the Requirements  
for the Degree of  
Doctor of Philosophy



California Institute of Technology  
Pasadena, California

2009  
(Defended May 5, 2009)

© 2009

Waheb Bishara

All Rights Reserved

To my family, and Giselle, for their unconditional support.

# Acknowledgments

I want to express my deep gratitude to my committee members: Chetan Nayak for willing to be my advisor in an unconventional arrangement, for providing the excitement and inspiration when needed, and for his guidance and understanding; Alexei Kitaev for his always eye-opening suggestions and ideas; Gil Refael for his enthusiasm and constant encouragement, both academically and personally; and Jim Eisenstein for his support and dedication to the condensed matter group. I would also like to thank Parsa Bonderson, Israel Klich, and Kirill Shtengel for being my academic big brothers and personal good friends. I have also had the privilege to meet many great scientists and interesting people with whom I have had many interesting discussions: Jason Alicea, Ryan Barnett, Ivailo Dimov, Lukasz Fidkowski, Olexei Motrunich, Tami Pereg-Barnea, Joost Slingerland, and Yue Zou, among others.

My stay in southern California would not have been nearly as much fun without the great friends I made here. They enriched my life in many different ways, but above all, they have always been there for me, as true friends do. In addition, I want to thank my teammates in the SOPS and the Lucky Bastards for the weekly dosage of escape and endorphin rush.

I am most grateful to my parents for their unconditional support and faith in me; to my sister Nesma, my brother Nafea and his wife Lana for always offering a different perspective; to my nephews and niece Munir, Arz and Rawi, for being little bundles of joy; and to Giselle, for her love, patience, and for convincing me that everything will be just fine.

# Abstract

The discovery of the fractional quantum Hall effect stimulated the investigation of anyons, particles with fractional statistics which are neither bosons nor fermions. This thesis focuses on the study of quantum Hall states which may support non-Abelian anyons. We first address the validity of assumptions used in the numerical study of such states, and then proceed with analyzing different experiments which can detect non-Abelian fractional statistics. We quantitatively analyze the two-point contact interferometer experiment, which is hoped to display clear-cut, direct evidence of non-Abelian fractional statistics. We calculate the temperature and voltage dependence of the interference experiment outcome, and the signal attenuation due to finite temperature loss of coherence. We then analyze the edge theory of a family of non-Abelian quantum Hall states in the second Landau level, and examine the tunneling between these states and a quantum dot. This tunneling problem maps onto the multi-channel Kondo problem, and will allow distinguishing between different quantum Hall states. Finally, we use the same theoretical methods for analyzing Sagnac interference in the conductance of a carbon nanotube loop, a one-dimensional system.

# Contents

<b>Acknowledgments</b>	<b>iv</b>
<b>Abstract</b>	<b>v</b>
<b>Contents</b>	<b>vi</b>
<b>1 Introduction</b>	<b>1</b>
1.1 Quantum mechanics in 2 spatial dimensions . . . . .	2
1.2 Integer Quantum Hall Effect . . . . .	6
1.3 Fractional Quantum Hall Effect . . . . .	8
1.4 Edge Excitations in Quantum Hall Liquids . . . . .	11
1.5 Overview . . . . .	12
<b>2 Landau Level Mixing</b>	<b>14</b>
2.1 Landau Levels, Coulomb Interaction and Particle-Hole Symmetry . .	16
2.2 Multi-Particle Pseudopotentials . . . . .	19
2.3 Perturbative Calculation of LLM . . . . .	23
2.4 Tree Level Interaction . . . . .	25
2.5 Lowest Order 3-Particle Interaction . . . . .	26
2.6 Lowest Order 3-Particle Pseudopotentials . . . . .	30
2.7 Results in Lowest and Second Landau Levels . . . . .	32
<b>3 Interferometry and Non-Abelian Statistics at 5/2 Filling Fraction</b>	<b>34</b>
3.1 Quantum Hall State at Filling 5/2 . . . . .	35
3.2 Fabry-Perot Interferometer . . . . .	36

3.3	Tunneling Operators and Conformal Blocks . . . . .	38
3.4	Temperature And Voltage Behavior . . . . .	46
3.5	Anti-Pfaffian Edge . . . . .	49
3.6	Discussion and Interpretation of Experimental Results . . . . .	54
<b>4</b>	<b>Quantum Hall States at <math>\nu = \frac{2}{k+2}</math></b>	<b>59</b>
4.1	Second Landau Level Quantum Hall States . . . . .	59
4.2	Particle-Hole Conjugation of Read-Rezayi states . . . . .	62
4.3	Properties of anti-RR States . . . . .	66
4.4	Candidate States for Filling 12/5 . . . . .	68
<b>5</b>	<b>Multi-Channel Kondo Effect in QH Edges</b>	<b>71</b>
5.1	Kondo Model Review . . . . .	73
5.2	Quantum Dot coupled to QH Edge . . . . .	74
5.3	Pfaffian Edge and Quantum Dot . . . . .	76
5.4	Anti-Pfaffian and Quantum Dot . . . . .	81
5.5	Read-Rezayi State and Quantum Dot . . . . .	82
5.6	Summary . . . . .	84
<b>6</b>	<b>Sagnac Interference in Carbon Nanotubes</b>	<b>85</b>
6.1	Introduction . . . . .	85
6.2	Sagnac interference in a single channel . . . . .	90
6.3	Interference in Nanotubes . . . . .	101
6.4	Summary and Conclusions . . . . .	107
	Appendix 6.A Diagonalizing the Hamiltonian with Degeneracies . . . . .	109
	Appendix 6.B Correlation functions . . . . .	112
	<b>Bibliography</b>	<b>115</b>

# Chapter 1

## Introduction

At an early stage of science education, students are taught that there are only two types of particles in the world: fermions and bosons. This often happens prior to the introduction of quantum mechanics. Fermions obey Pauli's exclusion principle, by which two fermions cannot occupy the same quantum mechanical state. Due to this simple rule, electrons circulating an atom's nucleus must fill high energy atomic shells, and even non-interacting electrons in a metal or a semiconductor must fill bands and form Fermi seas. Bosons, on the other hand, do not have such a restriction, and a macroscopic number of bosons may occupy the same quantum mechanical state. A macroscopic occupation of a single state leads to the formation of a Bose-Einstein condensate, a state of matter which displays quantum mechanical behavior at macroscopic length scales. The classic example of a Bose-Einstein condensate is liquid  $^4\text{He}$  below its critical temperature of  $2.17\text{K}$ . Bose-Einstein condensed  $^4\text{He}$  exhibits vanishing viscosity and quantized vortices, among other interesting properties.

When the number of spatial dimensions of a system is three or greater, it can be mathematically proven that quantum mechanics of that system can be consistent only when all particles are either bosons or fermions, perhaps with additional *local* degrees of freedom (e.g., [1]). Since our world has exactly 3 observed spatial dimensions, all elementary particles must be bosons or fermions. Indeed, all particles in the Standard Model [2, 3] of particle physics are either bosons or fermions. With the exception of the Higgs boson, all particles of the Standard Model have been observed.

In two spatial dimensions, on the other hand, particles which are neither bosons

nor fermions can exist without violating any of the requirements of quantum mechanics. Such particles have been dubbed anyons [4, 5], and are said to have fractional statistics. Fortunately, anyons may be more than a theoretical curiosity. A number of physical systems are effectively two-dimensional at low energies, including two-dimensional electron gases in semiconductor heterostructures [6, 7], single layer graphene [8, 9], and trapped atomic gases [10, 11].

In the remainder of this chapter, we discuss quantum mechanics in two spatial dimensions, and possible realization of anyons in physical systems, in particular in quantum Hall systems. In section 1.1 we describe how anyons arise in two-dimensions, and the different types of anyons. In section 1.2 we review the integer quantum Hall effect, and in section 1.3 we review the fractional quantum Hall effect, the most promising venue for the observation of anyons. Then we briefly discuss gapless edge excitations in quantum Hall systems and their importance for experiments in section 1.4. Finally, we provide an overview of the work reported in this thesis in section 1.5.

## 1.1 Quantum mechanics in 2 spatial dimensions

In quantum mechanics textbooks, the bosonic or fermionic statistics are introduced as a result of symmetry requirements on multi-particle wavefunctions. Under the exchange of the positions of any two particles, the wavefunction must be completely symmetric or completely antisymmetric:

$$\psi(x_2, x_1, \dots) = \pm \psi(x_1, x_2, \dots). \quad (1.1)$$

When the wavefunction is symmetric under exchanges it describes bosonic particles. When it is antisymmetric, it describes fermionic particles, since the wavefunction vanishes in that case when two particles are brought to the same position. To understand the origin of this symmetry requirement, it is useful to use the path integral representation of quantum mechanics [1, 12, 13].

Consider the quantum transition amplitude  $K(q', t'; q, t) = \langle q', t' | q, t \rangle$ , which is simply the probability of finding particles at the positions  $q'$  at time  $t'$  if they were at positions  $q$  at time  $t$ . We can write this matrix element as a path integral over all possible particle trajectories weighted by the action of the system [14]. In order to classify the possible particle trajectories, we must specify the configuration space of the particles. Since we are dealing with indistinguishable particles, particle configurations which differ by the interchange of two particles must be identified. Also, we assume two particles cannot be at a location at the same time (else they will be necessarily bosonic), i.e., we exclude the diagonal  $\mathcal{D}$  from the configuration space. The configuration space of  $n$  particles in  $d$  dimensions is therefore

$$\mathcal{C} = \frac{\mathbb{R}^{dn} - \mathcal{D}}{S_n}, \quad (1.2)$$

where  $S_n$  is the permutation group of  $n$  elements.

With this understanding of the configuration space we can proceed to write the path integral for the transition matrix elements:

$$K(q', t'; q, t) = \sum_{\alpha \in \pi_1(\mathcal{C})} \chi(\alpha) \int_{q(t) \in \alpha} Dq(t) \exp \left( i \int_t^{t'} dt_0 L(q(t_0)) \right). \quad (1.3)$$

On the right hand side of Equation 1.3, we divided all possible particle trajectories which obey the boundary conditions into groups of trajectories labeled by  $\alpha$ . All trajectories in the same homotopy class  $\alpha$  can be continuously deformed into each other. These classes form a group, the fundamental group  $\pi_1(\mathcal{C})$ . Each homotopy class is given a weight  $\chi(\alpha)$ , and we will see below that it is exactly this weight which determines the statistics of the particles.

Determining the allowed values of the weights  $\chi(\alpha)$  requires studying the group  $\pi_1(\mathcal{C})$  which classifies the possible trajectories of particles [12, 13]. The interpretation of the matrix element above as a probability forces the weights  $\chi$  to form a representation of the group  $\pi_1(\mathcal{C})$  [15]. When the number of spatial dimensions is  $d \geq 3$ , the group  $\pi_1(\mathcal{C})$  turns out to be simply the permutation group of  $n$  particles,  $S_n$ . This in

turn means that all paths which share the same end points can be continuously deformed into each other. The only one dimensional representation of  $S_n$  are the trivial representation and the alternating or permutation parity representation. Using the trivial representation gives  $\chi = 1$  to all trajectories of particles, resulting in bosonic wavefunctions. Using the parity representation gives  $\chi = \pm 1$ , where the sign depends on the parity of the permutation of particles from the start point to the end point. This in turn yields completely antisymmetric or fermionic wavefunctions. Higher dimension representations of the permutation group have been also studied [16], and have been found to be equivalent to bosonic or fermionic theories with additional hidden local degrees of freedom [17].

In two spatial dimension,  $d = 2$ , quantum mechanics is much richer. Heuristically, this can be motivated by thinking of the world lines of particles in the 3-dimensional space-time. If we imagine creating a pair of particles from the vacuum, winding these particles around each other, and then annihilating them back in to the vacuum, the world lines of these particles would form a knot in the space-time manifold. In a space-time manifold of dimension greater than three, there are no non-trivial knots, since there are enough dimensions to undo any knot to a simple loop. In  $2 + 1$  dimension, that is not possible, and non-trivial knots can exist. In terms of particle trajectories, this observation means that in  $2 + 1$  dimensions not only the end points of particle trajectories are important, but also the exact way particles wind around each other.

More formally, the first fundamental group  $\pi_1(\mathcal{C})$  of the configuration space of  $n$  particles in  $d = 2$  dimensions is the braid group  $B_n$  [18], an infinite non-Abelian group, rather than the permutation group  $S_n$  for  $d \geq 3$ . There is an infinite number of particle trajectories that share the same start and end points, but differ by the way particles are exchanged along the way. The braid group  $B_n$  can be generated by successive exchanges of particle positions, yet is different from the permutation group  $S_n$  due to the fact that in two spatial dimensions, clockwise and counter clockwise exchanges of particles are not equivalent.

The braid group has a family of one dimensional representations which can be

used to assign weights  $\chi$  to trajectories. Translated to requirements on wavefunctions, these representation lead to multi-valued wavefunctions:

$$\psi(x_2, x_1, \dots) = e^{i\pi\nu} \psi(x_1, x_2, \dots) \quad (1.4)$$

where  $0 \leq \nu \leq 1$ . Bosons and fermions correspond to  $\nu = 0$  and  $\nu = 1$ , respectively. An intermediate value for  $\nu$  makes this wavefunction one of *Abelian anyons*. They are Abelian since exchanging or braiding particles causes a simple multiplication by a phase, so the order of exchanges can be changed without effecting the final outcome.

Higher dimensional representations of the braid group give rise to *non-Abelian anyons*[19]. In such case, the wavefunction is a vector state, even for fixed particle positions. A particle exchange causes a rotation in the vector space, i.e., the wavefunction vector is multiplied by a matrix, as shown in Figure 1.1. Since matrix multiplication is not commutative, the order in which particle exchanges are performed is important, hence the non-Abelian statistics.

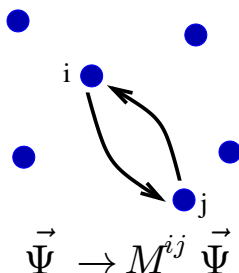


Figure 1.1: When non-Abelian particles are exchanged, the vector wavefunction is rotated in the degenerate subspace of states with the same particle positions.

Interest in anyons and fractional statistics surged in the condensed matter physics community following the observation of the fractional quantum Hall effect[7]. It was evident that the planar two-dimensional geometry of quantum Hall systems plays a crucial role in their physics. In particular, the wavefunctions suggested by Laughlin [20], which successfully explained the existence of the fractional quantum Hall effect,

had anyonic charged particles [21].

Fractional quantum Hall effect systems are still the most promising venue for the observation of fractional statistics in two dimensions, and are the focus of this thesis. We first review the integer Hall effect in section 1.2, and then we discuss the fractional quantum Hall effect in section 1.3.

## 1.2 Integer Quantum Hall Effect

The classical Hall effect, discovered by Edwin Hall in 1879 [22], is easily understood using simple electrodynamics. When moving charge carriers in a metal are placed in a magnetic field perpendicular to the current, they will be subject to the Lorentz force. The Lorentz force is perpendicular to both the current and the magnetic field, and is proportional to the charge unit and the magnitude of the magnetic field. Charge carriers will be forced to accumulate on the edges of the sample and develop a voltage drop perpendicular to the current in the sample, exactly enough voltage drop to cancel the Lorentz force. This voltage is the Hall voltage, and classically it is proportional to the magnetic field magnitude.

The quantum Hall effect (QHE) occurs in two-dimensional systems, at low temperature ( $T < 500\text{mK}$ ) and high magnetic fields ( $T \approx 2 - 10$  Tesla). Under these conditions, the Hall resistance, i.e., the ratio of the Hall voltage to the current running through the sample, deviates from the linear behavior in magnetic field predicted by the classical Hall effect. In fact, near certain magnetic fields, the Hall resistance forms plateaus, and its value is very precisely quantized to be of the form  $R_{xy} = \frac{1}{\nu} \frac{h}{e^2}$ , where  $\nu$  is a rational number. At the same time, the longitudinal resistance of the system vanishes. A typical experimental trace is shown in Figure 1.2.

The first quantum Hall effect observation was in a semiconductor heterostructure system, where electrons are trapped to the two-dimensional interface between two different semiconductors, such as GaAs and AlGaAs. At first, integer plateaus corresponding to integer value of  $\nu$  were observed [6]. This effect was labeled the integer quantum Hall effect. Soon after, non-integer fractions were also observed [7], the

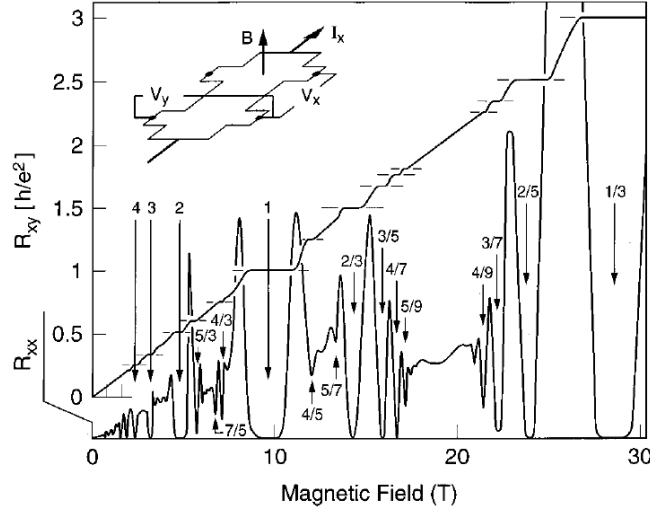


Figure 1.2: A trace showing the quantum Hall plateaus and the vanishing of the longitudinal resistance, taken from references [23, 24]

fractional quantum Hall effect.

It is instructive to examine the spectrum of non-interaction two-dimensional electrons in the presence of a magnetic field. The spectrum of a clean system breaks into a set of discrete energies called Landau levels. The energies of Landau levels are:

$$E_n = \hbar\omega_c \left( n + \frac{1}{2} \right), \quad n = 0, 1, 2, \dots \quad (1.5)$$

where  $\omega_c = \frac{eB}{m}$ . Each Landau level has degeneracy

$$g_{LL} = \frac{SB}{\phi_0}, \quad (1.6)$$

where  $S$  is the area of the system and  $\phi_0 = h/|e|$  is the magnetic flux quantum. The single-electron wavefunctions can also be calculated. For example, in the  $n = 0$  Landau level, the electron wavefunctions are holomorphic functions of  $z = x + iy$  multiplied by a gaussian factor, when using the symmetric gauge for the electromagnetic potential:

$$\varphi_m(\vec{r}) = C_m z^m e^{-|z|^2/4l_B^2}, \quad m = 0, 1, \dots, g_{LL}. \quad (1.7)$$

The magnetic length  $l_B = \sqrt{\hbar/|e|B}$  is the natural length scale in the quantum Hall regime, and  $C_m$  is a normalization constant. For more on Landau levels, see section 2.1.

It is easy to show that the Hall conductance of a filled Landau level is exactly  $\frac{e^2}{h}$ , and that its longitudinal resistance vanishes (see, e.g., the review article by Girvin [25]). It is therefore tempting to attribute the integer quantum Hall effect to simply filling an integer number of Landau levels. Luckily, the explanation cannot be this simple, since in a translationally invariant system, the Hall conductance must be linear in magnetic field, just like the classical Hall effect. It will be an integer multiple of  $\frac{e^2}{h}$  when the magnetic field is such that an integer number of Landau levels are filled, but deviations from that magnetic field change the filling of Landau levels and the Hall conductance accordingly. The existence of Landau levels does not explain the observed plateaus in the Hall conductance.

To understand the integer quantum Hall plateaus it is necessary to invoke disorder. In the presence of disorder, Landau levels acquires a finite width, and some of the states in each Landau level become localized. These localized states do not contribute to the conductance of the system, but act as a particle reservoir which can absorb particle density changes without effecting the conductance of the system, producing conductance plateaus (see [26] and references therein). The precise quantization of the conductance plateaus can be explained using Laughlin's gauge arguments [27]. Excellent review articles are [28] and [25].

### 1.3 Fractional Quantum Hall Effect

The picture described above for the integer quantum Hall effect had completely filled or nearly completely filled Landau levels as a starting point. This picture does not hold for the non-integer fractions observed, as seen in Figure 1.2 and Figure 1.3. The fraction  $\nu$  appearing in the Hall conductance  $\sigma_{xy} = \nu \frac{e^2}{h}$  corresponds to the filling fraction of electrons, i.e., the number of filled Landau levels, or equivalently, the ratio between the number of electrons in the sample and the number of magnetic

flux quanta threading the sample,  $\nu = \frac{N_e}{N\Phi_0}$ . When  $\nu$  is not an integer, for example  $\nu = 1/3$ , the ground state of free electrons at such a density is highly degenerate due to the flat dispersion of a Landau level. The fractional quantum Hall effect (FQHE) arises due to the interaction between electrons, which lifts the ground state degeneracy at these special rational filling fractions. The FQHE ground state is a strongly correlated state of electrons which has a gap for bulk excitations.

Laughlin's wavefunction for electrons [20] describes the FQHE at filling  $\nu = 1/m$ , with  $m$  an odd integer:

$$\Psi_m(z_1, z_2, \dots, z_N) = \prod_{i < j} (z_i - z_j)^m \exp\left(-\sum_i |z_i|^2 / 4l_0^2\right) \quad (1.8)$$

where  $l_0 = \sqrt{hc/eB}$  is the magnetic length. This wavefunction is entirely in the lowest Landau level, as can be seen from Equation 1.7. The wavefunction of Equation 1.8 has almost unity overlap with the exact ground state of electrons with Coulomb interaction at filling  $\nu = 1/m$ , and is the exact ground state wavefunction of a short range Hamiltonian [29]. Laughlin showed that electrons around these filling fractions have a gap to excitations, and also argued that these states support localized charged excitations which carry fractional charge  $e^* = e/m$ . These fractionally charged excitations were first observed in the  $\nu = 1/3$  state [30] in 1995. Using a hierarchy over the Laughlin series [29, 31] or a composite fermion picture [32], other observed fractions were explained, all with odd denominator filling fractions. Quasiparticle excitations in the Laughlin and hierarchy states are expected to have Abelian fractional statistics. These fractional statistics are yet to be observed.

The even denominator quantum Hall state observed at filling fraction  $\nu = 5/2$  [33] could not be explained using the hierarchy scheme or composite fermion picture. Moore and Read [34] constructed a wavefunction for electrons at  $\nu = 1/2$  as a candidate for the observed  $\nu = 5/2$  state, assuming the two lower filled Landau levels are inert:

$$\Psi_{Pf} = \text{Pf}\left(\frac{1}{z_i - z_j}\right) \prod_{i < j} (z_i - z_j)^2 \exp\left(-\sum_i |z_i|^2 / 4l_0^2\right) \quad (1.9)$$

where the Pfaffian is the completely antisymmetrized product

$$\text{Pf}\left(\frac{1}{z_i - z_j}\right) = \mathcal{A}\left(\frac{1}{z_1 - z_2} \frac{1}{z_3 - z_4} \dots\right). \quad (1.10)$$

The Moore-Read wavefunction is also referred to as the Pfaffian wavefunction. The Moore-Read wavefunction is written here in the lowest Landau level for simplicity, but we have in mind the equivalent wavefunction in the second Landau level (the first Landau level of both spins is completely filled). The wavefunction in Equation 1.9 can be raised to the second Landau level by applying the raising operators described in section 2.1. The Moore-Read wavefunction can be written as a conformal block of a conformal field theory, an approach which proved useful for generating quantum Hall candidate wavefunctions. The Moore-Read wavefunction suggested the existence of non-Abelian fractional statistics, since there is a ground state degeneracy for fixed positions of quasiparticles and a model Hamiltonian [35], and braiding quasiparticles causes a rotation in the degenerate subspace [35, 36].

Read and Rezayi generalized the Moore-Read construction and suggested a family of non-Abelian states at filling fraction  $\nu = k/(Mk+2)$  [37]. The  $k = 2, M = 1$  Read-Rezayi state is the Moore-Read state. The motivation for constructing additional non-Abelian states was the experimental observation of quantum Hall plateaus in the range  $2 < \nu < 4$ . (see Figure 1.3.)

Until recently, support for non-Abelian quantum Hall states has been largely due to numerical work. Support for the Moore-Read state as the ground state of electrons at  $\nu = 5/2$  was initiated by the numerical work of Morf [39], in 1998, on systems with a small number of electrons. Following numerical studies [40, 41, 42] further established that the ground state of electrons at  $\nu = 5/2$  is in the same universality class as the Moore-Read Pfaffian state. Support for the Read-Rezayi state as the ground state of electrons at filling fraction  $\nu = 12/5$  or its particle-hole conjugate  $\nu = 13/5$  is due to the numerical work of references [37, 43].

Experiments aimed at detecting the properties of the quantum Hall state at  $\nu = 5/2$  have been reported recently. These include experiments for measuring the charge

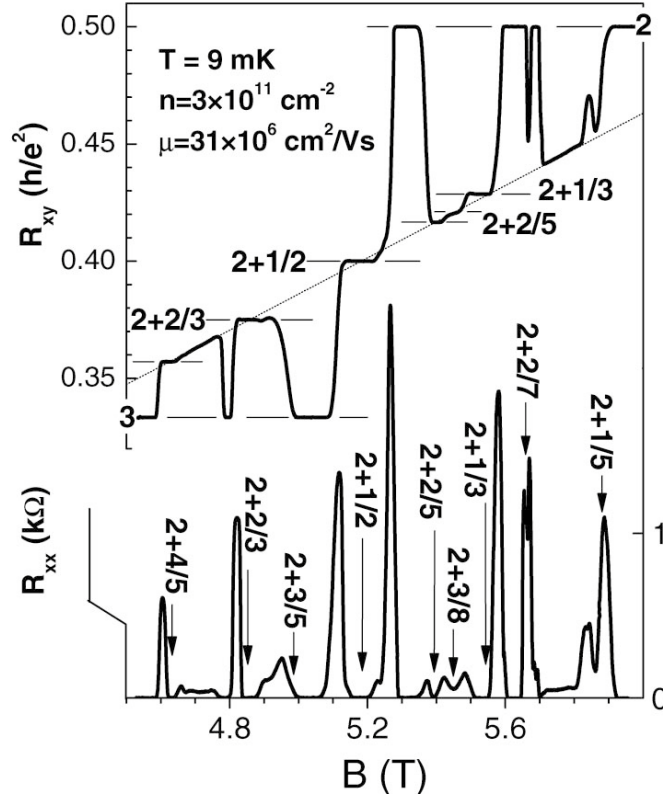


Figure 1.3: States in the first excited Landau level,  $2 < \nu < 3$ , at  $T = 9$  mK, taken from ref. [38]. Among others, plateaus at  $\nu = \frac{7}{3}, \frac{12}{5}, \frac{5}{2}, \frac{8}{3}$  are clearly observed, along with the vanishing of the longitudinal resistance.

of quasiparticles [44], I-V curves in a quantum point contact [45], thermopower [46], and two point contact interference [47].

## 1.4 Edge Excitations in Quantum Hall Liquids

Quantum hall states have a gap to excitations in the bulk. It was first pointed out by Halperin that integer quantum Hall systems must have gapless edge excitations [48]. By examining single particle energy levels, Halperin found that the edge theory of integer quantum Hall systems is the chiral one-dimensional Fermi liquid theory.

Based on general gauge invariance arguments, it can be shown [27, 49] that also fractional quantum Hall samples must have gapless edge excitations, though they cannot be described by Fermi liquid theory due to the strong correlations in the

fractional quantum Hall effect. The gapless edge theory is closely related to the conformal field theory of the bulk wavefunction [50], but it is also possible to deduce the edge theory from a hydrodynamical approach [49], or by examining microscopic wavefunctions of excitations of model Hamiltonians [51].

## 1.5 Overview

The gapless edge excitations of quantum Hall liquids dominate the transport properties of these systems due to the bulk gap to excitations. This is the reason for the extensive study of edge experiments for detecting properties of quantum Hall states.

Fractionally charged quasiparticles in the fractional quantum Hall regime have been observed [30, 44] through edge tunneling experiments. There are a number of proposed experiments for using edge tunneling to detect fractional statistics, both Abelian [52, 53, 54, 55] and non-Abelian [56, 57, 58, 59].

Support for the existence of non-Abelian quantum Hall states is so far only due to numerical work on systems with a small number of electrons. In this thesis, we first address Landau level mixing. It is often ignored in numerical work, and could significantly improve such work and enhance our theoretical understanding of quantum Hall systems. The bulk of the work reported in this thesis focuses on the analysis of possible edge experiments which are hoped to reveal evidence of non-Abelian states and statistics, either directly or indirectly.

In chapter 2 we perturbatively and systematically calculate the effects of Landau level mixing on the interaction of electrons in a given Landau level. We represent our results using multi-particle pseudopotentials and explain the significance of Landau level mixing to numerical work. In chapter 3 we quantitatively analyze the two-point contact interferometer in the  $\nu = 5/2$  quantum Hall state. This experiment is hoped to provide direct evidence of non-Abelian statistics. We address the finite temperature and voltages behavior of the measurable signal and the amplitude attenuation of the signal due to finite temperature. In chapter 4 we investigate a family of quantum Hall states at filling fractions  $2/(k+2)$ , which are relevant to the observed quantum

Hall fractions  $5/2$  and  $12/5$ . In chapter 5 we suggest an experimental setup involving electron tunneling between quantum Hall edges and a quantum dot. It is shown that the neutral modes of the edge theories lead to the mapping of the tunneling problem to the multi-channel Kondo problem, which can help distinguish between different states at filling  $\nu = 5/2$ . Finally, in chapter 6 we use the same bosonization technique extensively used in the study of quantum Hall edges to study Sagnac interference in carbon nanotube loops.

## Chapter 2

# Landau Level Mixing

Since the early days of the fractional quantum Hall effect (FQHE), numerical experiments on small systems have played a major role in the study of electrons in high magnetic fields. Laughlin's seminal paper [20], which initiated the approach of candidate wavefunctions for the FQHE, included the exact diagonalization results of a system with 3 and 4 electrons at filling fraction  $\nu = 1/m$ , with  $m$  an odd integer. Even with such small systems, Laughlin was able to verify that the FQHE system has a gap to excitations, that the excitations are localized and fractionally charged, and that his variational wavefunctions for the ground and excited states are indeed very close to the numerically calculated ones.

The observation of an even denominator quantum Hall plateau at  $\nu = 5/2$  [33] led to the proposal of wavefunctions with non-Abelian excitations for the FQHE. A paired electron wavefunction with non-Abelian statistics [34] was proposed to describe the observed state at  $\nu = 5/2$ . This approach was generalized to non-Abelian states at  $\nu = 2 + k/(k + 2)$ , where  $k$  is an integer [37]. Recent measurements of quasi-particle charge [44] and tunneling current [45] around  $\nu = 5/2$  are consistent with the Moore-Read paired state of Ref. [34] or its particle-conjugate [60], but are also consistent with Abelian wavefunctions [61]. Therefore, the support for non-Abelian FQHE states stems mainly from numerical calculations. In particular, the Moore-Read wavefunction emerged as the leading candidate for the  $\nu = 5/2$  state due to the investigation by Morf in '98 [39] and following works [40, 41, 42, 62]. The numerical studies of the quantum Hall system at  $\nu = 12/5$  [37, 43] support the  $k = 3$

Read-Rezayi state as the ground state.

Most numerical studies of quantum Hall systems truncate the Hilbert space to the partially filled Landau level in question. The electron-electron interaction is usually taken as the Coulomb interaction projected onto that Landau level, or a model interaction which captures the essential features of the projected interaction. These simplifications make the size of the Hilbert space of the system tractable and amenable to numerical calculations. The projection or approximation of the Coulomb interaction has had much success in the study of Abelian quantum Hall states since these states seem to be robust to small changes in the electron-electron interactions. The ground state of electrons in the second Landau level, however, seems to be sensitive to such small changes in the interaction between electrons [40, 63, 41, 42]. Though this sensitivity makes the justification of numerical results more difficult, it might also provide a control knob for engineering ground states of quantum Hall systems.

Another shortcoming of the projection of the Coulomb interaction onto a given Landau level is that the resulting interaction is particle-hole symmetric. With such a particle-hole symmetric interaction, it is not possible to differentiate energetically between a state and its particle-hole conjugate. For example, a particle-hole symmetric interaction will result in the same ground state energy for the Moore-Read state [34] and its particle-hole conjugate state, the anti-Pfaffian [60, 64], both states of electron at filling  $\nu = 5/2$ . Also, a particle-hole symmetric interaction will appear to be the same at filling fractions  $\nu = 12/5$  and  $\nu = 13/5$ , which is inconsistent with the experimental observation of the  $\nu = 12/5$  state and the lack of such observation of the  $\nu = 13/5$  state [38].

In this chapter we present a method for systematically incorporating the completely empty upper Landau levels or completely filled lower Landau levels into the effective interaction between electrons in a given Landau level. This effective interaction is usually referred to as Landau level mixing (LLM). Our approach allows us to better approximate the electron-electron interactions in the second Landau level, which can make a substantial difference in the properties of numerically calculated

ground states, as we argued above. In addition, our approach will generate interactions which are not particle-hole symmetric, and will allow us to differentiate between the Moore-Read state and the anti-Pfaffian state. Our results can be used as input for a numerical investigation of ground states in the second Landau level.

To our knowledge, there is no previously published systematic investigation of LLM.

## 2.1 Landau Levels, Coulomb Interaction and Particle-Hole Symmetry

In the presence of a magnetic field  $\vec{B} = B\hat{z}$  perpendicular to the  $x - y$  plane of a two dimensional electron gas, the single electron spectrum breaks into flat Landau levels. The  $n^{\text{th}}$  Landau level has energy

$$E_n = \hbar\omega_c \left( n + \frac{1}{2} \right), \quad n = 0, 1, 2, \dots \quad (2.1)$$

where  $\omega_c = \frac{eB}{m}$ , with  $m$  the effective mass of an electron. Each Landau level has degeneracy

$$g = \frac{SB}{\phi_0}, \quad (2.2)$$

where  $S$  is the area of the sample and  $\phi_0 = h/|e|$  is the magnetic flux quantum.

In the symmetric gauge,  $\vec{A} = (-By/2, Bx/2, 0)$ , the lowest Landau level ( $n = 0$ ) states are holomorphic functions of  $z = x + iy$ , multiplied by a decaying gaussian:

$$\varphi_{m,0}(\vec{r}) = C_m z^m e^{-|z|^2/4l_B^2}, \quad m = 0, 1, \dots, g. \quad (2.3)$$

The magnetic length  $l_B = \sqrt{\hbar/|e|B}$  is the natural length scale in the quantum Hall regime, and  $C_m$  is a normalization constant. Single electron states in higher  $n$  Landau levels can be obtained from the lowest Landau level states by application of the raising

operator  $a^\dagger = \frac{i}{\sqrt{2}} e^{-|z|^2/4l_B^2} (z^* - 2\frac{\partial}{\partial z}) e^{|z|^2/4l_B^2}$  for  $n$  times (see, for example, Ref. [65]):

$$\varphi_{m,n}(\vec{r}) = \frac{a^{\dagger n}}{\sqrt{n!}} \varphi_{m,0}(\vec{r}) \quad (2.4)$$

In the absence of interactions, a partially filled Landau level has many degenerate states due to its flat dispersion. The Coulomb interaction lifts this degeneracy, and gives rise to a gapped spectrum near certain filling fractions, as was first shown by Laughlin [20]. The Coulomb interaction can be written, using second quantization notation, as:

$$U = \frac{1}{2} \sum u(4, 3; 2, 1) c_4^\dagger c_3^\dagger c_2 c_1. \quad (2.5)$$

The creation operator  $c_i^\dagger \equiv c_{m_i, n_i}^\dagger$  creates an electron in the state  $m_i$  in the  $n_i$  Landau level. The matrix element  $U(4, 3; 2, 1)$  is the  $1/r$  Coulomb interaction matrix element:

$$u(4, 3; 2, 1) = \langle m_4, n_4; m_3, n_3 | \frac{e^2}{4\pi\epsilon r} | m_1, n_1; m_2, n_2 \rangle. \quad (2.6)$$

Note the ordering of the states in the matrix element. We can use the explicit wavefunctions and evaluate the Coulomb matrix elements of Equation 2.6. We cannot obtain a closed form for these matrix elements, but they can be expressed as an integral over a two dimensional linear momentum variable:

$$u(4, 3; 2, 1) = \frac{e^2}{4\pi\epsilon l_B} \tilde{\text{A}}\text{S} \left\{ \int \frac{d^2 q}{(2\pi)^2} \frac{2\pi}{|q|} e^{-q^2} G_{n_4, n_1}(q^*) G_{m_4, m_1}(q) G_{n_3, n_2}(-q^*) G_{m_3, n_2}(-q) \right\} \quad (2.7)$$

The function  $G_{a,b}(q)$ , for  $a > b$ , is [65]:

$$G_{a,b}(q) = \left( \frac{b!}{a!} \right) \left( \frac{-iq}{\sqrt{2}} \right)^{a-b} L_b^{a-b} \left( \frac{|q|^2}{2} \right) \quad (2.8)$$

where  $L_b^{a-b}(q)$  is the generalized Laguerre polynomial.  $\tilde{\text{A}}\text{S}$  antisymmetrizes with respect to the exchanges  $4 \leftrightarrow 3$  and  $2 \leftrightarrow 1$ , so that the matrix elements respect the fermionic statistics of electrons.

The full Coulomb interaction of Equation 2.5 includes all Landau levels, i.e., it

acts in an infinite Hilbert space. The full Hamiltonian of the system is then:

$$\begin{aligned}
 H &= H_0 + U \\
 &= \sum_{m,n} \hbar\omega_c \left(n + \frac{1}{2}\right) c_{m,n}^\dagger c_{m,n} + \frac{1}{2} \sum u(4, 3; 2, 1) c_{m_4, n_4}^\dagger c_{m_3, n_3}^\dagger c_{m_2, n_2} c_{m_1, n_1}
 \end{aligned} \tag{2.9}$$

The spacing in energy between Landau level is  $\hbar\omega_c \approx 20B$  Kelvins, when  $B$  is in Teslas. This spacing is much larger than the observed gap in the quantum Hall regime. For example, the fragile state at  $\nu = 5/2$  has an activation gap of about  $\Delta = 500\text{mK}$  [38]. It is also assumed in many cases that the typical Coulomb energy,  $e^2/4\pi\epsilon l_B$ , is much smaller than the Landau level spacing as well. It will be useful to define the ratio of the Coulomb energy to the cyclotron energy:

$$\kappa = \frac{e^2/4\pi\epsilon l_B}{\hbar\omega_c}. \tag{2.10}$$

Under the assumption that  $\kappa \ll 1$ , the cyclotron energy  $\hbar\omega_c$  is much larger than any other energy scale in the problem, and it would be a good approximation to ignore all higher or lower Landau levels other than the partially filled one. This will reduce the size of the Hilbert space and greatly reduce the numerical effort required for diagonalizing the system. Projection onto a single Landau level is equivalent to keeping only operator with labels  $n_i = n$  in the full Hamiltonian, Equation 2.9. We may suppress the  $n_i$  label in that case, and ignore the Landau level energy which is simply a constant:

$$H_{\text{projected}} = \frac{1}{2} \sum u^n(4, 3; 2, 1) c_{m_4}^\dagger c_{m_3}^\dagger c_{m_2} c_{m_1} \tag{2.11}$$

We will see that the Coulomb interaction can be easily calculated and represented by pseudopotentials when projected to a given Landau level in section 2.2.

As discussed in the introduction, the projected Hamiltonian in Equation 2.11 has a few shortcomings. The assumption that the ratio of the Coulomb energy to the cyclotron energy,  $\kappa$ , is small, does not hold in real systems. In addition, when

projected to a single Landau level, the Coulomb interaction is particle-hole symmetric, as can be seen from the simple transformation:

$$\begin{aligned} c_m^\dagger &\rightarrow c_m \\ c_m &\rightarrow c_m^\dagger \\ u^n(4, 3; 2, 1) &\rightarrow (u^n(4, 3; 2, 1))^* . \end{aligned} \tag{2.12}$$

Under this transformation, the two-particle interaction in Equation 2.11 is invariant, up to a shift of the chemical potential [60]. (It is useful to remember that the matrix elements satisfy  $(u^n(4, 3; 2, 1))^* = u^n(1, 2; 3, 4)$ .)

We show below how to incorporate systemically the neglected Landau levels into the effective interaction between electrons in a given Landau level. This effective interaction will not be particle-hole symmetric and will be able to resolve the difference between quantum Hall candidate states and their particle-hole conjugates. Also, we get the effective interaction as an expansion in powers of  $\kappa$ , which would allow a rigorous test of the usual assumptions which go into numerics of quantum Hall systems.

## 2.2 Multi-Particle Pseudopotentials

In this section we will review multi-particle pseudopotentials, a convenient way of parameterizing multi-particle interactions. It is most easily presented in first quantization notation, but can also be easily translated to second quantization notation, as we shall see. Two-particle pseudopotentials were first introduced by Haldane [29], and multi-particle pseudopotentials were introduced in [66].

In first quantization notation, a translationally invariant two-particle interaction can be written as the sum of interactions of pairs of particles:

$$H_{2p} = \sum_{i < j} V(\vec{r}_i - \vec{r}_j). \tag{2.13}$$

The two-particle Hamiltonian acts only on two particles at a time, so it is sufficient to analyze a two-particle wavefunction. A two-particle wavefunction can be always decomposed to a center of mass part and a relative part:

$$\Psi(\vec{r}_1, \vec{r}_2) = \sum_{b,c} A_{b,c} \Psi_b^{CM} \left( \frac{\vec{r}_1 + \vec{r}_2}{2} \right) \Psi_c^{rel}(\vec{r}_1 - \vec{r}_2). \quad (2.14)$$

When the interaction is translationally invariant, it acts only on the relative part of the wavefunction. If the interaction is also rotationally invariant, it cannot mix states with different relative angular momenta.

We will restrict our discussion to electrons in the lowest Landau level. Any higher Landau level can be analyzed by simply applying the raising operators described in section 2.1 to all electrons an appropriate number of times. In the lowest Landau level, we can write the relative wavefunction of two particles in a basis of defined angular momentum, as can be seen from the lowest Landau level states in Equation 2.3. The states in this relative basis are:

$$|m; i, j\rangle = N_m (z_i - z_j)^m, \quad (2.15)$$

where  $m$  is the relative angular momentum, and  $N_m$  is a normalization constant. Using this basis, we can write the two-particle Hamiltonian as:

$$\begin{aligned} H_{2p} &= \sum_{i < j} \sum_m |m; i, j\rangle \langle m; i, j| V(\vec{r}_i - \vec{r}_j) |m; i, j\rangle \langle m; i, j| \\ &\equiv \sum_{i < j} \sum_m V_{m,2} P_{ij}^m, \end{aligned} \quad (2.16)$$

where  $P_{ij}^m$  is the projector onto the state of relative angular momentum  $m$  between particles  $i$  and  $j$ , and  $V_{m,2}$  is the two-particle  $m^{\text{th}}$  pseudopotential [29]. Using the explicit relative wavefunctions of Equation 2.15 we can explicitly calculate  $V_{m,2}$  for the lowest Landau level [29]:

$$V_{m,2} = \langle m; i, j| V(\vec{r}_i - \vec{r}_j) |m; i, j\rangle = \int_0^\infty \frac{d^2q}{(2\pi)^2} V(q) L_m(q^2 l_B^2) e^{-q^2 l_B^2}, \quad (2.17)$$

where  $V(q)$  is the Fourier transform of  $V(\vec{r})$ . For the  $1/r$  Coulomb interaction we have

$$V_C(q) = \frac{e^2}{4\pi\epsilon} \frac{2\pi}{q}. \quad (2.18)$$

,

The 2-particle pseudopotentials  $V_{m,2}$  of the Coulomb interaction projected to the lowest Landau level decay as  $1/\sqrt{m}$  for large  $m$ , and therefore, one might suspect that higher  $m$  pseudopotentials are not as important as lower  $m$  ones. Indeed, that turns out to be true for the Laughlin states. For example, the  $\nu = 1/3$  Laughlin state is the exact ground state of a two-particle interaction where only  $V_{1,2}$  is non-zero, and it is very close to the ground state of the system with the full Coulomb interaction [20].

So far we have discussed two-particle pseudopotentials, but the same approach can be generalized to interaction of more than two particles. The derivation of multi-particle pseudopotentials follows the above derivation closely, with the only difference being the structure of the relative angular momentum basis.

If we are interested in an  $M$ -particle interaction, it is sufficient to consider an  $M$ -particle wavefunction. This wavefunction can be decomposed to a sum of products of a center of mass wavefunction and a relative wavefunction:

$$\Psi(\vec{r}_1, \dots, \vec{r}_M) = \sum A_{b,c} \Psi_b^{CM} \left( \frac{\vec{r}_1 + \dots + \vec{r}_M}{M} \right) \Psi_c^{rel}(\vec{r}_1 - \vec{r}_2, \dots, \vec{r}_1 - \vec{r}_M). \quad (2.19)$$

A rotationally and translationally invariant  $M$ -particle interaction acts only on the relative part of the wavefunction, and cannot mix relative wavefunctions with different angular momenta. If we restrict ourselves to the lowest Landau level once more, then we can define the angular momentum of the relative wavefunction as the total degree of the holomorphic polynomial  $\Psi^{rel}$ . If  $\Psi^{rel}$  is a homogeneous polynomial of degree  $m$ , then it is an angular momentum eigenstate with angular momentum  $m$ .

To write an angular momentum basis for the relative wavefunctions of  $M$  particles in the lowest Landau level we must find all the homogenous polynomials in  $z_1, \dots, z_M$  which are translationally invariant and completely antisymmetric, due to

the fermionic statistics. This has been carried out in Ref. [66]. For a given angular momentum  $m$ , there could be more than one state satisfying these conditions, and the  $M$ -particle interaction may mix these states since they have the same angular momentum. In such case, the pseudopotential  $V_{m,M}$  is a matrix rather than a scalar. A general translationally and rotationally invariant  $M$ -particle interaction can be written as:

$$H_{Mp} = \sum_{i_1 < \dots < i_M} \sum_{m, q, q'} |m, q; i_1, \dots, i_M\rangle V_{m,M}^{q, q'} \langle m, q'; i_1, \dots, i_M|. \quad (2.20)$$

The indices  $q$  and  $q'$  run over the multiple possible states for a given angular momentum  $m$ , if any.

As an example, we can write the lowest and second lowest angular momentum states of 3 electrons. The lowest angular momentum a relative wavefunction of 3 fermions can have is 3. The corresponding wavefunction is:

$$|m = 3, M = 3 \rangle = c(z_1 - z_2)(z_1 - z_3)(z_2 - z_3). \quad (2.21)$$

One can easily check that  $|m = 3, M = 3 \rangle$  is a homogenous polynomial which is completely antisymmetric and translationally invariant. There is no such 3-fermion state for  $m = 4$ . For  $m = 5$ , the state is:

$$|m = 5, M = 3 \rangle = c'(z_1 - z_2)(z_1 - z_3)(z_2 - z_3) \times (\tilde{z}_1 \tilde{z}_2 + \tilde{z}_1 \tilde{z}_3 + \tilde{z}_2 \tilde{z}_3), \quad (2.22)$$

where  $\tilde{z}_i = z_i - \frac{z_1 + z_2 + z_3}{3}$ . A systematic derivation of multi-particle angular momentum states of both bosons and fermions can be found in [66].

We will use the pseudopotential representation for the effective interactions between electrons generated by LLM.

## 2.3 Perturbative Calculation of LLM

Our approach for including the effects of fully filled or completely empty Landau levels on the interaction between electrons in a given partially filled Landau level is to integrate out the degrees of freedom belonging to those empty or full Landau levels. This will add to the interaction between the electrons of the partially filled level the virtual processes in which electrons hop to higher empty levels, or electrons from lower filled levels hop to the partially filled level. This approach is systematic, and we will calculate the effective interaction in powers of  $\kappa$ , the ratio of the Coulomb energy to the cyclotron energy, introduced in section 2.1.

This approach is essentially the same as energy or momentum shell Renormalization Group (RG). In energy or momentum shell RG, one attempts to integrate out high energy degrees of freedom and examine the resulting effective interaction between the remaining low energy degree of freedom. This procedure reduces the cutoff of the problem. Rescaling is required in the usual RG procedure, so that one can compare the flow of the interactions. In the case of LLM, we have no need to rescale. The RG approach for interacting fermions was pioneered by Shankar [67], and we largely follow his conventions for notation.

The starting point for our calculation is the path integral representation of the zero-temperature partition function of electrons in a magnetic field. The full partition function corresponding to the Hamiltonian in Equation 2.9 can be readily written as

$$Z = \int \prod_{m,n} [d\bar{c}_{m,n}(\omega) dc_{m,n}(\omega)] e^{S_0} e^{S_V}. \quad (2.23)$$

The variables  $\bar{c}_{m,n}(\omega)$  and  $c_{m,n}(\omega)$  are anti-commuting Grassman variables. The action  $S_0$  is the action of free electrons in a magnetic field:

$$S_0 = \int \frac{d\omega}{2\pi} \sum_{m,n} \bar{c}_{m,n}(\omega) (i\omega - E_n + \mu) c_{m,n}(\omega), \quad (2.24)$$

where  $E_n = \hbar\omega_c (n + \frac{1}{2})$  as before, and  $\mu$  is the chemical potential. The interaction

part of the action is:

$$\begin{aligned}
SU = & -\frac{1}{2} \int \prod_{i=0}^4 \frac{d\omega_i}{2\pi} u(4, 3; 2, 1) 2\pi \delta(\omega_4 + \omega_3 - \omega_2 - \omega_1) \\
& \times \bar{c}_{m_4, n_4}(\omega_4) \bar{c}_{m_3, n_3}(\omega_3) c_{m_2, n_2}(\omega_2) c_{m_1, n_1}(\omega_1). \tag{2.25}
\end{aligned}$$

We are interested in the situation where the chemical potential is such that one of the Landau levels is only partially filled. Let us call the index of that partially filled Landau level  $n_{par}$ . Higher Landau level are completely empty, while lower Landau levels are completely full, in the absence of electron interactions.

Borrowing notation and terminology from momentum shell RG, we shall call the degrees of variable within the  $n_{par}$  Landau level low energy degrees of freedom, and we will drop the Landau level index for these variables:

$$c_{m, n=n_{par}}(\omega) \equiv c_m(\omega), \tag{2.26}$$

and the same for  $\bar{c}(\omega)$ . We shall call all other degrees of freedom high energy degrees of freedom. Any variable in the interaction action, Equation 2.25, can be expressed as the sum of low and high energy variable:

$$c_{m, n}(\omega) = \delta_{n, n_{par}} c_m(\omega) + (1 - \delta_{n, n_{par}}) c_{m, n}(\omega). \tag{2.27}$$

Our plan from this point onwards is to use the decomposition above, Equation 2.27, to rewrite the action. Then, we will integrate out all the degrees of freedom with  $n \neq n_{par}$ , in powers of the interaction  $u$ , to generate new interactions between the degree of freedom with  $n = n_p$ . The generated interactions will include  $n$ -particle contributions, i.e. 2-particle, 3-particle interactions and more:

$$\begin{aligned}
U_{eff} = & \sum u_{eff}^{(2)}(4, 3; 2, 1) \bar{c}_{m_4} \bar{c}_{m_3} c_{m_2} c_{m_1} \\
& + \sum u_{eff}^{(3)}(6, 5, 4; 3, 2, 1) \bar{c}_{m_6} \bar{c}_{m_5} \bar{c}_{m_4} c_{m_3} c_{m_2} c_{m_1} + \dots \tag{2.28}
\end{aligned}$$

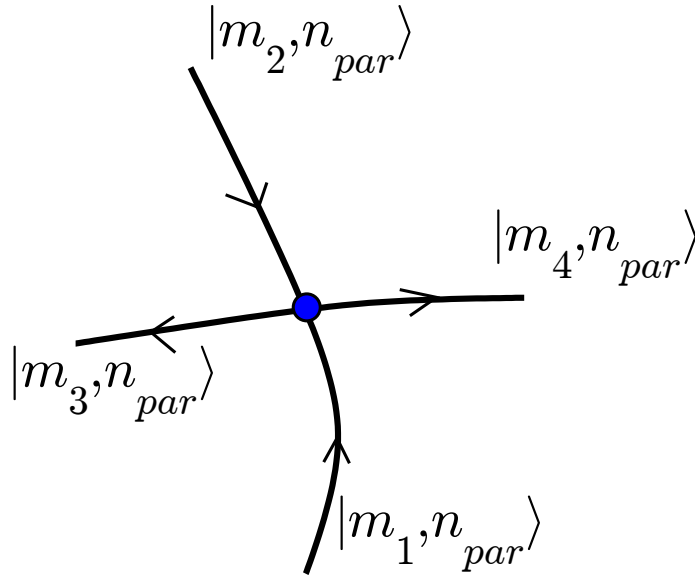


Figure 2.1: The tree level diagram. The vertex corresponds to the Coulomb matrix elements. In the tree level diagram, all the legs are low energy variable, i.e., they are all in the partially filled Landau level  $n_{par}$

This procedure is well known, and it is extremely helpful to use diagrams to simplify bookkeeping. As the review [67] provides a detailed description of the expansion in powers of the interaction, the diagrammatic representation, and the integration procedure, we will not review these here. We will simply show the diagrams we are interested in and explain the corresponding interactions.

## 2.4 Tree Level Interaction

The lowest order contribution to the interaction between electrons in the partially filled Landau level comes from simply ignoring the other Landau levels in the action  $S_U$  of Equation 2.25, and restricting the sums to  $n = n_p$ . The tree level diagram is shown in Figure 2.1.

The tree level diagram and all other diagrams have a corresponding mathematical expression. Each vertex contributes a Coulomb matrix element and the  $\omega$  conserva-

tion. For each vertex in a diagram, we need to include the following term:

$$-\frac{1}{2}u(4, 3; 2, 1) 2\pi\delta(\omega_4 + \omega_3 - \omega_2 - \omega_1). \quad (2.29)$$

We need to sum over all possible high energy legs. In the tree level diagram, there are no high energy legs, so the interaction is simply the Coulomb interaction, but with all Landau level indices set to  $n = n_{par}$ . This is equivalent to the projection of the Coulomb interaction to the partially filled Landau level, as discussed in section 2.1:

$$u_{tree}(4, 3; 2, 1) = u^{n_{par}}(4, 3; 2, 1). \quad (2.30)$$

As mentioned earlier, the Coulomb interaction conserves angular momentum. The basis states we chose are angular momentum eigenstates. The angular momentum of the state  $\varphi_{m,n}(\vec{r})$  is:

$$J^z|m, n\rangle = (m - n)|m, n\rangle. \quad (2.31)$$

In the tree level diagram, all Landau level indices are  $n = n_{par}$ , so angular momentum conservation forces:

$$m_4 + m_3 = m_2 + m_1 \quad (2.32)$$

In short, the tree level interaction is simply the projected Coulomb interaction. Keeping only the tree level diagram is equivalent to setting all the Landau level indices in the Hamiltonian of Equation 2.9 to  $n_i = n_{par}$ . It is still a 2-particle interaction that does not break particle-hole symmetry, and does not know about the other Landau levels, as evident from the lack of  $\hbar\omega_c$  in these expressions.

## 2.5 Lowest Order 3-Particle Interaction

Higher order contributions to the effective actions come from more complicated diagrams which also include high energy degrees of freedom. In such diagrams, the external legs are set to be in the Landau level of interest,  $n = n_{par}$ , while internal legs are allowed to be in any other Landau level, as long as angular momentum is

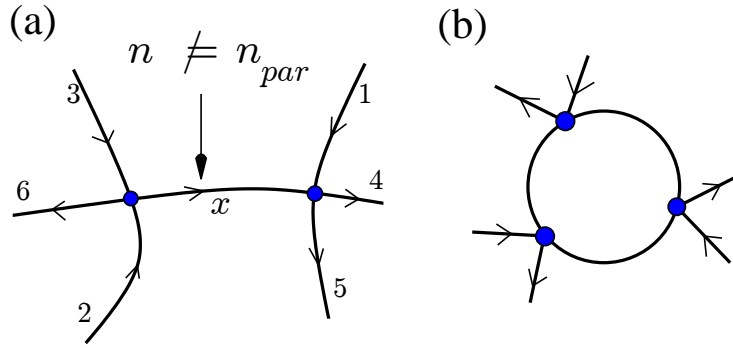


Figure 2.2: Diagrams corresponding to 3-particle interaction. Figure (a) is a second order diagram, since it contains two vertices. All external legs are in the partially filled Landau level  $n = n_{par}$ . Incoming legs are labeled 1, 2, 3 and outgoing legs are labeled 4, 5, 6. The inner leg indices  $m_x$  and  $n_x$  run over all possible values with  $n \neq n_{par}$ . Figure (b) is a third order diagram.

conserved at each vertex. Examples of such diagrams are those in Figure 2.2.

We are interested in the 3-particle interaction since it is the first interesting interaction which is not invariant under the particle-hole symmetry, Equation 2.12. This interaction will split the energies of a state and its particle-hole conjugate.

Let us examine the diagram in Figure 2.2(a). This is the lowest order 3-particle interaction, in powers of  $\kappa$ . It is second order in  $u$  and first order in  $\kappa$ , as we shall see. Note that in the usual Fermi-liquid RG, this diagram would vanish, since it is hard to satisfy the conservation laws at a vertex when 3 of the legs are low energy variables and the remaining leg a high energy variable. In the case of quantum Hall, this diagram does not vanish since even for a large Landau level index, a state can have small angular momentum when  $m$  is large enough, as can be seen from Equation 2.31.

The effective action for any diagram can be written using the following rules: External legs are labeled by their  $m_i$  values and their corresponding frequencies  $\omega_i$ , with the  $n$  index suppressed since they all have  $n = n_{par}$ . Each internal leg with indices  $(m_x, n_x \neq n_{par})$  comes with a propagator, as a result of integration:

$$G_{m_x, n_x}(\omega_x) = \frac{1}{i\omega_x - (E_{n_x} - \mu)}. \quad (2.33)$$

Each vertex carries a contribution shown in Equation 2.29. There is also an overall constant factor of  $1/r!$ , where  $r$  is the order of the diagram (number of vertices), and a combinatorial factor depending on the exact diagram considered. Finally, we sum over all possible values of the internal indices  $m_x, n_x$  and the integrate over the frequencies of the internal legs.

The diagram shown in Figure 2.2(a) corresponds to the following expression:

$$c_{comb} \frac{1}{2!} \left(-\frac{1}{2}\right)^2 \sum_{m_x, n_x \neq n_{par}} \int \frac{d\omega_x}{2\pi} \frac{1}{i\omega_x - (E_{n_x} - \mu)} \\ \times u(6, x; 3, 2) u(5, 4; x, 1) 2\pi\delta(\omega_6 + \omega_x - \omega_3 - \omega_2) 2\pi\delta(\omega_5 + \omega_4 - \omega_x - \omega_1), \quad (2.34)$$

where  $c_{comb}$  is a combinatorial factor arising from the different possible ways of contacting operators using Wick's theorem [67]. The energy  $E_{n_x} - \mu$  is approximately  $\hbar\omega_c(n_x - n_{par})$ . The  $\omega_x$  integral in this particular diagram simply enforces energy conservation. The resulting interaction Lagrangian to this order is:

$$\tilde{u}(m_6, \dots, m_1) = -c_{comb} \frac{1}{2!} \left(-\frac{1}{2}\right)^2 \times \\ \sum_{m_x, n_x \neq n_{par}} \frac{u(6, x; 3, 2) u(5, 4; x, 1)}{i(\omega_3 + \omega_2 - \omega_6) - (E_{n_x} - \mu)} 2\pi\delta(\omega_6 + \omega_5 + \omega_4 - \omega_3 - \omega_2 - \omega_1). \quad (2.35)$$

There is an additional minus sign in Equation 2.35 compared to Equation 2.34 due to the definition  $S \sim -U$ .

The tilde in  $\tilde{u}$  indicates that this is the interaction appearing in the *Lagrangian* in the frequency domain. In this form,  $\tilde{u}$  is frequency dependent, i.e., describes a time-retarded interaction, and will not simply translate to a Hamiltonian. A Hamiltonian, on the other hand, is much more useful for numerical calculations. Luckily, we can argue that ignoring the frequency dependence is a good approximation. We know that the cyclotron energy  $\hbar\omega_c$  is much larger than the energy scales we are interested

in, therefore it is possible to ignore the frequency dependence in the term

$$\frac{1}{i(\omega_3 + \omega_2 - \omega_6) - (E_{n_x} - \mu)}. \quad (2.36)$$

A slightly more formal way to justify this approximation is to imagine expanding Equation 2.36 in powers of  $\omega_i$ . The lowest order term, the one with all the  $\omega_i$ 's set to zero is the most relevant in the RG sense since it has the lowest powers of frequencies. For these reasons, we shall make the approximation  $\hbar\omega_c \gg \omega_i$  in all the diagrams we evaluate.

Once we've ignored the  $\omega_i$  dependence in Equation 2.35, it is straightforward to go back to a Hamiltonian for this interaction. In terms of creation and annihilation operators, this lowest order 3-particle interaction Hamiltonian is

$$H_{3b}^{2^{\text{nd order}}}(m_6, \dots, m_1) = \sum_{\{m_i\}} u(m_6, \dots, m_1) c_{m_6}^\dagger c_{m_5}^\dagger c_{m_4}^\dagger c_{m_3} c_{m_2} c_{m_1} \quad (2.37)$$

with

$$u(m_6, \dots, m_1) = -c_{comb} \frac{1}{2!} \left(-\frac{1}{2}\right)^2 \sum_{m_x, n_x \neq n_{par}} \frac{u(6, x; 3, 2) u(5, 4; x, 1)}{-(E_{n_x} - \mu)}. \quad (2.38)$$

The Hamiltonian in Equation 2.37 came about from evaluating the diagrams in Figure 2.2(a) with a particular assignment of external legs labels. To get the correct result, we must sum over the different label permutations of the external legs. We will do this implicitly when we report our results. The resulting correct Hamiltonian acts entirely in the  $n_{par}$  Landau level. It is not particle-symmetric, and it incorporates the effect of LLM to lowest order.

In the next section, we explicitly evaluate the expressions for the 3-particle interaction and calculate the corresponding 3-particle pseudopotentials.

## 2.6 Lowest Order 3-Particle Pseudopotentials

We have obtained a formal expression for the lowest order 3-particle interaction generated by LLM, Equation 2.37. It is instructive to represent this interaction using 3-particles pseudopotentials. This will allow us to conveniently parameterize the interaction with a list of numbers, and will give us insight regarding the short and long distance behavior of this interaction.

As described in section 2.2, a 3-particle interaction can be decomposed to a sum of operators acting in defined relative angular momentum subspaces:

$$V(\vec{r}_i, \vec{r}_j, \vec{r}_k) = \sum_{m,q,q'} |m, q; i, j, k\rangle V_{m,3}^{q,q'} \langle m, q'; i, j, k|. \quad (2.39)$$

The state  $|m, q; i, j, k\rangle$  is a state of the three particles  $i$ ,  $j$ , and  $k$  with angular momentum  $m$ . The label  $q$  runs over all such possible states. To extract a particular pseudopotential element  $V_{m,3}^{q,q'}$  of  $V(\vec{r}_i, \vec{r}_j, \vec{r}_k)$ , one simply needs to evaluate the matrix element

$$V_{m,3}^{q,q'} = \langle m, q; i, j, k | V(\vec{r}_i, \vec{r}_j, \vec{r}_k) | m, q'; i, j, k \rangle. \quad (2.40)$$

In Ref. [66] the wavefunctions of the states  $|m, q'; i, j, k\rangle$  have been explicitly calculated. For fermions, the lowest three particle relative angular momentum possible is  $m = 3$ . For all angular momenta up to  $m = 8$  there is only one state with that angular momentum, and  $V_{m \leq 8, 3}^{q,q'}$  is a single number  $V_{m,3}$ . The wavefunctions of these states are, in the lowest Landau level:

$$\begin{aligned} |m = 3; z_1, z_2, z_3\rangle &\propto (z_1 - z_2)(z_1 - z_3)(z_2 - z_3) \\ |m = 5; z_1, z_2, z_3\rangle &\propto (z_1 - z_2)(z_1 - z_3)(z_2 - z_3)(\tilde{z}_1\tilde{z}_2 + \tilde{z}_1\tilde{z}_3 + \tilde{z}_2\tilde{z}_3) \\ |m = 6; z_1, z_2, z_3\rangle &\propto (z_1 - z_2)(z_1 - z_3)(z_2 - z_3)\tilde{z}_1\tilde{z}_2\tilde{z}_3 \\ |m = 7; z_1, z_2, z_3\rangle &\propto (z_1 - z_2)(z_1 - z_3)(z_2 - z_3)(\tilde{z}_1\tilde{z}_2 + \tilde{z}_1\tilde{z}_3 + \tilde{z}_2\tilde{z}_3)^2 \\ |m = 8; z_1, z_2, z_3\rangle &\propto (z_1 - z_2)(z_1 - z_3)(z_2 - z_3)\tilde{z}_1\tilde{z}_2\tilde{z}_3(\tilde{z}_1\tilde{z}_2 + \tilde{z}_1\tilde{z}_3 + \tilde{z}_2\tilde{z}_3), \end{aligned} \quad (2.41)$$

where  $\tilde{z}_i = z_i - \frac{z_1+z_2+z_3}{3}$ . There is no translationally invariant and completely

antisymmetric wavefunction of 3 particles with  $m = 4$ . The exponentially decaying factors are always implicitly assumed, since they are the same for all wavefunctions.

We have calculated the lowest order 3-particle interaction in second quantization language, Equation 2.37. To calculate the matrix elements of Equation 2.40 we must also represent the relative angular momentum states of Equation 2.41 in term of creation and annihilation operators. The normalized occupation number basis for three particles is:

$$\begin{aligned} |m_1, m_2, m_3 \rangle &= c_{m_3}^\dagger c_{m_2}^\dagger c_{m_1}^\dagger |0\rangle \\ &= N_{m_1 m_2 m_3} \text{AS} \{z_1^{m_1} z_2^{m_2} z_3^{m_3}\} e^{-\sum |z_i|^2 / 4l_B^2}, \end{aligned} \quad (2.42)$$

where the state  $|0\rangle$  is the empty Landau level, AS stands for antisymmetrization, and the normalization constant  $N_{m_1 m_2 m_3}$  is

$$N_{m_1 m_2 m_3} = \sqrt{\frac{1}{6(2\pi)^3 2^{m_1+m_2+m_3} m_1! m_2! m_3!}}. \quad (2.43)$$

For example, the lowest relative angular momentum state  $|m = 3; z_1, z_2, z_3\rangle$  is simply the state  $|0, 1, 2\rangle = c_2^\dagger c_1^\dagger c_0^\dagger |0\rangle$ , since the antisymmetrization yields:

$$\text{AS} \{z_1^0 z_2^1 z_3^2\} = (z_1 - z_2)(z_1 - z_3)(z_2 - z_3) \propto |m = 3; z_1, z_2, z_3\rangle. \quad (2.44)$$

The relative angular momentum states up to  $m = 8$  are written using occupation number states, Equation 2.42, as follows:

$$\begin{aligned} |m = 3; z_1, z_2, z_3\rangle &\propto \frac{|0,1,2\rangle}{N_{012}} \\ |m = 5; z_1, z_2, z_3\rangle &\propto 2 \frac{|0,1,4\rangle}{N_{014}} - 4 \frac{|0,2,3\rangle}{N_{023}} \\ |m = 6; z_1, z_2, z_3\rangle &\propto -2 \frac{|0,1,5\rangle}{N_{015}} + 5 \frac{|0,2,4\rangle}{N_{024}} - 20 \frac{|1,2,3\rangle}{N_{123}} \\ |m = 7; z_1, z_2, z_3\rangle &\propto -1 \frac{|0,1,6\rangle}{N_{016}} + 3 \frac{|0,2,5\rangle}{N_{025}} - 5 \frac{|0,3,4\rangle}{N_{034}} \\ |m = 8; z_1, z_2, z_3\rangle &\propto 2 \frac{|0,1,7\rangle}{N_{017}} - 7 \frac{|0,2,6\rangle}{N_{026}} + 7 \frac{|0,3,5\rangle}{N_{035}} + 21 \frac{|1,2,5\rangle}{N_{125}} - 35 \frac{|1,3,4\rangle}{N_{134}}. \end{aligned} \quad (2.45)$$

It is simple to normalize these states since  $\{|m_1, m_2, m_3\rangle\}$  are normalized and orthogonal.

## 2.7 Results in Lowest and Second Landau Levels

Using the second quantization representation of Equation 2.45, we can calculate the matrix elements corresponding to the pseudopotentials  $V_{m,3}$  as in Equation 2.40, for the lowest order 3-particles interactions we calculated, Equation 2.37. The results are summarized in Table 2.7 and Figure 2.3, where we have calculated the effective interaction in both the lowest Landau level and the second Landau level.

$m$	$V_{m,3}$ (LLL)	$V_{m,3}$ (SLL)
3	-0.0181	-0.0147
5	0.0033	-0.0054
6	-0.0107	-0.0099
7	0.0059	0.0005
8	-0.0048	-0.0009

Table 2.1: Lowest order 3-particle pseudopotentials. The pseudopotentials are in units of  $\left(\frac{e^2/4\pi\epsilon l_B}{\hbar\omega_c}\right) \frac{e^2}{4\pi\epsilon l_B}$ , and therefore are of order  $\kappa$ . The first column are the 3-particles pseudopotentials in the lowest Landau level, i.e., with  $n_{par} = 0$ , while the second column is the effective pseudopotentials in the second Landau level,  $n_{par} = 1$ .

The lowest order diagram we have evaluated, shown in Figure 2.2a, is first order in the ratio of Coulomb energy to cyclotron energy,  $\kappa$ . As expected, the lowest angular momentum pseudopotential is the largest in magnitude. If that was the only non-zero pseudopotential, then the ground state of the quantum Hall state at filling  $\nu = 5/2$  is exactly the anti-Pfaffian state [60, 64], since the first pseudopotential in the second Landau level is negative. If it were positive, the ground state would be the Moore-Read Pfaffian state [68, 41], but our explicit calculation finds it is negative to lowest order in  $\kappa$ .

It is clear from Table 2.7 and Figure 2.3 that even to lowest order in  $\kappa$ , higher angular momentum pseudopotentials cannot be ignored compared to the lowest angular momentum one. Higher angular momentum pseudopotentials are comparable to the

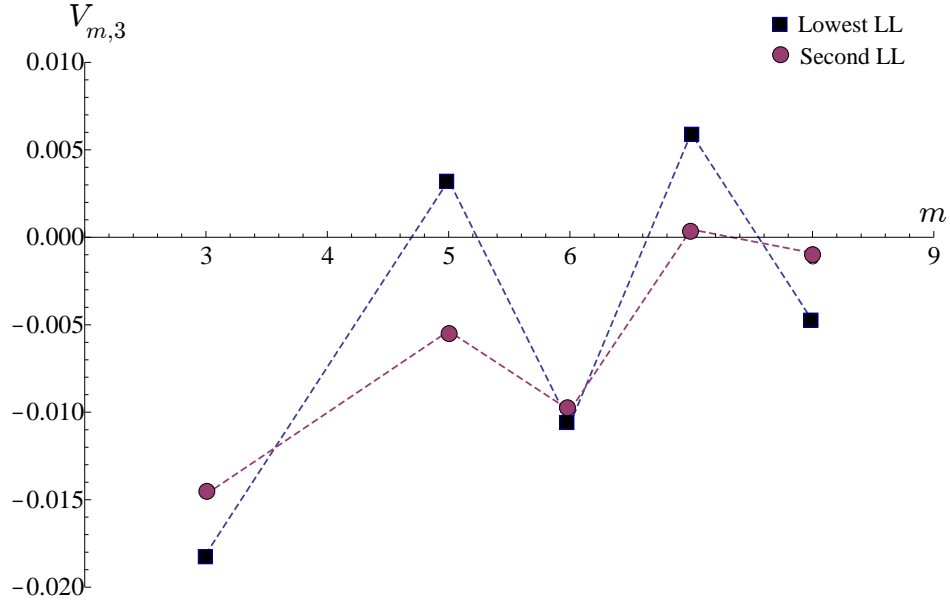


Figure 2.3: 3-particle pseudopotentials of the lowest order interactions generated by LLM, for both the lowest Landau level and the second Landau level. The lowest order interaction are generated by the diagram shown in Figure 2.2a.

lowest angular momentum one, and can even flip signs. When keeping these higher angular momentum pseudopotentials, it is no longer clear what the ground state of electrons at filling  $\nu = 5/2$  is, and whether it is close to the Pfaffian or anti-Pfaffian states.

The pseudopotentials calculated in this chapter should provide a better starting point for numerical calculations of ground states of quantum Hall systems, especially in the second Landau level. We find that the electron interactions, even to lowest order in the ratio of Coulomb energy to cyclotron energy, do not seem to be well approximated by projection to a given Landau level, or by keeping only the lowest angular momentum pseudopotential, as is often done. Numerical calculations using the interaction calculated here, and higher order interactions in  $\kappa$  generated in the same fashion, will give more accurate answers regarding the nature of quantum Hall states in the second Landau level, and whether they are indeed non-Abelian.

## Chapter 3

# Interferometry and Non-Abelian Statistics at $5/2$ Filling Fraction

Utilizing quantum Hall edges in interference experiments may provide a path for the direct observation of fractional statistics. It is not yet possible to braid quantum Hall quasiparticles by manipulating their positions in the bulk of a sample. Using the edges of a quantum Hall sample, it is possible to design quasiparticle trajectories along the edges which enclose trapped quasiparticles in the bulk. In such a scenario, the effect of fractional statistics should be discernable by comparison with a topologically inequivalent quasiparticle trajectory, i.e., a trajectory which encloses a different set of bulk quasiparticles. Interference between two such trajectories would provide information about the braiding of quasiparticles.

For Abelian fractional statistics, the effect of braiding one quasiparticle around another is a multiplicative phase factor. A simple phase factor might be hard to disentangle from other sources of phase factors in an experiment, such as the Aharonov-Bohm effect or dynamical phases arising from the propagation of quasiparticles.

Non-Abelian statistics, on the other hand, could provide more direct clear-cut evidence of fractional statistics. When quasiparticles are braided, the wavefunction is rotated in the degenerate subspace of the system. The difference between the states of the system before and after quasiparticle braiding is more than a mere phase factor, and it should be possible to observe this difference even without complete control of the Abelian phase factors described above.

In this chapter, we discuss the two-quantum point contact (QPC) interferometer, which is equivalent to a Fabry-Perot interferometer of quantum Hall edge quasiparticles. We analyze this experiment in the  $\nu = 5/2$  quantum Hall state, where it is hoped to have a striking, measurable signature. In particular, we calculate  $I - V$  curves and their temperature dependence assuming the  $\nu = 5/2$  state is described by the Moore-Read Pfaffian state, or its particle-hole conjugate. We address the ambiguities in the calculation arising from the non-Abelian statistics, and verify that non-Abelian statistics have a clear, distinct experimental signature. We determine the temperature and length scales for which this signature should be observable. Finally, we discuss recent experimental results, compare with our predictions, and critically examine the applicability of our analysis to those experiments.

This chapter has been adapted from our published article [69].

### 3.1 Quantum Hall State at Filling 5/2

Quantum Hall (QH) devices are the only systems known to be in topological phases. The  $\nu = 1/3$  Laughlin state is in an Abelian topological phase. The excitations of such a phase carry a fraction of an electron charge and have fractional statistics which are intermediate between bosonic and fermionic statistics. The fractional charge has been confirmed experimentally [30, 70, 71] and experiments showing indications of fractional statistics have been carried out [72].

The observed [33, 73, 38] Quantum Hall state at filling fraction  $\nu = 5/2$  is the primary candidate for a system in a non-Abelian topological phase, and is believed to be described by the Moore-Read Pfaffian state [34, 68] as a result of numerical evidence [39, 40]. The excitations of the Pfaffian carry fractional charge  $e/4$  and have non-Abelian braiding statistics: for given quasiparticle positions, there are several linearly-independent quantum states of the system, and braiding the quasiparticles causes a rotation in this space [35, 74, 75, 76, 77]. In addition to their novelty, these properties could be useful for topological quantum computation [56]. The non-Abelian statistics of the Moore-Read Pfaffian state are explained in more detail in

section 3.3.

In the absence of Landau Level mixing, the Hamiltonian of a half-filled Landau level is particle-hole symmetric. The Pfaffian state, if it is the ground state of such a Hamiltonian, spontaneously breaks particles-hole symmetry. The particle-hole conjugate of the Pfaffian, dubbed the anti-Pfaffian [60, 64], has exactly the same energy as the Pfaffian in the absence of Landau level mixing. Hence, it is a serious candidate for the  $\nu = 5/2$  state observed in experiments, where Landau level mixing, which is not small, will favor one of the two states. Therefore, it is important to find experimental probes which can distinguish between these two states. Although the two states are related by a particle-hole transformation and are both non-Abelian, they differ in important ways: their quasiparticle statistics differ by Abelian phases, and the anti-Pfaffian has three counter-propagating neutral edge modes while the Pfaffian edge is completely chiral. In this chapter we consider edge tunneling experiments for both the Pfaffian and the anti-Pfaffian states, and we find quantitative differences between the two resulting from these distinctions.

## 3.2 Fabry-Perot Interferometer

The double point contact geometry has been proposed as a probe for non-Abelian statistics [75, 57, 58, 78, 79, 80, 81]. In this setup, a QH bar is gated so that two constrictions are created, as shown in Figure 3.1, and quasiparticles can tunnel from one edge to the other at either constriction. The dashed line in Figure 3.1 serves as a reminder that the two edges are actually different sections of a single edge which is the boundary of the system; consequently, inter-edge tunneling satisfies topological conservation laws which are important in the non-Abelian case. An edge quasiparticle entering the sample from the left can tunnel to the lower edge through either point contact, and the measured tunneling current is sensitive to the interference between these two possible trajectories. The phase difference between the quantum amplitudes of these two trajectories depends on the applied voltage between the top and bottom edges, the magnetic flux enclosed between the two trajectories, and the number of

quasiparticles localized in the bulk between the two trajectories. If the quasiparticles have non-Abelian statistics, the quantum state of the system can change when the edge quasiparticle encircles the localized bulk ones, and the effect on the interference term is more than merely a phase shift. The Pfaffian and anti-Pfaffian states exemplify the most extreme case: if there is an even number of localized quasiparticles enclosed between the tunneling trajectories, there will be interference that depends on the magnetic flux and applied voltage, while in the presence of an odd number of bulk quasiparticles in the bulk, the interference pattern will be completely lost. We will recover these striking results using an explicit edge theory calculation.

The visibility of the interference pattern in the even quasiparticle case will be obscured by thermal smearing as well as the difference between the charged and neutral mode velocities. Naively, the latter is particularly acute in the anti-Pfaffian case, where the velocities have opposite sign. However, as we will see quantitatively from the edge state calculation below, the difference between the even and odd quasiparticle cases will be visible for sufficiently low temperature in both the Pfaffian and anti-Pfaffian states. The required temperature vanishes as the distance between the contacts or the difference in velocities is increased.

The principle conceptual difficulty in analyzing inter-edge tunneling stems from the non-Abelian nature of the bulk state, which causes ambiguities in edge correlation functions (or, more properly, *conformal blocks*). We show how these are resolved, following Refs. [82, 83] and further refinements introduced in Refs. [79, 78].

In section 3.3 we set up the perturbative calculation to lowest order, explain the ambiguity that arises in evaluating correlation functions due to the non-Abelian nature of the edge, and show how to resolve this ambiguity, following Refs. [82, 83]. We proceed in section 3.4 to find the expected tunneling current behavior as a function of bias voltage and temperature in the Pfaffian state, taking into consideration the different velocities of charged and neutral modes on the edge. We show that for sufficiently low temperature, interference will be visible in the even quasiparticle case. In section 3.5, we repeat the calculation for the anti-Pfaffian state and show the quantitative differences with the Pfaffian case.

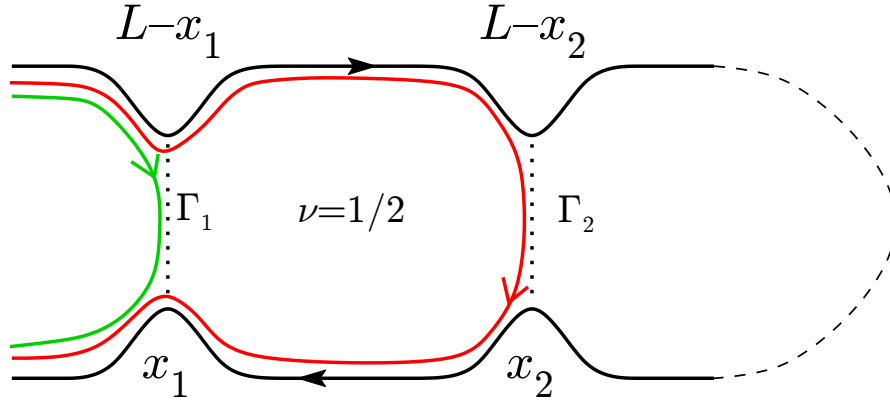


Figure 3.1: The double point contact geometry. Edge quasiparticles can tunnel between the top and bottom edges at the point contacts  $j = 1, 2$ , with tunneling amplitude  $\Gamma_j$ . The dashed line serves as a reminder that both top and bottom edges are two sections of the same edge. The two ends of point contact  $j$  are two points on the same edge separated by a distance  $L - 2x_j$ , where  $L$  is the length of the edge.

### 3.3 Tunneling Operators and Conformal Blocks

We now set up the calculation of the tunneling current to lowest order and discuss the basic issues which arise. The Pfaffian and anti-Pfaffian cases are conceptually similar, so we focus on the Pfaffian for the sake of concreteness. The edge theory of the Pfaffian state has a chiral bosonic charge mode and a chiral neutral Majorana mode [51, 59, 82, 83]

$$\mathcal{L}_{\text{Pf}}(\psi, \phi) = \frac{1}{4\pi} \partial_x \phi (\partial_t + v_c \partial_x) \phi + i\psi (\partial_t + v_n \partial_x) \psi \quad (3.1)$$

Both modes propagate in the same direction, but will have different velocities in general. One expects the charge velocity  $v_c$  to be larger than the neutral velocity  $v_n$ . The electron operator is a charge 1 fermionic operator:

$$\Phi_{el} = \psi e^{i\sqrt{2}\phi} \quad (3.2)$$

and the  $e/4$  quasiparticle operator is:

$$\Phi_{1/4} = \sigma e^{i\phi/2\sqrt{2}} \quad (3.3)$$

where  $\sigma$  is the Ising spin field of the Majorana fermion theory[83]. When inter-edge tunneling is weak, we expect the amplitude  $\Gamma$  for charge- $e/4$  to be transferred from one edge to the other to be larger than for higher charges  $ne/4$ , which should be  $\sim \Gamma^n$ . It is also the most relevant tunneling operator in the Renormalization Group sense [82, 83], so we will focus on it. Since it is relevant, its effective value grows as the temperature is decreased, eventually leaving the weak tunneling regime. We assume that the temperature is high enough that the system is still in the weak tunneling regime and a perturbative calculation will be valid, but still much lower than the bulk energy gap.

Following Ref. [53], we write the tunneling Hamiltonian in the form:

$$H_t(t) = \Gamma_1 e^{-i\omega_J t} V_1(t) + \Gamma_2 e^{i\Phi/4\Phi_0} e^{-i\omega_J t} V_2(t) + h.c. \quad (3.4)$$

The frequency  $\omega_J = \frac{eV}{4}$  is the Josephson frequency for a charge  $e/4$  quasiparticle with voltage  $V$  applied between the top and bottom edges. The difference in the magnetic fluxes enclosed by the two trajectories around the interferometer is  $\Phi$ . We have chosen a gauge in which the vector potential is concentrated at the second point contact so that  $\Phi$  enters only through the second term above. Both edges are part of the boundary of the same Hall droplet, so we can denote the point on the upper edge which is on the other side of point contact  $j$  from  $x_j$  by  $L - x_j$ , where  $j = 1, 2$  and  $L$  is large. The operator  $V_j(t)$  tunnels a quasiparticle between  $x_j$  and  $L - x_j$ :

$$V_j(t) = \sigma(x_j, t) \sigma(L - x_j, t) e^{\frac{i}{\sqrt{8}} \phi(x_j, t)} e^{-\frac{i}{\sqrt{8}} \phi(L - x_j, t)} \quad (3.5)$$

The current operator can be easily found from the commutator of the tunneling Hamiltonian and the charge operator on one edge, which involves only the bosonic

field:

$$I(t) = \frac{ie}{4} (\Gamma_1 e^{-i\omega_J t} V_1(t) - \text{h.c.}) + \frac{ie}{4} (\Gamma_2 e^{i\Phi/4\Phi_0} e^{-i\omega_J t} V_2(t) - \text{h.c.}) \quad (3.6)$$

To lowest order in perturbation theory, the tunneling current is found to be:

$$\langle I(t) \rangle = -i \int_{-\infty}^t dt' \langle 0 | [I(t), H_t(t')] | 0 \rangle \quad (3.7)$$

In order to compute the current, we substitute Equation 3.4 and Equation 3.6 into Equation 3.7. We obtain:

$$I(t) = \frac{e}{4} \sum_{j,k} \Gamma_j \Gamma_k^* e^{i(j-k)\Phi/4\Phi_0} \times \int_{-\infty}^t dt' e^{i\omega_J(t'-t)} \left( \langle V_j(t) V_k^\dagger(t') \rangle - \langle V_k^\dagger(t') V_j(t) \rangle \right) \quad (3.8)$$

Therefore, we must compute the correlation function

$$\langle V_j(t) V_k^\dagger(t') \rangle = \langle \sigma(x_j, t) \sigma(L - x_j, t) \sigma(L - x_k, t') \sigma(x_k, t') \rangle \times \langle e^{\frac{i}{\sqrt{8}}\phi(x_j, t)} e^{-\frac{i}{\sqrt{8}}\phi(L-x_j, t)} e^{\frac{i}{\sqrt{8}}\phi(L-x_k, t')} e^{-\frac{i}{\sqrt{8}}\phi(L-x_k, t')} \rangle \quad (3.9)$$

This correlation function is at the heart of our calculation. The correlations involving the bosonic fields are straightforward to calculate and, in the limit of a long sample,  $L \rightarrow \infty$ , the bosonic correlation function breaks into a product of two-point correlation functions of fields on the same edge:

$$\langle e^{\frac{i}{\sqrt{8}}\phi(x_j, t)} e^{-\frac{i}{\sqrt{8}}\phi(x_k, t')} \rangle \langle e^{-\frac{i}{\sqrt{8}}\phi(L-x_j, t)} e^{\frac{i}{\sqrt{8}}\phi(L-x_k, t')} \rangle = \prod_{r=\pm} [\delta + i(v_c(t-t') + r(x_j - x_k))]^{-1/8} \quad (3.10)$$

However, the four  $\sigma$  correlation function is actually ill-defined without further information, namely the fusion channels of the four  $\sigma$  operators. (Technically, the correlation function is what is called a *conformal block*.) These are determined by the

physical situation, as we elaborate below.

In the Ising Conformal Field Theory, the  $\sigma$  operators have non-trivial fusion rules:

$$\sigma \times \sigma = I + \psi \quad (3.11)$$

These two fusion possibilities,  $I$  and  $\psi$ , correspond directly to the two degenerate ground states of a system with two  $\sigma$  particles in the bulk. A correlation function of  $2n$   $\sigma$  particles is non-vanishing only if all of the operators fuse together to the identity, but there are a number of ways in which the fields can do that. In the four  $\sigma$  operators case, the correlation  $\langle \sigma(z_1)\sigma(z_2)\sigma(z_3)\sigma(z_4) \rangle$  has two different conformal blocks corresponding to the two possible fusions. In the standard notation explained, for instance, in this context in Ref. [83], these two conformal blocks/fusion channels are:

$$\mathcal{F}_c \equiv \frac{1 \quad 2 \quad 3 \quad 4}{I \quad | \quad | \quad c \quad | \quad | \quad I}$$

where  $c = 1$  or  $\psi$  is the fusion product of the fields at the space-time points  $z_1$  and  $z_2$ . Their explicit forms are:

$$\begin{aligned} \mathcal{F}_I &= \left( \frac{1}{z_{12}z_{34}(1-x)} \right)^{1/8} (1 + \sqrt{1-x})^{1/2}, \\ \mathcal{F}_\psi &= \left( \frac{1}{z_{12}z_{34}(1-x)} \right)^{1/8} (1 - \sqrt{1-x})^{1/2}, \end{aligned} \quad (3.12)$$

where  $z_{ij} = z_i - z_j$  and  $x = z_{12}z_{34}/z_{13}z_{24}$ .

Now for an obvious question: which conformal block enters the perturbative calculation? As explained in Ref. [83], when there are no quasiparticles in the bulk, the correct choice is the conformal block in which the  $\sigma$  operators in the tunneling operator  $V_j(t)$ , i.e.  $\sigma(x_j, t)$  and  $\sigma(L - x_j, t)$ , fuse to the identity. Since all this operator does is transfer a quasiparticle from one side of the Hall sample to the other, it should not change the topological charge on the edge, which would involve the creation of a fermion. In the bottom half of Figure 3.2a, we show two successive tunneling events. Each can be envisioned as the creation out of the vacuum of a quasiparticle-quasihole

pair in the bulk. Saying that they are created ‘out of the vacuum’ is equivalent to saying that they fuse to  $I$ . The quasiparticle then goes to one edge and the quasi-hole goes to the other. A second tunneling event (either at the same or a different point contact) occurs in the same way. Let us, for the sake of concreteness call the quasiparticle and quasihole which are created in the first tunneling process 1 and 2; in the second tunneling process, 3 and 4 are created. (For these purposes, there is no need to distinguish between quasiparticles and quasiholes.) Let us assume that quasiparticles 1 and 3 go to the top edge while 2 and 4 go to the bottom edge. If the two edges are independent (as occurs in the  $L \rightarrow \infty$  limit), this process has a non-zero amplitude only if 1, 3 fuse to  $I$  and 2, 4 fuse to  $I$ , as depicted in the top half of Figure 3.2a. ( $I$  is depicted by the absence of a line. If a fermion were the result of fusing the two quasiparticles, there would be a wavy line emanating upward from each of the two fusion points at the top of Figure 3.2a.) This picture can be interpreted as the matrix element between the state in which quasiparticle-quasihole pairs 1, 2 and 3, 4 are created in the bulk and go to the edges (bottom) and the state in which quasiparticles 1, 3 fuse to  $I$  and 2, 4 fuse to  $I$  (top).

Hence the correlation function in Equation 3.9 is actually the conformal block:

$$\mathcal{F}_I = \frac{(x_j, t)(L - x_j, t) (L - x_k, t')(x_k, t')}{I \quad | \quad | \quad I \quad | \quad | \quad I}$$

On the other hand, in the  $L \rightarrow \infty$  limit, we expect the  $\sigma$  correlation in Equation 3.9 to break into a product of correlators of fields on the same side of the sample:

$$\langle \sigma(x_j, t)\sigma(x_k, t') \rangle \langle \sigma(L - x_j, t)\sigma(L - x_k, t') \rangle \quad (3.13)$$

As noted above, this correlation function is non-vanishing only if the fields on the same side of the sample fuse to the identity. This conformal block is given pictorially by:

$$\mathcal{G}_I = \frac{(x_j, t)(x_k, t') \quad (L - x_j, t)(L - x_k, t')}{I \quad | \quad | \quad I \quad | \quad | \quad I}$$

In the  $\mathcal{G}_{cS}$ , we specify the fusions of fields on the same side of the edge rather than

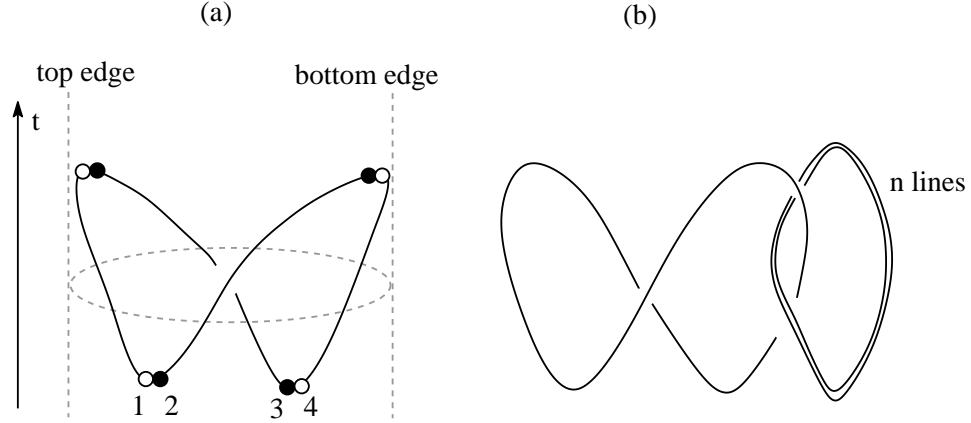


Figure 3.2: (a) The knot corresponding to the matrix element between the state in which two quasiparticle-quasihole pairs, 1, 2 and 3, 4 are created out of the vacuum (top half) and go to opposite edges and a state in which the two quasiparticles on each edge (e.g. 1, 3 on the top edge) fuse to  $I$ . Equivalently, it is one element of the  $F$ -matrix, which transforms between the basis of conformal blocks in which 1, 2 has a fixed fusion channel (and, therefore, 3, 4 does as well) and the basis in which 1, 3 has a fixed fusion channel. (b) The same matrix element with  $n$  quasiparticles in the bulk. The  $n$  quasiparticles are assumed to have been created in pairs in the distant past, with one member of each pair taken inside the interferometer and the other member left outside. The two tunneling events are assumed to occur at different point contacts. The figure then gives the matrix element between the states in which 1, 2 and 3, 4 are created out of the vacuum (top half), go to opposite edges, and encircle the bulk quasiparticles; and a state in which 1, 3 fuse to  $I$ .

opposite sides of a point contact. In the  $L \rightarrow \infty$  limit,  $\mathcal{G}_\psi$  vanishes. The conformal blocks  $\mathcal{G}_c$  are linear combinations of the  $\mathcal{F}_c$ s; both form bases for the two-dimensional vector space of conformal blocks. The basis change between the two is called the  $F$ -matrix, which is part of the basic data characterizing a topological phase. We can write:

$$\mathcal{F}_I = a_I \mathcal{G}_I + a_\psi \mathcal{G}_\psi \quad (3.14)$$

where the coefficients  $a_I$  and  $a_\psi$  are two of the entries in the  $F$ -matrix. They can be calculated by computing the Kauffman bracket for a braid that corresponds to this

change of basis, as was done in Ref. [82, 83]:

$$a_I = \frac{1}{\sqrt{2}} \quad (\text{no qps in bulk}) \quad (3.15)$$

For the purposes of our calculation, we only need the long sample limit of the correlation function  $\mathcal{F}_I$ . As explained above, we find that it is proportional to  $\mathcal{G}_I$ , which can be easily evaluated since it is simply the product of two two-point correlation functions (it can also be obtained by taking the large- $L$  limit of the expression for  $G_I$  as in Equation 3.12):

$$\begin{aligned} \mathcal{F}_I |_{L \rightarrow \infty} &= a_I \mathcal{G}_I |_{L \rightarrow \infty} \\ &= a_I \prod_{\epsilon=\pm} [\delta + i(v_n(t-t') + \epsilon(x_j - x_k))]^{-1/8} \end{aligned} \quad (3.16)$$

We now generalize this to the case in which there are  $n$  quasiparticles in the bulk between the two point contacts. Correlation functions in which all of the fields are at the same point contact are unchanged. However, as pointed out in Refs. [79, 78], when two tunneling processes occur at different point contacts, the two quasiparticle-quasihole pairs are created out of the vacuum as before, but quasiparticle 1 must encircle the bulk quasiparticles before it can be fused with quasiparticle 3. This difference modifies the matrix element with the state in which 1, 3 fuse to  $I$  and 2, 4 fuse to  $I$ , as depicted in Figure 3.2b. Let us consider the simplest case, in which there is a single quasiparticle in the bulk. We can imagine that a quasiparticle-quasihole pair was created in the distant past and one member of the pair was brought into the interferometer while the other member was left outside. Then we create the quasiparticle-quasihole pairs 1, 2 and 3, 4 and take 4 around the bulk quasiparticle. This process is depicted in the bottom half of Figure 3.2b. We can compute the resulting  $a_I$  by computing the matrix element between the resulting state and the state in which 1, 3 fuse to  $I$  (as do 2, 4). This matrix element can be computed from the Kauffman bracket of the link in Figure 3.2b or, equivalently, by using the  $F$  and  $R$  matrices of the theory. By either method, we find  $a_I = 0$ . The reason is that, after

4 is taken around the bulk quasiparticle, either 1, 3 or 2, 4 (but not both) must fuse to  $\psi$  rather than  $I$ . Therefore, there is no amplitude for 1, 3 and 2, 4 to fuse to  $I$ . For the same reason,  $a_\psi = 0$ , so even for  $L$  finite, there is no contribution from such a process. In fact, the same result is obtained for any odd  $n$  since an odd number of quasiparticles must fuse to  $\sigma$ . Therefore, their effect is the same as if there were a single quasiparticle in the bulk:

$$a_I = 0 \quad (\text{odd number } n \text{ of qps in bulk}) \quad (3.17)$$

For  $n$  even, the  $n$  bulk quasiparticles can fuse to either  $I$  or  $\psi$ . The former case is the same as in the absence of quasiparticles; in the latter case, there is an additional minus sign which is acquired when a  $\sigma$  goes around a  $\psi$ :

$$a_I = \pm \frac{1}{\sqrt{2}} \quad (\text{even number } n \text{ of qps in bulk}) \quad (3.18)$$

With the correct conformal block in hand, as specified by the corresponding value of  $a_I$ , we can now give a meaning to expressions such as Equation 3.9 and can use Equation 3.7 to compute the current through our interferometer.

In the preceding discussion, we have focussed on the neutral sector of the theory, where the interesting non-Abelian effects occur. However, there is also a charged sector of the theory. The full conformal theory describing the edge includes both parts. As a result, there are additional phases which result from the change of basis when there are quasiparticles in the bulk. Furthermore, we must exercise a little more care in distinguishing quasiparticles from quasiholes since they have different Abelian phases. By recalculating Figure 3.2b with the Abelian part of the theory included, we find that  $a_I$  acquires an additional phase  $n\pi/4$  when there are  $n$  quasiparticles in the bulk and 1 and 4 are quasiparticles while 2 and 3 are quasiholes. The opposite phase results when 2 and 3 are quasiparticles while 1 and 4 are quasiholes.

### 3.4 Temperature And Voltage Behavior

To lowest order in  $\Gamma_1, \Gamma_2$ , the current naturally breaks into the sum of three terms:

$$I = I_1 + I_2 + I_{12} \quad (3.19)$$

where

$$I_j = \frac{e}{4} |\Gamma_j|^2 \int_{-\infty}^0 dt e^{i\omega_j t} \left( \langle V_j(0) V_j^\dagger(t) \rangle - \langle V_j^\dagger(t) V_j(0) \rangle \right) \quad (3.20)$$

and

$$I_{12} = \frac{e}{4} \Gamma_1 \Gamma_2^* \int_{-\infty}^0 dt e^{i\omega_j t} \left( \langle V_1(0) V_2^\dagger(t) \rangle - \langle V_2^\dagger(t) V_1(0) \rangle \right) + \text{c. c.} \quad (3.21)$$

$I_j, j = 1, 2$  would be the backscattered current if only point contact  $j$  were present.  $I_{12}$  is due to interference between the process in which a quasiparticle tunnels between the two edges at  $x_1$  and the process in which it continues to  $x_2$  and tunnels there. As a result,  $I_{12}$  depends on the magnetic flux and the number of bulk quasiparticles between the two point contacts; it reflects the non-Abelian statistics of quasiparticles, namely the difference between even and odd numbers of bulk quasiparticles. Meanwhile,  $I_1, I_2$ , and  $I_{12}$  all depend on the bias voltage and temperature. In this section we quantitatively analyze the dependence of  $I$  on all of these parameters.

We first consider the zero-temperature case. The single point contact current term,  $I_1 + I_2$ , is identical to the backscattering current due a single impurity in a Luttinger Liquid. The current is a power law in voltage:

$$I_1 + I_2 = \frac{1}{\sqrt{2}} \frac{e}{4} \frac{\pi}{\Gamma(\frac{1}{2})} (|\Gamma_1|^2 + |\Gamma_2|^2) v_n^{-1/4} v_c^{-2/8} \times \text{sgn}(V) \left( \frac{e|V|}{4} \right)^{-1/2} \quad (3.22)$$

The factor of  $\frac{1}{\sqrt{2}}$  is  $a_I$  discussed in the previous section. We now consider  $I_{12}$ . For an odd number of quasiparticles in the bulk,

$$I_{12} = 0 \quad (\text{odd number } n \text{ of qps in bulk}) \quad (3.23)$$

For an even number  $n$  of quasiparticles in the bulk,  $I_{12}$  can be evaluated analytically in the special case in which the two velocities are equal:

$$I_{12} = \pm \frac{1}{\sqrt{2}} \frac{e}{4} \frac{\pi^{3/2} 2^{9/4}}{\Gamma(\frac{1}{4})} |\Gamma_1| |\Gamma_2| \cos\left(\frac{\Phi}{4\Phi_0} + n\frac{\pi}{4} + \alpha\right) \times \text{sgn}(V) |V|^{-1/2} \times \left(\frac{e|x_1 - x_2|}{4v} |V|\right)^{1/4} J_{-1/4}\left(\frac{e|x_1 - x_2|}{4v} |V|\right) \quad (3.24)$$

In this expression, the  $\pm$  sign is obtained if the quasiparticles in the bulk fuse to total non-Abelian charge 1 or  $\psi$ , respectively;  $J_{-1/4}$  is the Bessel function;  $\Phi$  is the flux enclosed in the interference loop; and  $n$  is the (even) number of bulk quasiparticles inside the loop. The phase  $n\pi/4$  is statistical phase due to the Abelian part of the theory. The phase  $\alpha$  is  $\arg(\Gamma_1 \Gamma_2^*)$ . When the charge and neutral velocities are not equal, the current and differential conductance will oscillate at two different frequencies as seen in Figure 3.3, and both charge and neutral velocities can be extracted from the two different periods. The smaller period corresponding to the fast oscillations is roughly  $\frac{16\pi}{e|x_1 - x_2|} (1/v_n + 1/v_c)^{-1}$ , and the larger period corresponding to the oscillations of the envelope is roughly  $\frac{16\pi}{e|x_1 - x_2|} (1/v_n - 1/v_c)^{-1}$ .

Finite-temperature correlation functions can be obtained from the zero temperature correlation functions by a conformal transformation from the plane to the cylinder, which amounts to the following substitution:

$$\frac{1}{(\delta + i(t \pm x/v))^{1/8}} \rightarrow \left( \frac{\pi T}{\sin(\pi T(\delta + i(t \pm x/v)))} \right)^{1/8} \quad (3.25)$$

We find that the general form of the current is:

$$I_1 + I_2 = (|\Gamma_1|^2 + |\Gamma_2|^2) |V|^{-1/2} A \left( \frac{eV/4}{k_B T} \right) \quad (3.26)$$

$$I_{12} = |\Gamma_1||\Gamma_2| \cos\left(\frac{\Phi}{4\Phi_0} + n\frac{\pi}{4} + \alpha\right) \text{sgn}(V)|V|^{-1/2} \times B_n\left(\frac{e|x_1 - x_2|}{4v_c}|V|, \frac{e|x_1 - x_2|}{4v_n}|V|, \frac{eV/4}{k_B T}\right) \quad (3.27)$$

where  $B_{2n+1}(x, y, z) = 0$ , and  $A(x)$  and  $B_{2n}(x, y, z)$  are scaling functions which reduce to Equation 3.22 and Equation 3.24 in the  $T = 0$  limit:  $A(\infty) = \text{const.}$ ,  $B_{2n}(x, x, 0) \propto x^{1/4} J_{-1/4}(x)$ . In the opposite limit,  $k_B T > eV$ ,  $A(x) \sim x^{3/2}$  as  $x \rightarrow 0$ , so that the conductance due to a single point contact is  $\sim T^{-3/2}$ . The explicit form of  $A(x)$  is

$$A(x) = \frac{1}{\sqrt{2}} \frac{e}{4} \frac{\pi \sqrt{x}}{\Gamma(\frac{1}{2})} \left| \Gamma\left(\frac{1}{4} + i\frac{x}{2\pi}\right) \right|^2 \sinh(x/2)$$

$B_{2n}(x, y, z)$  is more complicated, but it simplifies in the limit that  $(x + y)/z$  is large, where  $B_{2n}(x, y, z) \sim e^{-(x+y)/z}$ . Consequently, there is an effective dephasing length [84, 85, 86]

$$L_\phi = \frac{\beta}{2\pi} \left( \frac{1/8}{v_c} + \frac{1/8}{v_n} \right)^{-1} \quad (3.28)$$

such that

$$I_{12} \propto e^{-|x_1 - x_2|/L_\phi} \cos\left(\frac{\Phi}{4\Phi_0} + n\frac{\pi}{4} + \alpha\right) \quad (3.29)$$

Interference is only visible if the interferometer is smaller than  $L_\phi$ . Equivalently, there is a characteristic temperature scale [79]  $T^*$ :

$$k_B T^* = \frac{1}{2\pi|x_1 - x_2|} \left( \frac{1/8}{v_c} + \frac{1/8}{v_n} \right)^{-1} \quad (3.30)$$

Interference is only visible for  $T < T^*$  since Equation 3.29 can be rewritten as:

$$I_{12} \propto e^{-T/T^*} \cos\left(\frac{\Phi}{4\Phi_0} + n\frac{\pi}{4} + \alpha\right) \quad (3.31)$$

For fixed  $v_c$ , decreasing  $v_n$  causes  $T^*$  and  $L_\phi$  to decrease. If  $v_n$  becomes very small, interference will only be visible at extremely low temperatures or for extremely small interferometers (which, of course, suffer from other problems). In the extreme limit,  $v_n = 0$ , interference will not be visible at all. Numerical studies [87] indicate that

the two velocities might be quite different, in which case, it will be important that interferometry experiments be done at sufficiently low temperatures. Using commonly accepted values of edge velocities (see, for instance, Ref. [41]) of  $v_c \approx 5 \cdot 10^4 m/s$  and  $v_n = 0.1 v_c$ , we estimate the dephasing length  $L_\Phi$  to be about  $4\mu m$  at a temperature of  $10mK$ . We will see below that the direction of the propagation of the neutral mode is irrelevant for these DC interference measurements. Even when the neutral modes propagate in opposition to the charge modes, as in the anti-Pfaffian state, interference can be observable, and the dephasing length is only a function of the magnitude of the velocities of the edge modes.

Figure 3.3 shows the differential conductance  $\partial I/\partial V$  at a temperature much lower than  $T^*$  for both even and odd numbers of bulk quasiparticles. As may be seen from this figure, the difference between even and odd numbers of quasiparticles is still very dramatic, even for finite temperature and different charge and neutral velocities. The even quasiparticle differential conductance passes through zero twice at voltages which are small enough that the odd quasiparticle differential conductance is still appreciable (and, of course, due entirely to  $I_1 + I_2$ ).

### 3.5 Anti-Pfaffian Edge

If one ignores Landau level mixing, then the Hamiltonian for the  $\nu = 5/2$  FQH system is particle-hole symmetric when there is exactly half an electron per flux quantum (ignoring the filled Landau Levels). The Pfaffian state, on the other hand, does not possess this symmetry. The particle-hole conjugate of the Pfaffian state, the anti-Pfaffian ( $\overline{\text{Pf}}$ ) [60, 64], has the same energy in the absence of Landau level mixing as the Pfaffian, and should be considered a candidate for the observed  $\nu = 5/2$  state, even with finite Landau Level mixing.

The edge theory of the anti-Pfaffian can be considered by considering a Pfaffian state of holes in a filled  $\nu = 1$  Landau level (this procedure is covered at length in

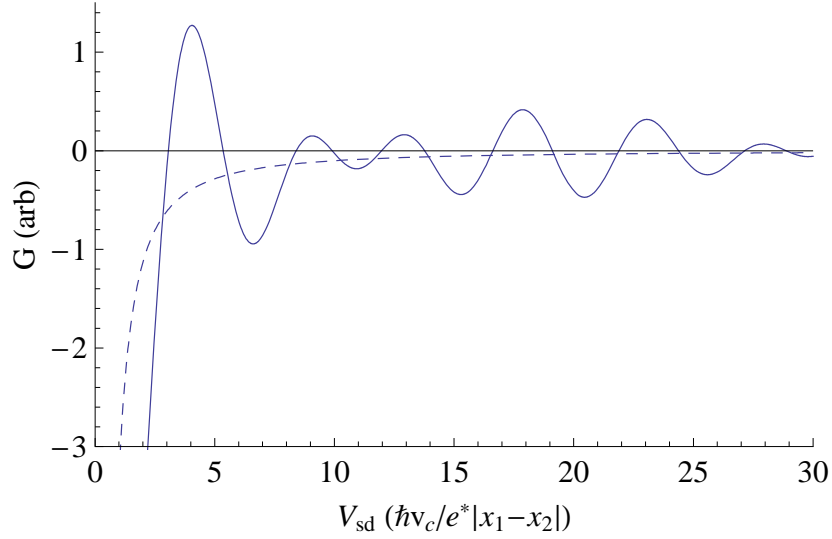


Figure 3.3: The differential conductance as a function of applied voltage at low temperature, for  $v_n = 0.75v_c$ . The dashed line is the conductance with an odd number of quasiparticles in the interference loop, and the solid line is for an even number. The charge and neutral velocities can be extracted from the two oscillation periods.

chapter 4):

$$\begin{aligned} \mathcal{L} = & \frac{1}{4\pi} \partial_x \phi_1 (-i\partial_t + v_1 \partial_x) \phi_1 + \mathcal{L}_{\text{Pf}}(\psi_1, \phi_2) \\ & + \frac{1}{4\pi} 2v_{12} \partial_x \phi_1 \partial_x \phi_2 + \xi(x) \psi_1 e^{i(\phi_1 - 2\phi_2)} + \text{h.c.} \end{aligned} \quad (3.32)$$

Here,  $\mathcal{L}_{\text{Pf}}(\psi_1, \phi_2)$  is the Pfaffian edge action, Equation 3.1, but for counter-propagating edge modes. The coupling  $v_{12}$  is short-ranged Coulomb repulsion between the edge mode of the filled Landau level and the charged edge mode of the Pfaffian state of holes while  $\xi(x)$  is random tunneling of electrons between the  $\nu = 1$  edge and the edge of the Pfaffian of holes. For large  $v_{12}$  and arbitrarily weak  $\xi$  or for small  $v_{12}$  and sufficiently large  $\xi$ , the theory flows in the infrared to a theory of a forward propagating bosonic charge mode and three *backward propagating* neutral Majorana modes [60, 64]:

$$\mathcal{L}_{\bar{P}f} = \frac{2}{4\pi} \partial_x \phi_\rho (\partial_t + v_c \partial_x) \phi_\rho + \sum_{a=1,2,3} i\psi_a (-\partial_t + v_n \partial_x) \psi_a \quad (3.33)$$

We will discuss quasiparticle tunneling in this phase of the anti-Pfaffian edge. The three Majorana fermions form an  $SU(2)_2$  triplet, which means that the non-Abelian statistics due to this part of the theory are associated with  $SU(2)_2$  Chern-Simons theory [75]. The electron operator in this theory is  $(\psi_2 - i\psi_3)e^{i2\phi_\rho}$ . The charge  $e/4$  quasiparticles are the primary fields  $\phi_{1/2}^\pm e^{i\phi_\rho/2}$ , where  $\phi_{1/2}^\pm$  are the spin-1/2 fields of  $SU(2)_2$ , and can be written in terms of the Ising order and disorder fields  $\sigma_a$  and  $\mu_a$ . The  $\phi_{1/2}^\pm$  fields consist of linear combinations of products of 3  $\sigma_a$  or  $\mu_a$  operators, and therefore has dimension 3/16. Consequently, the  $e/4$  quasiparticle operator in the anti-Pfaffian state has dimension 1/4, as opposed to dimension 1/8 in the Pfaffian case. This difference in the scaling dimension causes the Pfaffian and anti-Pfaffian to have different temperature and voltage dependence for transport through point contacts which, in principle, allows one to experimentally distinguish between the two states. Another important difference is that in the anti-Pfaffian case, the charge  $e/2$  quasiparticle operator has the same scaling dimension as the  $e/4$  quasiparticle and its tunneling is just as relevant, but one expects the bare tunneling element for the  $e/2$  quasiparticle to be smaller than the  $e/4$  one ( $|\Gamma_{e/2}| \sim |\Gamma_{e/4}|^2$ ).

The above discussion implies that  $e/4$  quasiparticle tunneling is the dominant one also in the anti-Pfaffian case. The tunneling current calculation in the double quantum point setup proceeds in a very similar fashion to the Pfaffian case. To lowest-order, we must compute four-quasiparticle correlation functions, and the relevant conformal block is the one in which quasiparticle fields on both ends of a point contact should fuse the identity. In the long sample limit, we seek the projection of these correlation function on the conformal block in which quasiparticles on the same edge fuse to the identity.

$SU(2)_2$  non-Abelian statistics are similar to the Ising statistics that appear in the Pfaffian. In the  $SU(2)_2$  theory there are only 3 particle types, 0, 1/2, and 1, with the fusion rule:

$$\frac{1}{2} \times \frac{1}{2} = 0 + 1 \quad (3.34)$$

which is analogous to the the fusion rule in Equation 3.11. Hence, the enumeration

of conformal blocks in  $SU(2)_2$  theory is the same as in the Ising theory if we identify the operators  $I, \sigma$  and  $\psi$  with 0, 1/2, and 1 operators respectively. Also, the matrix elements of the F-matrix which describes the change of basis between different fusion channels turn out to be the same in both theories, up to a phase[50]. An equation analogous to Equation 3.16 holds for the anti-Pfaffian case also, but with different power laws since the spin 1/2 operator has a different scaling dimension than the  $\sigma$  operator:

$$\begin{aligned} \mathcal{F}_I |_{L \rightarrow \infty} &= \tilde{a}_I \mathcal{G}_I |_{L \rightarrow \infty} \\ &= \tilde{a}_I \prod_{\epsilon=\pm} [\delta + i(v_n(t-t') - \epsilon(x_j - x_k))]^{-3/8} \end{aligned} \quad (3.35)$$

The tunneling current behavior in the anti-Pfaffian case is qualitatively the same as but quantitatively different from the Pfaffian case. One might worry that no interference should take place at all since the  $e/4$  quasiparticle operator is made up of a bosonic part moving in one direction and a fermionic part moving in the opposite direction, and in a semiclassical picture these two parts are moving away from each other. In fact, the sign of the neutral mode velocity makes no difference, as may be seen by comparing Equation 3.16 and Equation 3.35. As a result of the product over  $\epsilon = \pm$ , the sign of the neutral mode velocity drops out of the problem. The point is that the quantum mechanical tunneling process involves creating a quasiparticle and a quasihole, and regardless of the chirality of the mode, one excitation will move to the left and one to the right. We note that this breakdown of semiclassical intuition represented by the insensitivity to the neutral mode direction is a feature of a DC measurement. A finite frequency measurement might be more sensitive to the difference between the charge and neutral velocities.

At zero temperature in the anti-Pfaffian state,

$$I_1 + I_2 = \frac{1}{\sqrt{2}} \frac{e}{4} \pi (|\Gamma_1^2| + |\Gamma_2|^2) v_n^{-6/8} v_c^{-2/8} \text{sgn}(V) \quad (3.36)$$

The conductance will behave as  $V^{-1}$ ; the differential conductance will be sharply

peaked at  $V = 0$  (with a peak width of order  $k_B T$ ) and vanishing elsewhere. For  $k_B T > eV$ , the conductance varies as  $T^{-1}$ . In both cases, there are quantitative differences from the Pfaffian.

Again, for an odd number of quasiparticles in the interference loop,

$$I_{12} = 0 \quad (3.37)$$

For an even number of bulk quasiparticles, the tunneling current will oscillate with magnetic field and voltage, similar to the Pfaffian case. Again, for charge and neutral velocities which are equal in absolute value (although opposite in sign),  $I_{12}$  can be found analytically:

$$I_{12} = \pm \frac{1}{\sqrt{2}} \frac{e}{4} \frac{2\pi^{3/2}}{\Gamma(\frac{1}{2})} |\Gamma_1| |\Gamma_2| \cos\left(\frac{\Phi}{4\Phi_0} + n\frac{\pi}{4} + \alpha\right) \times \text{sgn}(V) J_0\left(\frac{e|x_1 - x_2|}{4v_c} |V|\right) \quad (3.38)$$

Although the phase acquired in the anti-Pfaffian state by an  $e/4$  quasiparticle going around another  $e/4$  quasiparticle is different (in either fusion channel) from in the Pfaffian state, the phase acquired by an  $e/4$  quasiparticle going around a charge  $e/2$  is  $\pm i$  in either state, with the minus sign corresponding to the presence of a neutral fermion.

A difference between the absolute values of the neutral and charge velocities will again be evident through a beating pattern in the differential conductance.  $I_{12}$  is exponentially decaying with temperature with characteristic scale:

$$k_B T^* = \frac{1}{2\pi|x_1 - x_2|} \left(\frac{1/8}{v_c} + \frac{3/8}{v_n}\right)^{-1} \quad (3.39)$$

and the corresponding dephasing length is:

$$L_\phi = \frac{\beta}{2\pi} \left(\frac{1/8}{v_c} + \frac{3/8}{v_n}\right)^{-1}. \quad (3.40)$$

## 3.6 Discussion and Interpretation of Experimental Results

As we have seen from the preceding formulas, the Pfaffian and anti-Pfaffian state have qualitatively similar behavior in a two point-contact interferometer. In particular, the reversal of the neutral modes in the latter state makes little difference. However, the temperature and voltage dependences of the backscattered current are quantitatively different. The difference is clear in the behavior of a single-point contact, where the associated power laws are different,  $I \sim V^{-1/2}$  in the case of the Pfaffian and  $I \sim V^0$  in the case of the anti-Pfaffian. However, there are also differences in the detailed temperature and voltage dependence of the interference contribution to the current, as may be seen from Equation 3.24 and Equation 3.38.

The relative insensitivity of quantum interference effects to the difference between the charge and neutral mode velocities runs counter to semi-classical thinking (and shows its limitations): naively, one might think that when a quasiparticle decays into its charged and neutral parts, interferometry would be hopeless. Fortunately, this picture is inadequate for the DC measurement discussed in this chapter, as explicit calculation shows. This also augurs well for the suitability of either one for quantum computation along the lines of Refs. [56, 88]. The downside is that the experimental difference between the Pfaffian and anti-Pfaffian states is muted. It can be extracted from the behavior in an interferometer, but it would still be useful to have a probe which is more sensitive to the direction of the neutral modes.

Both the Pfaffian and anti-Pfaffian states show the effect of non-Abelian statistics on the interference experiment in its strongest manifestation. The interference oscillations corresponding to charge  $e/4$  quasiparticles disappear when the number of trapped quasiparticles in the interference loop is odd. In the case of Abelian states, the interference pattern would simply shift as a function of trapped quasiparticles, while in the case of other non-Abelian states, the interference oscillations can be suppressed by changing the number of quasiparticles in the bulk, but it might not be possible to make them vanish [79].

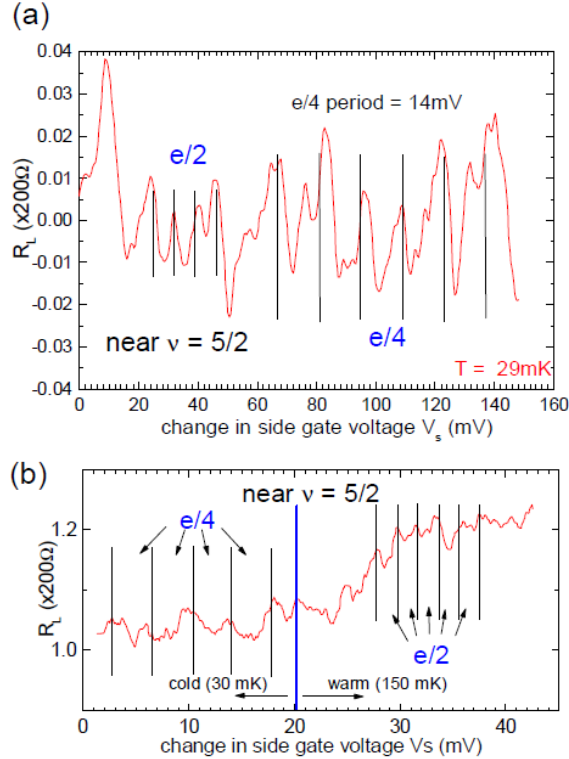


Figure 3.4: The longitudinal resistance of a two point contact interferometer, which is proportional to the current tunneling from one side of the sample to the other. The sample is near filling  $\nu = 5/2$ . Figure (a) shows the observed oscillations at a  $T = 29\text{mK}$ , where two oscillation periods are apparent, with the larger period present only for certain ranges of side gate voltage. Figure (b) shows that the larger period oscillation does not persist to  $T = 150\text{mK}$ , while the smaller period oscillation does persist, though attenuated.

A recent experiment [47] attempted to measure tunneling current in the exact geometry discussed in this chapter, the two point contact interferometer, in the  $\nu = 5/2$  quantum Hall regime. In this experiment, the control knob was the voltage on an electrostatic side gate. Changing the voltage on this side gate deforms the shape of the edge, therefore modifying the trajectory of quasiparticles and the area enclosed by the interference loop. Changing the area of the interference loop, in the absence of bulk quasiparticles, causes oscillations in the tunneling current due to the change of magnetic flux threading the loop area. Of course, in addition to the  $e/4$  quasiparticle tunneling which would show the effect of non-Abelian statistics, tunneling of Abelian  $e/2$  quasiparticles is always present. Interference of  $e/2$  quasiparticle current does

not vanish for any number of bulk quasiparticles.

Figure 3.4 shows some results of Ref. [33]. Figure 3.4a shows the longitudinal resistance of the sample in the presence of two point contact, which is proportional to the tunneling current going from one side of the sample to the other [83]. The authors observe oscillations which they attribute to a period of two magnetic flux quanta through the interference loop, a period which would arise from tunneling of  $e/2$  quasiparticles. They also observe a period corresponding to four flux quanta through the loop, which could arise from tunneling of  $e/4$  quasiparticles. The oscillations corresponding to charge  $e/4$  quasiparticles vanishes for certain regions of side gate voltage, or equivalently for certain positions of the sample edge. We will refer to this as the switching behavior. Another observation concerns the temperature behavior of these oscillations: The  $e/2$  oscillations survive up  $T = 150\text{mK}$ , while  $e/4$  oscillations are not seen at that temperature.

If the observed oscillations are indeed due to tunneling of  $e/2$  and  $e/4$  quasiparticles, then the results of Ref. [47] are consistent with the behavior of the two point contact interferometer analyzed in this chapter, under the assumption that the  $\nu = 5/2$  state is described by the Pfaffian or anti-Pfaffian state. The observed switching behavior can be due to changes in the number of quasiparticles in the bulk. If there are trapped quasiparticles in the bulk, pinned to certain positions by impurities, then as the side gate voltage is swept, these trapped quasiparticles would be excluded one by one from the interference loop. Each such exclusions would toggle the number of quasiparticles in the interference loop between an even and an odd number, causing the  $e/4$  quasiparticle oscillation amplitude toggle between zero and non-zero.

The temperature behavior is also consistent with our analysis. The  $e/2$  quasiparticles involve only the bosonic charge mode, which propagates with velocity  $v_c$ . The  $e/4$  quasiparticle, on the other hand, involves the slower neutral mode. If the neutral mode is much slower than the charge mode, the neutral mode will dominate the temperature scale of the  $e/4$  oscillations,  $T_{e/4}^*$ . The temperature scale  $T_{e/2}^*$  is much larger since it is set by the charge velocity. According to our estimate in section 3.4, the temperature  $T = 150\text{mK}$  is much higher than  $T_{e/4}^*$ , therefore the  $e/4$  oscillation

is strongly attenuated at that temperature and cannot be observed there.

It is tempting to accept the above explanation for the observed oscillations and take the results of Ref. [47] to be the first observation of non-Abelian statistics. Yet, there are a number of checks which can be performed to verify the nature and origin of the observed oscillations. We discuss these checks and offer a critical analysis of the observed oscillations in Ref. [89].

The different oscillation periods could arise without invoking non-Abelian statistics. For example, if the dependence of the interference loop area on the side gate voltage was not a simple linear dependence, perhaps due to density inhomogeneities in the electron density distribution, then the inferred oscillation period would also change with the side gate voltage. Coulomb blockade would also give rise to two different oscillation periods [58, 90, 89], though it seems unlikely Coulomb blockade is the origin of the two different periods in the interferometer of Ref. [47].

Additional measurements using the same experimental setup in different configurations would help clarify the origin of the oscillations. If one of the point contacts is turned off, i.e., it is completely transmitting, then tunneling at a single point contact should give power law behavior of the current at low temperatures, and power law behavior in temperature at low voltages, as shown in section 3.4. That would allow disentangling the temperature behavior of the oscillatory interference current from the temperature behavior of the effective tunneling strength at a single point contact. Power laws would be a strong indication that it is indeed quasiparticles tunneling at a single point contact.

It is also desirable to verify the relation between side gate voltage and the area of the interference loop. For example, the magnetic field and side gate voltage can be simultaneously varied, and the periodicity in the magnetic field can be used to determine the change in area for different side gate voltages. Additional checks are described in Ref. [89].

In conclusion, the results of Ref. [47] are, at first glance, consistent with the picture of quasiparticles with non-Abelian statistics tunneling at the point contacts and encircling trapped bulk quasiparticles. A number of additional measurements

[89] can solidify the agreement between the experimental results and the non-Abelian statistics scenario discussed in this chapter. If these additional measurements indeed give the results predicted in this chapter, the interference experiment of [33] would be a direct observation of a novel physical phenomena, non-Abelian statistics.

## Chapter 4

# Quantum Hall States at $\nu = \frac{2}{k+2}$

Quantum Hall states in the second Landau level,  $2 < \nu < 4$ , sparked the study of non-Abelian statistics in condensed matter systems. The observed quantum Hall state at  $\nu = 5/2$  is the most well studied state in the second Landau level, and is the most promising candidate for the observation of non-Abelian statistics. Due to the difference of electron interactions in the first and second Landau levels, it is possible that other observed states in the second Landau level are non-Abelian as well.

In this chapter, we study a family of quantum Hall states at filling  $\nu = \frac{2}{k+2}$ , and suggest them as candidates for states in the second Landau Level. In particular, the observed fractions  $\nu = 2 + \frac{1}{2}$  and  $\nu = 2 + \frac{2}{5}$  fall in this family of states. We analyze the edge theory of these states and calculate experimentally measurable quantities. We then focus on the state  $\nu = 2 + \frac{2}{5}$ , and compare it to other candidate states at the same filling fraction. This state is of particular interest since it might support non-Abelian statistics which are elaborate enough to enable universal quantum computation.

The work in this chapter has been published in Ref. [91].

### 4.1 Second Landau Level Quantum Hall States

The most robust state in the second Landau level (SLL) is the  $\nu = 5/2$  state [33, 92, 73]. As a result of its even-denominator, it cannot belong to the usual hierarchy/‘composite fermion’ sequence of Abelian states [20, 29, 31, 32, 93, 49] which seems to explain all of the observed states in the lowest Landau level (LLL). The

leading candidate theories of the  $\nu = 5/2$  state are non-Abelian: the Pfaffian state [34, 68, 35] and its particle-hole conjugate, the anti-Pfaffian state [60, 64]. Thus, one may wonder whether the other fractions observed in the second Landau level, such as  $\nu = 7/3, 12/5, 8/3$  and  $14/5$  [92, 38, 94], are also non-Abelian even though they occur at odd-denominator filling fractions. The state at  $\nu = 12/5 = 2 + \frac{2}{5}$  has been the subject of particular interest because its filling fraction is the particle-hole conjugate<sup>1</sup> of that of the  $k = 3$  Read-Rezayi state [37]. This is an exciting possibility because this state is capable of supporting universal topological quantum computation [95, 50]. Alternatively, a state at the lowest level of a non-Abelian hierarchy built on a  $\nu = 5/2$  Pfaffian state also occurs at  $\nu = 12/5$  [96]. Finally, the  $\nu = 12/5$  state may simply be the transposition to the second Landau level of the Abelian state which is believed to occur at  $\nu = 2/5$ .

The action of the edge of the level  $k$ -RR state [37] at filling fraction  $\nu = \frac{k}{k+2}$  is composed of charged and neutral sectors. The charged sector is described by a chiral bosonic field propagating with velocity  $v_c$ . The neutral sector is a chiral  $\mathbb{Z}_k$  parafermionic theory [97] propagating with velocity  $v_n$ . The  $\mathbb{Z}_k$  parafermion theory is an  $SU(2)_k/U(1)$  coset with central charge  $c = \frac{2k-2}{k+2}$  which can be represented by an  $SU(2)_k$  chiral Wess-Zumino-Witten (WZW) model in which the  $U(1)$  subgroup has been gauged [98] (note that the gauge field is not minimally coupled [99]). Thus, we can write:

$$S = \frac{1}{4\pi\nu} \int dx d\tau \partial_x \varphi \bar{\partial} \varphi + S_{\text{WZW},k} + \frac{k}{4\pi} \int dx d\tau \text{tr} \left( A_x \bar{\partial} g \cdot g^{-1} - \bar{A} g^{-1} \partial_x g + A_x g \bar{A} g^{-1} - A_x \bar{A} \right), \quad (4.1)$$

where  $\bar{\partial} \equiv i\partial_\tau + v_c \partial_x$  and  $\bar{A} \equiv A_\tau - i v_n A_x$ . The neutral sector is the sum of the second and third terms which we will call  $S_{\mathbb{Z}_k} = \int \mathcal{L}_{\mathbb{Z}_k}$ . The second term, the WZW

---

<sup>1</sup>We note that the  $k = 2, 3$  RR states in the SLL appear to be weaker than the corresponding RR states, in contrast with the LLL, where the Jain states are stronger than their particle-hole conjugates.

action, is given by:

$$S_{\text{WZW},k} = \frac{k}{16\pi} \int d\tau dx \text{tr} (\partial_x g^{-1} \bar{\partial} g) - i \frac{k}{24\pi} \int dx d\tau dr \epsilon^{\mu\nu\lambda} \text{tr} (\partial_\mu g g^{-1} \partial_\nu g g^{-1} \partial_\lambda g g^{-1}). \quad (4.2)$$

The field  $g$  takes values in  $\text{SU}(2)$ . The second integral is over any three-dimensional manifold  $M$  which is bounded by the two-dimensional spacetime of the edge  $\partial M$ . The value of this integral depends only on the values of the field  $g$  at the boundary  $\partial M$ . As a result of the gauging Equation 4.1, the primary fields  $\Phi_{j,m}$  of this model are essentially the spin- $j$  primary fields of the WZW model, Equation 4.2, dressed by charge- $m$  Wilson lines of the  $\text{U}(1)$  gauge field; as a result of the latter, they are invariant under the  $\text{U}(1)$  subset of the gauge group. The  $k(k+1)/2$  primary fields  $\Phi_{j,m}$  are, consequently, indexed by half-integers  $j, m$  satisfying  $0 \leq j \leq k/2$ ,  $m \in (-j, -j+1, \dots, j)$  with the identifications  $(j, m) \cong (\frac{k}{2} - j, m + \frac{k}{2})$ ,  $(j, m) \cong (j, m+k)$ . The field  $\Phi_{j,m}$  has dimension  $\Delta_{j,m} = \frac{j(j+1)}{k+2} - \frac{m^2}{k}$ . Of particular importance is the parafermion field  $\psi_1 \equiv \Phi_{\frac{k}{2}, -\frac{k}{2}+1}$  of dimension  $\Delta = 1 - \frac{1}{k}$ . For  $k=1$ , the theory is trivial; the  $k=1$  RR state is simply the  $\nu = 1/3$  Laughlin state which has no neutral sector. The  $k=2$  RR state is the Pfaffian state; in the special case  $k=2$ , the  $\text{SU}(2)_2/\text{U}(1)$  coset can be alternately represented as a Majorana fermion. The three primary fields are then  $\Phi_{0,0} = 1$ ,  $\Phi_{1/2,1/2} = \sigma$ ,  $\Phi_{1,0} = \psi$ .

In the RR state, the electron creation operator is a charge-1 fermionic operator, and hence must be a combination of charge and neutral operators:

$$\Psi_e^\dagger = \psi_1 e^{i \frac{k+2}{k} \phi}, \quad (4.3)$$

where  $\psi_1$  is the  $\mathbb{Z}_k$  parafermion field described above (simply the Majorana fermion in the  $k=2$  case). With the bosonic field  $\phi$  normalized as in Equation 4.1, the scaling dimension of  $e^{i\alpha\phi}$  is

$$\dim[e^{i\alpha\phi}] = \nu \frac{\alpha^2}{2}. \quad (4.4)$$

Consequently, the electron operator has scaling dimension  $\frac{3}{2}$ . The neutral sector does not enter the charge current,  $J = \frac{1}{2\pi}\partial\varphi$ , so the level- $k$  RR state has a quantized Hall conductance  $\sigma_{xy} = \frac{k}{k+2}\frac{e^2}{h}$ . If this fractional quantum Hall state occurs in the second Landau level and the lowest Landau level (of both spins) is filled and inert, then  $\sigma_{xy} = \left(2 + \frac{k}{k+2}\right)\frac{e^2}{h}$ . The energy momentum tensor is the sum of the two energy momentum tensors,  $T = T_c + T_{\mathbb{Z}_k}$ . Consequently, the thermal Hall conductivity of the level- $k$  RR state is proportional to the sum of the two central charges [76]:

$$\kappa_{xy}^{\text{RR}} = \frac{3k}{k+2} \frac{\pi^2 k_B^2}{3h} T. \quad (4.5)$$

If this this fractional quantum Hall state occurs in the second Landau level, then  $\kappa_{xy} = \left(2 + \frac{3k}{k+2}\right)\frac{\pi^2 k_B^2}{3h} T$ .

## 4.2 Particle-Hole Conjugation of Read-Rezayi states

Our goal is to analyze the particle-hole conjugates of the general level- $k$  Read-Rezayi states, which we call the level- $k$   $\overline{\text{RR}}$  states. These states possess multiple gapless modes of edge excitations, which are of particular interest for charge and heat transport. We formulate the low-energy effective field theories of the edges of the level- $k$   $\overline{\text{RR}}$  states and show that an  $\text{SU}(2)_k$  Kac-Moody symmetry emerges when the different edge modes equilibrate. One notable feature is that the thermal Hall conductance due to this state  $\kappa_{xy} = -\left(\frac{2k-2}{k+2}\right)\pi^2 k_B^2 T/3h$ , is opposite in sign to the electrical Hall conductance,  $\sigma_{xy} = \frac{2}{k+2}\frac{e^2}{h}$ . We then focus on the  $k = 3$   $\overline{\text{RR}}$  state and compare it to other possible  $\nu = 2 + 2/5$  states. We show that charge transport through a quantum point contact and thermal transport can distinguish this state from its competitors.

To find the edge structure of the level  $k$  anti-RR state ( $\overline{\text{RR}}$ ), we generalize the analysis done for  $k = 1$  in Ref. [100] and for  $k = 2$  in Refs. [60, 64]. Ignoring filled Landau levels (if any), we perform a particle-hole transformation of the partially filled Landau level (the second Landau level in the case of  $\nu = 12/5$ ). The particle-hole conjugate of a particular state can be built by placing that state, but with holes

replacing electrons, on top of a filled LL of electrons. Using this construction, the edge between the level- $k$   $\overline{\text{RR}}$  state ( $\nu = 1 - \frac{k}{k+2} = \frac{2}{k+2}$ ) and the vacuum ( $\nu = 0$ ) is mapped to the edge between the level  $k$ -RR state ( $\nu = \frac{k}{k+2}$ ) and a  $\nu = 1$  state. Hence, the theory of this edge is described by a level  $k$ -RR edge theory and a counter-propagating bosonic charge mode which is the edge theory of the  $\nu = 1$  state. The low-energy effective Lagrangian is:

$$\begin{aligned} \mathcal{L}_{\overline{\text{RR}}} = & \frac{1}{4\pi} \partial_x \phi_1 (i\partial_\tau + v_1 \partial_x) \phi_1 + \left( \frac{k+2}{k} \right) \frac{1}{4\pi} \partial_x \phi_2 (-i\partial_\tau + v_2 \partial_x) \phi_2 + \mathcal{L}_{\mathbb{Z}_k} \\ & - \frac{2}{4\pi} v_{12} \partial_x \phi_1 \partial_x \phi_2 + \xi(x) \psi_1 e^{i\frac{k+2}{k}\phi_2} e^{-i\phi_1} + h.c., \end{aligned} \quad (4.6)$$

where  $\phi_1$  is the  $\nu = 1$  edge charge mode,  $\phi_2$  and the parafermions  $\mathbb{Z}_k$  belong to the RR edge, and  $v_{12} > 0$  is a repulsive density-density interaction along the edge.

The final term in Equation 4.6 is inter-mode electron tunneling which tunnels electrons from the outer  $\nu = 1$  edge to the inner edge with a random coefficient  $\xi$  which, for simplicity, we take to be of Gaussian white noise form:  $\langle \xi(x) \xi^*(x') \rangle = W \delta(x - x')$ . In the absence of inter-mode tunneling, this theory will not realize the universal value of the two-terminal conductance we seek,  $\sigma_{xy} = 1 - \frac{k}{k+2}$ . Heuristically, if there are only two terminals, we cannot distinguish between forward and backward propagation, and the charge conductivities of the filled Landau level and the RR state of holes will add up in absolute value. The tunneling term allows the counter-propagating modes to equilibrate and achieve a universal two-terminal conductance, as is the case for the  $\nu = 2/3$  quantum Hall state [100].

To determine the relevance of the random inter-edge tunneling, we need to examine the scaling dimension of  $W$ . In general, the Renormalization Group flow of the strength of the tunneling,  $W$ , follows [101]:

$$\frac{dW}{d\ell} = (3 - 2\Delta)W \quad (4.7)$$

where  $\Delta$  is the scaling dimension of the term coupled to the random  $\xi(x)$ . In the absence of density-density interactions,  $v_{12} = 0$ , the scaling dimension of the tunneling

operator  $\psi_1 e^{i\frac{k+2}{k}\phi_2} e^{-i\phi_1}$  is  $\Delta = \frac{3}{2} + \frac{1}{2} = 2$ . The inter-mode electron tunneling term is irrelevant in this case:  $dW/d\ell = -W$ , as may be seen by using the replica trick to integrate out  $\xi$ . However, for  $v_{12}$  sufficiently large,  $W$  becomes relevant. To see this, we introduce a new set of fields defined by

$$\phi_\rho = \phi_1 - \phi_2, \quad \phi_\sigma = \phi_1 - \phi_2(k+2)/k, \quad (4.8)$$

corresponding to charged and neutral bosonic modes, respectively. In these variables, the Lagrangian takes the form  $\mathcal{L}_{\overline{\text{RR}}} = \mathcal{L}_\rho + \mathcal{L}_\sigma + \mathcal{L}_{\text{tun}} + \mathcal{L}_{\rho\sigma}$ , with:

$$\begin{aligned} \mathcal{L}_\rho &= \frac{1}{4\pi} \left( \frac{k+2}{2} \right) \partial_x \phi_\rho (i\partial_\tau + v_\rho \partial_x) \phi_\rho, \\ \mathcal{L}_\sigma &= \frac{1}{4\pi} \frac{k}{2} \partial_x \phi_\sigma (-i\partial_\tau + v_\sigma \partial_x) \phi_\sigma + \mathcal{L}_{\mathbb{Z}_k}(v_n), \\ \mathcal{L}_{\rho\sigma} &= 2v_{\rho\sigma} \partial_x \phi_\sigma \partial_x \phi_\rho, \\ \mathcal{L}_{\text{tun}} &= \xi(x) \psi_1 e^{i\phi_\sigma} + \xi^*(x) \psi_1^\dagger e^{-i\phi_\sigma}, \end{aligned} \quad (4.9)$$

and  $v_\sigma, v_\rho, v_{\rho\sigma}$  are functions of  $v_1, v_2$  and  $v_{12}$ , e.g.,

$$4\pi v_{\rho\sigma} = (k/2)^2 v_1 + (k+2/2)^2 v_2 - (k(k+2)/4 + (k/2)^2) v_{12}. \quad (4.10)$$

If  $v_{\rho\sigma} = 0$ , then the electron tunneling operator has scaling dimension  $[\psi_1 e^{i\phi_\sigma}] = 1$  and the inter-mode electron tunneling term is *relevant*:  $dW/d\ell = W$ .

We now show that when the disorder is a relevant perturbation, the edge theory flows to a new fixed point described by a freely-propagating charged boson (responsible for the universal quantized Hall conductance) and a backward propagating neutral sector that possesses an  $SU(2)$  symmetry. We will argue that due to the disordered tunneling the neutral modes will equilibrate and propagate at common average velocity  $\bar{v}$  and show that the velocity mismatch and the mixing term  $\mathcal{L}_{\rho\sigma}$  are irrelevant. An  $SU(2)$  symmetry will thus emerge in the neutral sector. Note that for  $k=2$  this reduces to the result obtained for the anti-Pfaffian [60, 64].

Let us write the neutral sector action  $\mathcal{L}_\sigma$  as  $\mathcal{L}_{SU(2)_k} + \mathcal{L}_{\delta v}$ , with:

$$\begin{aligned}\mathcal{L}_{SU(2)_k} &= \frac{1}{4\pi} \frac{k}{2} \partial_x \phi_\sigma (-i\partial_\tau + \bar{v}\partial_x) \phi_\sigma + \mathcal{L}_{\mathbb{Z}_k}(\bar{v}), \\ \mathcal{L}_{\delta v} &= (\mathcal{L}_{\mathbb{Z}_k}(v_n) - \mathcal{L}_{\mathbb{Z}_k}(\bar{v})) + \frac{1}{4\pi} \frac{k}{2} (v_\sigma - \bar{v})(\partial_x \phi_\sigma)^2.\end{aligned}\tag{4.11}$$

The Lagrangian  $\mathcal{L}_{SU(2)_k}$  is, in fact, equivalent to (the opposite chirality version of) the chiral WZW action, Equation 4.2: the chiral boson  $\phi_\sigma$  restores the U(1) which was gauged out in Equation 4.1. A simple way to see this is to note that the currents:

$$J^+ = \sqrt{k}\psi_1 e^{i\phi_\sigma}, \quad J^- = \sqrt{k}\psi_1^\dagger e^{-i\phi_\sigma}, \quad J^z = \frac{k}{2}\partial_x \phi_\sigma,\tag{4.12}$$

obey the same  $SU(2)_k$  Kac-Moody commutation relations as the WZW currents:

$$J^a = -\frac{ik}{2\pi} \text{tr} (T^a g^{-1} (i\partial_\tau - \bar{v}\partial_x) g),\tag{4.13}$$

where  $T^a$ ,  $a = x, y, z$  are  $SU(2)$  generators and  $J^\pm = J^a \pm iJ^y$ .

We notice that the tunneling term  $\mathcal{L}_{\text{tun}}$  can be written in terms of the currents:

$$\mathcal{L}_{\text{tun}} = \xi(x)J^+ + \xi^*(x)J^-\tag{4.14}$$

It is convenient to use the WZW representation since the tunneling term can be eliminated from the action by the gauge transformation  $g \rightarrow gU$  with

$$U = P e^{\frac{i}{v} \int^x dx' \vec{\xi}(x') \cdot \vec{T}}\tag{4.15}$$

where  $P$  denotes path ordering and  $\vec{\xi}(x') = (2\text{Re}(\xi(x')), -2\text{Im}(\xi(x')), 0)$ . Under this gauge transformation

$$\mathcal{L}_{SU(2)_k} \rightarrow \mathcal{L}_{SU(2)_k} - \vec{\xi} \cdot \vec{J},\tag{4.16}$$

thus with this gauge transformation we are able to eliminate the tunneling term  $\mathcal{L}_{\text{tun}}$

from the action of the edge..

We now turn to the effect of this gauge transformation on the velocity anisotropy terms. The velocity terms in  $\mathcal{L}_\sigma$  can be written in the form:

$$v_a \text{tr} (S_a \partial_x g^{-1} \partial_x g), \quad (4.17)$$

where  $S_a$  is a matrix satisfying  $\text{tr}(S_a T_b T_c) = \delta_{ab} \delta_{ac}$  and  $v_a$ ,  $a = x, y, z$  can be expressed in terms of  $v_\sigma$ ,  $v_n$ . The matrix  $v_a S_a$  picks out the current  $J_a$ , Equation 4.13, from the action, and gives it the velocity  $v_a$ . Let us separate the traceless part  $M$  of the matrix  $v_a S_a$ :

$$M = v_a S_a - \text{tr}(v_a S_a) \times \mathbb{I}/3. \quad (4.18)$$

Then  $\mathcal{L}_{\delta v}$  takes the form  $\mathcal{L}_{\delta v} = \text{tr}(M \partial_x g^{-1} \partial_x g)$  Under the gauge transformation  $g \rightarrow gU$ ,  $\mathcal{L}_{\delta v} \rightarrow \text{tr}(M' \partial_x g^{-1} \partial_x g)$ , where  $M' = U M U^\dagger$  is random since the gauge transformation is a function of  $\xi(x)$ . The renormalization group flow of the mean square average of  $M'$ ,  $W_{M'}$ , is  $dW_{M'}/dl = (3 - 2\Delta)W_{M'}$  [101], where  $\Delta$  is the scaling dimension of the term to which  $M'$  couples. In this case,  $M'$  couples to  $\partial_x g^{-1} \partial_x g \propto J^2$  which has scaling dimension  $\Delta = 2$  (i.e.  $M'$  is a velocity). Hence  $W_{M'}$  and the velocity anisotropy are irrelevant. The part of the velocity term which is invariant under the gauge transformation is the average velocity  $\bar{v} = \text{tr}(v_a S_a)/3$ .

The mixing term,  $\mathcal{L}_{\rho\sigma}$  is irrelevant. It can be written as  $\mathcal{L}_{\rho\sigma} = 2v_{\rho\sigma}(\frac{2}{k}J^z) \cdot \partial_x \phi_\rho$ ; under the gauge transformation  $g \rightarrow gU$  the current  $J^z$  gets rotated with a random coefficient. Consequently, deviations from  $v_{\rho\sigma} = 0$  are irrelevant, much like the velocity anisotropy term above.

### 4.3 Properties of anti-RR States

We have found that at the fixed point where the edge modes equilibrate due to random electron tunneling, the edge theory of the anti-RR state is described by a single bosonic charge mode,  $\mathcal{L}_\rho$ , and an  $SU(2)_k$  neutral sector,  $\mathcal{L}_{SU(2)_k}$ , moving in the opposite direction. The electron operator of the  $\nu = 1$  edge in the unequilibrated

theory with  $\xi = 0$  in Equation 4.6 is  $e^{i\phi_1}$ , and can be rewritten in the form  $e^{i\phi_1} = e^{-i\frac{k}{2}\phi_\sigma} e^{i\frac{k+2}{2}\phi_\rho}$ . As a result of equilibration, the dimension of this operator changes, from  $\Delta_e = 1/2$  to  $\Delta_e = (k+1)/2$ . (The conformal spin, the difference between the right and left scaling dimensions, remains  $1/2$ , however.) Noting that  $e^{i\phi_1}$  can be rewritten as  $\chi_{j=k/2}^{m=-k/2} e^{i\frac{k+2}{2}\phi_\rho}$ , we see that this operator is the lowest  $J^z$  eigenvalue,  $m$ , of a multiplet  $\chi_{j=k/2}^m e^{i\frac{k+2}{2}\phi_\rho}$  with  $m = -k/2, -k/2 + 1, \dots, k/2$ . The other electron creation operators in this SU(2) multiplet are obtained by acting multiple times on  $e^{i\phi_1}$  with the raising operator  $J^+ = \psi_1 e^{i\phi_\sigma}$ ; thus, they create an electron in the original  $\nu = 1$  edge and transfer multiple electrons from the RR edge to the  $\nu = 1$  edge. As a result of equilibration, all  $k+1$  of these operators have the same scaling dimension. When electrons tunnel between two level- $k$   $\overline{\text{RR}}$  droplets, the tunneling conductance  $G \sim T^{2k}$  and, for finite  $V > T$ ,  $I_{\text{tun}} \sim V^{2k+1}$ .

Quasiparticle operators can be obtained by the requirement that they are local with respect to these electron operators. The allowed quasiparticle operators (modulo the creation or annihilation of an electron) and their scaling dimensions are:

$$\Phi_{\text{qp}}^{j,N} = \chi_j e^{i(j+N)\phi_\rho}. \quad (4.19)$$

The  $J^z$  eigenvalue is suppressed here; there is an SU(2) multiplet of each of these operators all of which belong to the same quasiparticle species because they have the same topological properties.  $\Phi_{\text{qp}}^{j,N}$  has right scaling dimension  $(j+N)^2/(k+2)$  and left scaling dimension  $j(j+1)/(k+2)$  and, therefore, total scaling dimension  $[(j+N)^2 + j(j+1)]/(k+2)$  and topological spin  $[(j+N)^2 - j(j+1)]/(k+2)$ . For  $k$  even,  $N = 0, 1, \dots, \frac{k}{2}$ . For  $k$  odd,  $N = 0, 1, \dots, \frac{k+1}{2}$  for integer  $j$  and  $N = 0, 1, \dots, \frac{k-1}{2}$  for half-integer  $j$ . Therefore, there are  $(k+1)(k+2)/2$  different quasiparticle species. This is also the ground state degeneracy of the  $\overline{\text{RR}}$  theory on the torus (which is 10 in the case of the  $\nu = 12/5$  state). The corresponding RR state has the same degeneracy. The minimal dimension of a quasiparticle operator is  $[\Phi_{\text{qp}}^{1/2,0}] = [\Phi_{\text{qp}}^{0,1}] = \frac{1}{k+2}$ . Consequently, when quasiparticles tunnel between the edges at a point contact,  $R_{xx} \sim T^{-2k/(k+2)}$  and, at finite  $V > T$ ,  $I_{\text{tun}} \sim V^{(2-k)/(2+k)}$ .

The thermal Hall conductivity of the anti-RR state is determined by the central charge of the edge theory [76]. Ignoring the filled Landau levels, the central charge of the bosonic charge sector is  $c = 1$  and the central charge of the  $SU(2)_k$  theory is  $\bar{c} = 3k/(k + 2)$ . The thermal Hall conductivity of the anti-RR state is then:

$$\kappa_{xy}^{\overline{\text{RR}}} = \left(1 - \frac{3k}{k + 2}\right) \frac{\pi^2 k_B^2}{3h} T. \quad (4.20)$$

Thus, the conductivity due to the partially filled second Landau level is negative for all  $k$ .

## 4.4 Candidate States for Filling 12/5

Focusing on the  $\nu = 2/5$  anti-RR state ( $k=3$ ) its thermal Hall conductivity is  $-\frac{4}{5}$  (in units of  $\frac{\pi^2 k_B^2}{3h} T$ ), while the Abelian hierarchy state at  $\nu = 2/5$  has a positive thermal Hall conductance of  $+2$ , and the  $\nu = 2/5$  non-Abelian hierarchy state of Ref. [96], built on the  $\nu = 1/2$  Pfaffian state, would have a thermal Hall conductance of  $+\frac{1}{2}$ . We note that the construction of Ref.[96] can also produce a  $\nu = 2/5$  state built on the anti-Pfaffian state, with thermal Hall conductance  $-\frac{3}{2}$ . These thermal conductivities are achieved at length scales longer than the equilibration length of the edges. In the case of the  $\nu = 12/5$  state, the filled lower Landau level gives an additional contribution of  $+2$ , which would make all of the thermal conductivities positive, though differing in magnitude. Therefore, in order to distinguish the non-Abelian  $\nu = 12/5$  states from the Abelian one through the signs of their thermal Hall conductivities, it would be necessary to measure the thermal conductivity along an edge between  $\nu = 2$  and  $\nu = 2 + \frac{2}{5}$ , which would only have a contribution from the partially-filled Landau level. On shorter length scales, the different modes on the edge do not equilibrate, in which case both the anti-RR state and the non-Abelian hierarchy state will have heat flow both upstream and downstream while the Abelian state will have purely chiral heat transport. In this case, the filled Landau levels simply give an additional contribution to the downstream heat transport.

The difference between the various proposed  $\nu = 12/5$  states would also be evident from the transport through a point contact. Such experiments have been performed in the second Landau level [45]. As a result of weak quasiparticle tunneling from one edge to the other, there is a non-zero longitudinal resistance (see, e.g., the appendices of ref. [83]):

$$R_{xx} \sim T^{4\Delta_{\text{qp}}-2} \quad (4.21)$$

where  $\Delta_{\text{qp}}$  is the scaling dimension of the tunneling quasiparticle. At finite voltage  $V > T$ , we instead have  $I_{\text{tun}} \sim V^{4\Delta_{\text{qp}}-1}$ . In the Abelian hierarchy  $\nu = 2/5$  state, the most relevant tunneling operator is that of the charge  $\frac{2}{5}e$  quasiparticle with  $\Delta_{\text{qp}} = \frac{1}{5}$  [49, 102], leading to  $R_{xx} \sim T^{-6/5}$ . In the non-Abelian hierarchy state of Ref. [96], the most relevant tunneling operator is that of charge  $\frac{1}{5}e$  quasiparticles with dimension  $\Delta_{\text{qp}} = \frac{9}{80}$ , leading to  $R_{xx} \sim T^{-31/20}$ . Its sister state, built on the anti-Pfaffian, rather than the Pfaffian has  $\Delta_{\text{qp}} = \frac{19}{80}$ , hence  $R_{xx} \sim T^{-21/20}$ . Finally, in the  $k = 3 \overline{\text{RR}}$  state, the operator  $\Phi_{1/5} = \Phi_{(\frac{1}{2})} e^{i\frac{1}{2}\phi_\rho}$  carries charge  $\frac{1}{5}e$  and has scaling dimension  $\Delta_{\text{qp}} = \frac{1}{5}$ , while the operator  $\Phi_{2/5} = e^{i\phi_\rho}$  carries charge  $\frac{2}{5}e$  and has the same scaling dimension. Therefore, the longitudinal resistance in this theory will behave as  $R_{xx} \sim T^{-6/5}$ , precisely as in the Abelian hierarchy state. However, shot noise experiments [70, 71, 44] can detect the charge of the tunneling quasiparticles. In the Abelian hierarchy state, the current is carried by charge  $2e/5$  quasiparticles at the lowest temperatures, where the most relevant operator (in the Renormalization Group sense) will dominate. In the non-Abelian hierarchy state, charge  $e/5$  quasiparticle tunneling is the most relevant operator. In the  $k = 3 \overline{\text{RR}}$  state, charge  $e/5$  and charge  $2e/5$  quasiparticle tunneling are equally relevant, but the bare tunneling matrix element for charge  $e/5$  quasiparticles is presumably larger than for charge  $2e/5$  quasiparticles ( $\Gamma_{2/5} \sim (\Gamma_{1/5})^2$ ), so tunneling will be dominated by the former. In summary, we expect shot noise experiments in either of the non-Abelian states to result in a charge of  $e/5$ , as compared to charge  $2e/5$  in the Abelian state. The two non-Abelian states can be distinguished from each other by the power-laws with which  $R_{xx}$  depends on  $T$  or  $I_{\text{tun}}$  on  $V$  for  $V > T$  in the limit of weak tunneling. In the opposite limit of

Candidate State	$R_{xx}$	$\kappa_{xy}$	$e^*/e$
$k = 3$ anti-RR	$T^{-6/5}$	$-4/5$	$1/5$
Generalized Hierarchy over Pf	$T^{-31/20}$	$1/2$	$1/5$
Generalized Hierarchy over $\overline{\text{Pf}}$	$T^{-21/20}$	$-3/2$	$1/5$
Abelian Hierarchy	$T^{-6/5}$	$+2$	$2/5$

Table 4.1: Comparison between different candidate states for electrons at  $\nu = 12/5$ . We compare the state analyzed in this chapter, the  $k = 3$  anti-RR state, the the generalized hierarchy states of Ref. [96], and to the Abelian hierarchy state [102]. Listed are the longitudinal resistance in the presence of point contact,  $R_{xx}$ , the thermal Hall conductivity due to the upper LL,  $\kappa_{xy}$ , and the charge of the quasiparticle with the most relevant tunneling,  $e^*$ .

strong tunneling, the droplet effectively breaks in two and all that remains is the weak tunneling of electrons between the two droplets. In this case,  $G \sim T^{4\Delta_e-2}$ ; in both the Abelian and non-Abelian hierarchy states,  $\Delta_e = 3/2$  while in the  $k = 3$   $\overline{\text{RR}}$  state,  $\Delta_e = 2$ . These results are listed in Equation 4.4.

To conclude, we have studied the edge theory of the anti-RR states, a family of quantum Hall states at filling fractions  $\nu = \frac{2}{k+2}$ . These states are relevant to the observed  $\nu = 12/5$  state. We compared the anti-RR state at  $k = 3$  to other candidate states for  $\nu = 12/5$ . Quantitative measurements of quasiparticle charge, tunneling exponents, and thermal conductance would allow the determination of the ground state of electrons at filling  $\nu = 12/5$ , and whether it is described by the  $k = 3$  anti-RR state or a different non-Abelian, or Abelian, state.

## Chapter 5

# Multi-Channel Kondo Effect in QH Edges

Following the general theme of this thesis, we will discuss in this chapter an experiment which could reveal properties of non-Abelian quantum Hall states, including the structure of the neutral part of the edge theory, through charge measurements. In particular, this experiment might allow distinguishing between the Pfaffian and anti-Pfaffian states, two states at the same filling fraction. This experiment involves electron tunneling only, and therefore will not show a direct signature of fractional non-Abelian statistics.

Non-Abelian quantum Hall states have sparked considerable interest recently because of their novel physical properties and their potential application to topological quantum computing [103]. Though it is not known whether such states exist, it is suspected that the observed plateaus at  $\sigma_{xy} = \nu \frac{e^2}{h}$  with  $\nu = 5/2$  [33] and  $\nu = 12/5$  [38] are due to non-Abelian quantum Hall states.

The current evidence for the existence of non-Abelian quantum Hall states comes primarily from numerical studies [39, 40, 43] which found that the ground states of small numbers of electrons had large overlap with the Moore-Read Pfaffian wavefunction [34, 68, 35] and the particle-hole conjugate of the  $k = 3$  Read-Rezayi (RR) wavefunction [37, 91] at  $\nu = 5/2$  and  $\nu = 12/5$  respectively, and from recent noise and tunneling measurements [44, 45]. It has been argued that these wavefunctions are representatives of two universality classes which exhibit non-Abelian quasi-particle

statistics, which is a necessary ingredient for topological quantum computing [50]. Recently, further numerical studies [62, 42] have bolstered the argument that these states occur in the experiments of Refs. [33, 38].

Some theoretical proposals have been made to determine experimentally whether or not the  $\nu = 5/2$  state possesses the non-Abelian quasi-particle statistics of the Pfaffian [75, 56, 58, 57]. While fabricating high-mobility samples of mesoscopic size to test these proposals presents a significant challenge, recent experiments on quantum point contacts at  $\nu = 5/2$  give one reason to believe that such devices are within reach [104]. Experiments on such devices have recently shed light, for the first time, on quasiparticle properties at  $\nu = 5/2$ . Shot noise [44] and non-linear current-voltage characteristics [45] at quantum point contacts at  $\nu = 5/2$  are both consistent with a quasi-particle charge of  $e/4$ , as required by the Moore-Read Pfaffian state.

However, a wrinkle in the theoretical picture appeared recently when it was realized that another state, the ‘anti-Pfaffian’, is an equally good candidate at  $\nu = 5/2$  [60, 64]. The anti-Pfaffian is the conjugate of the Pfaffian under particle-hole symmetry within a Landau level, which is an exact symmetry in the limit of large magnetic field. This symmetry must be spontaneously broken in order for one of these two degenerate ground states to occur; the system sizes studied in numerics on the torus were simply too small to observe anything other than the symmetric combination of the two [40]. In the case of numerics on the sphere [39], the finite geometry explicitly breaks the symmetry; the anti-Pfaffian occurs at a different value of the magnetic flux and was, consequently, missed.

The Pfaffian and anti-Pfaffian states differ significantly in the nature of their edge excitations. This leads to a difference in tunneling characteristics and thermal transport along the edge [64, 91]. Both states possess charge  $e/4$  quasi-particles, so the existing noise experiments do not allow one to distinguish between them [44]. Current-voltage characteristics at a point contact can distinguish between the two states; measurements appear to be more consistent with the anti-Pfaffian state although they cannot fully rule out the Pfaffian [45]. Therefore, there is urgent need for further experiments to determine not only whether the  $\nu = 5/2$  state is Abelian or non-

Abelian, but to indicate which non-Abelian state.

We show that tunneling between a level- $k$  Read-Rezayi (RR) quantum Hall state and a quantum dot maps to  $k$ -channel Kondo problem, which is *channel symmetric* without fine tuning. This would allow verifying some properties of the edge states, and would provide a realization of the channel symmetric Kondo problem. The level- $k$  anti-RR state (chapter 4) maps to a channel asymmetric  $k$ -channel Kondo problem.

This chapter is based on the published article [105], by G. Fiete, W. Bishara and C. Nayak.

## 5.1 Kondo Model Review

The Kondo model is a model of a localized point-like magnetic impurity interacting with a Fermi sea of free electrons in three dimensions. There is vast literature on the Kondo model. A classic review is [106], and a review of the Kondo model and its literature can be found in [107].

The Hamiltonian for the Kondo model, for a single species of fermions, is

$$H_{\text{Kondo}} = H_0[\psi] + \lambda \vec{S} \cdot \vec{s}(0), \quad (5.1)$$

where  $H_0$  is the the Hamiltonian of free electron,  $\vec{S}$  is the spin of the impurity, and  $\vec{s}(0)$  is the spin of the electrons at the position of the impurity:

$$\vec{s}(0) = \psi_\alpha^\dagger(0) \vec{\sigma}_{\alpha\beta} \psi_\beta(0) \quad (5.2)$$

If the magnetic impurity is a point-like impurity, then the problem is isotropic, and the free electron Hamiltonian can be reduced to a chiral one-dimensional Hamiltonian of radial degree of freedom, the incoming and outgoing isotropic modes. The one-dimensional theory can be bosonized to give:

$$H_0[\psi] = \int dx \frac{v_F}{4\pi} (\partial_x \varphi(x))^2, \quad (5.3)$$

with  $\psi(x) \propto e^{i\varphi(x)}$ . If there are a number of fermion species, the Hamiltonian becomes

$$H_{\text{Kondo}} = \sum_i \left\{ H_0[\psi_i] + \lambda_i \vec{S} \cdot \vec{s}_i(0) \right\}. \quad (5.4)$$

This is the multi-channel Kondo problem. If all the  $\lambda_i$ 's are equal, then Equation 5.4 is the *channel symmetric* Kondo model. The multi-channel Kondo problem is interesting since it displays non-Fermi-Liquid behavior. For example, the  $k$ -channel, channel symmetric Kondo model gives for the magnetic susceptibility of the impurity:

$$\chi_{\text{imp}} \propto \left( \frac{1}{T} \right)^{\frac{k-2}{k+2}}. \quad (5.5)$$

For  $k = 2$ , the susceptibility has a logarithmic divergence,  $\chi_{\text{imp}} \propto \ln(1/T)$ . For  $k = 1$ , the magnetic susceptibility approaches a constant for low temperatures, reminiscent of the behavior of Fermi liquids.

It is useful in the study of the Kondo model to relax the assumption of spin isotropy. The spin-anisotropic coupling between the impurity and the fermi liquid spin is usually written as:

$$\lambda_i^\perp (S^+ s_i^-(0) + S^- s_i^+(0)) + \lambda_i^z S^z s_i^z(0) \quad (5.6)$$

## 5.2 Quantum Dot coupled to QH Edge

The experimental setup we have in mind is depicted in Figure 5.1. The bulk quantum Hall state on the left is assumed to be in a non-Abelian fractional quantum Hall state at  $\nu = 2 + k/(k+2)$  or  $\nu = 2 + 2/(k+2)$ , corresponding to a level- $k$  Read-Rezayi state or its particle hole conjugate, respectively (chapter 4). A quantum point contact may be used to pinch off a finite region of the quantum Hall fluid and form a quantum dot separated from the bulk by a tunneling barrier. We assume that the lower two Landau levels are not pinched off and therefore do not backscatter at the point contact, i.e. the barrier region is assumed to have  $\nu = 2$ . For an infinite system, the edge modes of

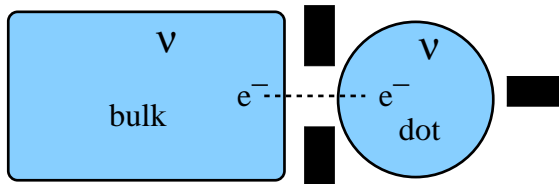


Figure 5.1: (color online) Schematic of our model. Gates are shown in black. They may be used to form a point contact to pinch off the dot from the rest of the quantum Hall bulk. The gate on the right of the figure may be used to shift the energy levels of the dot by changing its area  $S$ . The bulk is assumed to be at filling fraction  $\nu = 2 + k/(k + 2)$  or  $\nu = 2 + 2/(k + 2)$ . The white region between the dot and the bulk is assumed to be at  $\nu = 2$ . The charge on the dot may be measured capacitively [108].

the quantum dot are gapless, but for a finite system they acquire a discrete spectrum [109, 90]. We focus on fluctuations of the quantum dot charge  $Q \equiv e\langle \hat{N}_e \rangle$  near a degeneracy point in the energy, that is when the energy of a dot with  $N_e$  electrons is equal to that of a dot with  $N_e + 1$  electrons:

$$E(N_e, S, B) = E(N_e + 1, S, B). \quad (5.7)$$

The energy of the dot depends on its area  $S$ , which may be altered by a gate potential shown in Figure 5.1; and on the magnetic field  $B$ . Adjusting either  $S$  or  $B$  may be used to achieve the desired degeneracy and also to slightly tune away from it. The charge of the dot can be measured capacitively [108].

We are interested in energy and temperature scales much less than the level-spacing of the dot edge states. Under this assumption, only two levels on the quantum dot (the degenerate or nearly degenerate ones) are important for the physics. In our formulation, these two levels will act as an effective, local spin-1/2 degree of freedom. The crucial feature of the Read-Rezayi states is that the coupling of their edge states to this effective spin degree of freedom via electron tunneling to the dot can be mapped to the  $k$ -channel Kondo model. (We emphasize that our analysis applies to an effective spin degree of freedom which accounts for the charge on the dot; the Read-Rezayi states and their particle-hole conjugates [91] are spin polarized, so there

are no spin-flips in the quantum Hall edge states). This allows us to exploit known results from the multi-channel Kondo models [110].

A detuning from degeneracy maps to the coupling of an external magnetic field to the spin in the  $k$ -channel Kondo model. Thus, charge susceptibilities in our quantum dot set-up can be obtained from magnetic susceptibility in the Kondo model. A remarkable feature of the scenario we discuss here is that the channel *isotropic* limit is automatically obtained for Read-Rezayi states *without any fine tuning*. Again, this feature follows from the form of the coupling of the edge states to the quantum dot degrees of freedom. On the other hand, for their particle-hole conjugates [60, 64, 91], the generic case is channel anisotropic. Since the channel isotropic and channel anisotropic Kondo models are very different, one can exploit the thermodynamics of the multi-channel Kondo model applied to the charge susceptibility to distinguish the Pfaffian from the anti-Pfaffian. This is one of our central results.

### 5.3 Pfaffian Edge and Quantum Dot

We begin with the case of a quantum dot coupled to a bulk quantum Hall state in the Moore-Read Pfaffian state, at filling fraction  $\nu = 2 + 1/2$ . Here and henceforth, we ignore the 2 filled lower Landau levels. The Hamiltonian for our problem is

$$H = H_{\text{edge}} + H_{\text{dot}} + H_{\text{tun}}. \quad (5.8)$$

where  $H_{\text{edge}}$  is the Hamiltonian of the inner half filled Landau level. This is justified by the sequence of modes pinched off in a point contact [44]. The edge theory for the Pfaffian state is the product of a free, charged chiral bosonic sector and a neutral Majorana sector. The edge Hamiltonian takes the form (note the different normalization in section 5.1)

$$H_{\text{edge}} = \int dx \left( v_c \frac{(k+2)/k}{4\pi} (\partial_x \varphi(x))^2 + i v_n \psi \partial_x \psi \right), \quad (5.9)$$

Here,  $k = 2$  and  $v_n < v_c$  is the velocity of the neutral mode(s). The Hamiltonian of the dot describes a two level system which we can take to be “empty” or “occupied” (later to be mapped to “up” or “down”) [111, 112]. It thus has a fermionic character and we label the fermionic annihilation (creation) operator for this state  $d$  ( $d^\dagger$ ). Thus,

$$H_{\text{dot}} = \epsilon_d d^\dagger d, \quad (5.10)$$

where  $\epsilon_d = 0$  at the degeneracy point and  $\epsilon_d \neq 0$  when one is tuned away from degeneracy. The tunneling Hamiltonian is

$$H_{\text{tun}} = t(d^\dagger \Psi_e(0) + \Psi_e^\dagger(0)d) + V d^\dagger d \Psi_e^\dagger(0) \Psi_e(0), \quad (5.11)$$

where  $t$  is the tunneling amplitude to the dot;  $x = 0$  is the location of the point contact;  $V$  is the Coulomb repulsion between the edge and the dot, and  $\Psi_e$  ( $\Psi_e^\dagger$ ) is the annihilation (creation) operator for the electron,

$$\Psi_e^\dagger = \psi e^{i2\varphi}. \quad (5.12)$$

With the above normalization, the scaling dimension of  $e^{i\alpha\varphi}$  is  $\dim[e^{i\alpha\varphi}] = \nu \frac{\alpha^2}{2}$ , so that the dimension of the electron operator is

$$\dim[\Psi_e] = 3/2. \quad (5.13)$$

As a result of the scaling  $\dim$  of  $\Psi_e$ ,  $t$  is naively irrelevant in the Renormalization Group sense:

$$\begin{aligned} \frac{dt}{d\ell} &= (1 - \dim[\Psi_e]) t + \mathcal{O}(tV) + \mathcal{O}(t^3) \\ &= -\frac{1}{2} t + \mathcal{O}(tV) + \mathcal{O}(t^3). \end{aligned} \quad (5.14)$$

However, for  $V$  sufficiently large,  $t$  flows to the 2-channel Kondo fixed point, not to  $t = 0$ . (One might guess this from the second term above, but we will show this

directly.) To see this, we we apply a unitary transformation  $U = e^{2id^\dagger d\varphi(0)}$  to  $H$ , which rotates  $\varphi(0)$  out of the tunneling term.  $H$  now takes the form

$$\begin{aligned} UHU^\dagger &= H_{\text{edge}} + H_{\text{dot}} + t\psi(d - d^\dagger) \\ &+ (V - 2v_c) d^\dagger d \partial_x \varphi(0). \end{aligned} \quad (5.15)$$

For  $V - 2v_c = 0$ , this is a purely quadratic theory which can be solved exactly. Thus,  $t$  is clearly relevant in this limit; we will see below that it is actually relevant over a range of values of  $V$ . Note that only the Majorana combination  $d - d^\dagger$  couples to the the quantum Hall edge. This is precisely the same feature which leads to non-Fermi liquid behavior in the two-channel Kondo problem [113]: the spectral function  $\text{Im} \langle d^\dagger d \rangle$  has both a  $\delta$ -function piece, coming from  $d^\dagger + d$  and a Lorentzian piece coming from  $d - d^\dagger$ . As we will see, the coupling of a quantum dot to an anti-Pfaffian quantum Hall state does not have this property.

To see the connection to the two-channel Kondo model, it is useful to represent the two-level system on the dot by a spin:

$$\begin{aligned} S^\dagger &= d^\dagger; \quad S^- = d; \\ \text{and} \quad S^z &= d^\dagger d - \frac{1}{2}. \end{aligned} \quad (5.16)$$

(up to Klein factors we have suppressed.) Then, we apply a unitary transformation  $U = e^{i\alpha S^z \varphi(0)}$  to  $H$  as before, but now we take  $\alpha = 2 - \sqrt{2}$ , i.e. rather than fully rotate  $\varphi(0)$  out of the tunneling term, we partially rotate it.  $H$  now takes the form:

$$\begin{aligned} UHU^\dagger &= H_{\text{edge}} + \epsilon_d S^z + (V - v_c \alpha) S^z \partial_x \varphi(0) \\ &+ t(\psi^\dagger e^{-i\sqrt{2}\varphi(0)} S^\dagger + \psi e^{i\sqrt{2}\varphi(0)} S^-). \end{aligned} \quad (5.17)$$

We now compare this to the Hamiltonian for the Kondo model (see Equation 5.6):

$$H_{\text{imp}} = \lambda_\perp (J^+(0)S^- + J^-(0)S^+) + \lambda_z J^z(0)S^z + hS^z, \quad (5.18)$$

where  $\vec{S}$  is the impurity spin;  $\vec{J}(0)$  is conduction electron spin density at the impurity site;  $\lambda_{\perp}$ ,  $\lambda_z$  are the exchange couplings which are not assumed to be equal; and  $h$  is the magnetic field. The impurity spin only interacts with conduction electrons in the  $s$ -wave channel about the origin. Retaining only this channel, we have a chiral one-dimensional problem in which the impurity is at the origin and the incoming and outgoing modes are right-moving modes at  $x < 0$  and  $x > 0$ , respectively. Affleck and Ludwig observed [114, 110] that the Hamiltonian of the conduction electrons  $H_{\text{cond}}$  in the  $k$ -channel Kondo model admits a *conformal decomposition*,

$$H_{\text{cond}} = H_{U(1)} + H_{SU(2)_k} + H_{SU(k)_2}. \quad (5.19)$$

This decomposition follows from simply using the appropriate combinations of electron fields. The Hamiltonian  $H_{U(1)}$  involves only the totally charge mode, which in the bosonized version is simply  $\varphi_{\rho}(x) = \frac{1}{k} \sum_i \varphi_i(x)$ . The Hamiltonian  $H_{SU(2)_k}$  involves the combinations of fields representing the spin density. The remaining degrees of freedom enter  $H_{SU(k)_2}$ .

The spin density combination of fields,

$$J^a = \sum_i \psi_{i,\alpha}^{\dagger} \sigma_{\alpha\beta}^a \psi_{i,\beta} \quad (5.20)$$

obey the  $SU(2)_k$  Kac-Moody algebra:

$$[J_m^a, J_n^b] = i\epsilon^{abc} J_{n+m}^c + nk\delta_{a,b}\delta_{m+n,0}, \quad (5.21)$$

where the labels  $n, m$  correspond to the spatial Fourier transform components of the spin currents. For  $k = 2$ , we can express the  $J^a$  in terms of a Majorana fermion,  $\psi$ , and a free boson  $\varphi$ :

$$J^{\dagger} = \sqrt{2}\psi e^{i\sqrt{2}\varphi}, \quad J^{-} = \sqrt{2}\psi e^{-i\sqrt{2}\varphi}, \quad J^z = \sqrt{2}\partial_x\varphi. \quad (5.22)$$

The operators  $\psi$  and  $\varphi$  have a complicated, non-local relation to the original conduc-

tion electron operators, but they have the virtue of satisfying the  $SU(2)_2$  Kac-Moody algebra via Equation 5.22.

Substituting Equation 5.22 into Equation 5.18, we see that our problem in Equation 5.17 maps onto the 2-channel Kondo model with anisotropic exchange if we identify

$$\begin{aligned}\lambda_{\perp} &= t, \\ \sqrt{2}\lambda_z &= V - (2 - \sqrt{2})v_c, \\ h &= \epsilon_d.\end{aligned}\tag{5.23}$$

For  $\lambda_z < 0$ , the Kondo model is ferromagnetic. In the ferromagnetic Kondo model, the coupling to the impurity is irrelevant, as we naively expected above in Equation 5.14. However, when  $V$  is sufficiently large,  $\lambda_z > 0$ , corresponding to the antiferromagnetic Kondo model. In this case, the Hamiltonian is controlled in the infrared by the exchange and channel isotropic antiferromagnetic spin-1/2 2-channel Kondo fixed point [115]. This fixed point is characterized by non-Fermi liquid correlations, including anomalous exponents for the temperature dependence of the impurity contribution to the specific heat and spin susceptibility and the magnetic field dependence of the zero-temperature magnetization. The latter two translate to the charge susceptibility and charge of the quantum dot [110]:

$$\chi_{\text{charge}} \propto \ln(T_K/T), \quad \Delta Q \propto V_G \ln(k_B T_K / e^* V_G),\tag{5.24}$$

where the Kondo temperature depends on non-universal values  $v_n, t$  and is given by  $T_K \propto \exp(-c_1 v_n / t)$  with  $c_1 > 0$ . Here,  $\Delta Q = Q - e(N_e + \frac{1}{2})$  is the charge on the dot measured relative to the average electron number at the degeneracy point of the energy. In the case  $k = 2$ , which corresponds to the Pfaffian state, possibly realized at  $\nu = 5/2$ , there are logarithmic corrections: Ordinarily, fine tuning would be required to realize channel isotropy in the Kondo model [116] but, as we have seen, the coupling between a quantum dot and the edge of a Pfaffian quantum Hall state automatically

realizes the channel isotropic 2-channel Kondo model.

## 5.4 Anti-Pfaffian and Quantum Dot

We now turn to the coupling of the anti-Pfaffian state to the two degenerate levels of the quantum dot. The edge theory of the anti-Pfaffian state is [60, 64]:

$$\mathcal{L}_{\text{Pf}} = \frac{2}{4\pi} \partial_x \phi_\rho (\partial_t - v_\rho \partial_x) \phi_\rho + i\psi_a (-\partial_t - v_\sigma \partial_x) \psi_a. \quad (5.25)$$

There is a charged boson  $\phi_\rho$  and three counter-propagating Majorana fermions  $\psi_a$ ,  $a = 1, 2, 3$ . There are three different dimension-3/2 electron operators,  $\psi_a e^{2i\phi_\rho}$ . The combination  $(\psi_1 - i\psi_2) e^{2i\phi_\rho}$  is inherited from the electron operator of the  $\nu = 1$  integer quantum Hall state in which a Pfaffian state of holes forms (see chapter 4). Thus, we expect it to have the largest tunneling amplitude. The other two electron operators are complicated charge- $e$  combinations of the  $\nu = 1$  electron operator and the electron operator of the Pfaffian state of holes. The tunneling Hamiltonian is (the repeated index  $a$  is summed over):

$$H_{\text{tun}} = (t_a \psi_a e^{-2i\phi_\rho} d^\dagger + \text{h.c.}) + V d^\dagger d \partial_x \phi_\rho \quad (5.26)$$

Performing a unitary transformation as before to rotate out the  $\phi_\rho$  dependence of the first term, we obtain  $U H U^\dagger = H_{\text{edge}} + H_{\text{dot}} + \tilde{H}_{\text{tun}}$  where

$$\begin{aligned} \tilde{H}_{\text{tun}} &= (t_a \psi_a d^\dagger + \text{h.c.}) + (V - 2v_c) d^\dagger d \partial_x \phi_\rho \\ &= i\chi_1 (\lambda_1 (d^\dagger - d)/i + \lambda'_1 (d^\dagger + d)) \\ &\quad + i\lambda_2 \chi_2 (d^\dagger + d) + (V - 2v_c) d^\dagger d \partial_x \phi_\rho \end{aligned} \quad (5.27)$$

where  $\chi_1 = u_a \psi_a / \sqrt{u^2}$ ,  $\chi_2 = w_a \psi_a / \sqrt{w^2}$ ,  $u_a = \text{Re } t_a$ ,  $v_a = \text{Im } t_a$ ,  $w_a = v_a - u_a (u \cdot v / u^2)$ ,  $\lambda_1 = \sqrt{u^2}$ ,  $\lambda_2 = \sqrt{w^2}$ ,  $\lambda'_1 = u \cdot v / \sqrt{u^2}$ , and  $\{\chi_1, \chi_2\} = 0$ . Note that, for generic  $t_a$ s, both  $(d^\dagger - d)$  and  $(d^\dagger + d)/i$  couple to the edge modes, as in the *one-channel* Kondo model. This is in contrast to the Pfaffian case, in which only  $(d^\dagger - d)$  couples to the

edge modes, as in the two-channel Kondo model. At the Toulouse point, the *one-channel* Kondo model can be mapped to a form similar to Equation 5.27 with  $V = 2v_c$ . The charge susceptibility and charge of the quantum dot have the temperature and voltage dependence characteristic of a Fermi liquid:

$$\chi_{\text{charge}} \propto \text{const.}, \quad \Delta Q \propto V_G. \quad (5.28)$$

Consequently, measurements of the behavior of the dot would distinguish the Pfaffian and anti-Pfaffian states.

## 5.5 Read-Rezayi State and Quantum Dot

Now we analyze the Read-Rezayi state with filling  $k/(k+2)$ , generalizing our discussion in section 5.3 of the Pfaffian state, which is the  $k = 2$  case. The  $k = 1$  case is the Laughlin  $\nu = 1/3$  state, while the  $k = 3$  case is the  $3/5$  Read-Rezayi state. The edge Hamiltonian of a Read-Rezayi state has the form (section 4.1):

$$H_{\text{edge}} = H_c + H_{Z_k} \quad (5.29)$$

with  $H_c$  the same as the first term in Eq. (5.9).  $H_{Z_k}$  can be written as a gauged  $SU(2)_k$  WZW model in which the  $U(1)$  subgroup has been gauged, thereby realizing an  $SU(2)_k/U(1)$  coset with central charge  $c = \frac{3k}{k+2} - 1 = \frac{2k-2}{k+2}$ , but we will not need this representation here.

The electron operator now takes the form:

$$\Psi_e^\dagger = \psi_1 e^{i\frac{k+2}{k}\varphi}, \quad (5.30)$$

where  $\psi_1$  is a parafermion field. Since  $\dim[\psi_1] = 1 - 1/k$ ,  $\dim[\Psi_e] = 3/2$ , the same scaling dimension of an electron operator in the Pfaffian edge.

As before, we apply a unitary transformation  $U = e^{i\alpha S^z \varphi(0)}$  to  $H$ , which now takes

the form

$$\begin{aligned} UHU^\dagger = & H_{\text{edge}} + H_{\text{dot}} + (V - v_c\alpha) S^z \partial_x \varphi(0) \\ & + t(\psi_1^\dagger e^{-i\tilde{\alpha}\varphi(0)} S^\dagger + \psi_1 e^{i\tilde{\alpha}\varphi(0)} S^-) \end{aligned} \quad (5.31)$$

where  $\tilde{\alpha} \equiv \frac{k+2}{k} - \alpha$ . The choice  $\alpha^* = \frac{k+2}{k} - \sqrt{\frac{k+2}{k}} \sqrt{\frac{2}{k}}$  makes the connection to the  $k$ -channel Kondo problem explicit because the  $SU(2)_k$  current operators can be represented in terms of the  $\mathbb{Z}_k$  parafermions [117]:

$$J^\dagger = \sqrt{k}\psi_1 e^{i\beta\varphi}, J^- = \sqrt{k}\psi_1^\dagger e^{-i\beta\varphi}, J^z = \frac{k}{2}\beta\partial_x\varphi, \quad (5.32)$$

where  $\beta = \sqrt{2(k+2)}/k$ . Substituting these expressions into Equation 5.18 we see that our problem, Equation 5.31, is equivalent to the  $k$ -channel Kondo problem if we identify

$$\begin{aligned} \lambda_\perp &= t, \\ \beta\lambda_z &= V - v_c\alpha^*, \\ , \quad h &= \epsilon_d. \end{aligned} \quad (5.33)$$

For  $V > v_c\alpha^*$ , this is the antiferromagnetic Kondo problem, which has an intermediate coupling fixed point. Thus, we see that the Read-Rezayi states offer a novel scenario to realize the non-Fermi liquid behavior of the  $k$ -channel Kondo model,

$$\chi_{\text{charge}} \propto T^{-(k-2)/(k+2)}, \Delta Q \propto V_G^{2/k} \quad (5.34)$$

which would otherwise require an incredible amount of fine-tuning for  $k \geq 3$ . Moreover, observing the predicted non-Fermi liquid behavior would provide strong evidence that the quantum Hall state is of the Read-Rezayi type.

It can also be shown that the particle-hole conjugate of the Read-Rezayi state at  $\nu = 2 + 2/(k+2)$  generalizes the result obtained above for the anti-Pfaffian: the Kondo model realized is not channel isotropic [118].

## 5.6 Summary

In summary, we have shown that a quantum dot coupled via tunneling to a Pfaffian quantum Hall state realizes the channel isotropic 2-channel Kondo model while a quantum dot coupled to a Read-Rezayi state of filling factor  $\nu = 2 + k/(k + 2)$  leads to a channel isotropic  $k$ -channel Kondo problem, both without any fine tuning of parameters. These systems will thus exhibit all the known non-Fermi liquid properties in their thermodynamics, expressed through the charge on the dot, which may be measured capacitively. Because the coupling of a quantum dot to an anti-Pfaffian state generically exhibits Fermi liquid properties our results may be used to distinguish between the two leading candidate states for  $\nu = 5/2$ , the Pfaffian and the anti-Pfaffian.

## Chapter 6

# Sagnac Interference in Carbon Nanotubes

The method of bosonization, which is used extensively in the study of quantum Hall edge theories, has application in many one-dimensional systems. In this chapter, we use bosonization to study Sagnac interference in non-chiral Carbon nanotube loops, motivated by the experimental results reported in Ref. [119].

Unlike quantum Hall edges, where the Luttinger parameter of the bosonized edge theory is fixed to rational number set by the topological bulk state, the Luttinger parameter in a Carbon nanotube has no such constraint. In addition to explaining the origin of the Sagnac interference in Carbon nanotube loops, we make quantitative predictions regarding the interference amplitude as a function of temperature, bias voltage and Luttinger liquid parameter.

### 6.1 Introduction

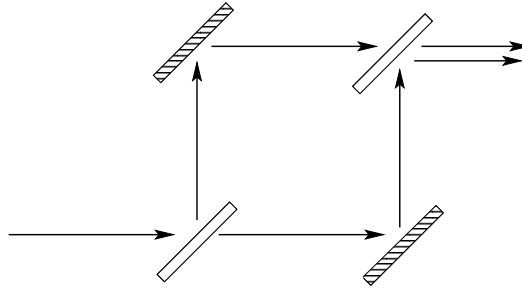
One of the most tantalizing effects predicted by quantum mechanics is the appearance of interference fringes when two *matter* beams come together. These fringes provided the ultimate testimony to the pertinence of quantum mechanics and the Schrödinger equation. Interferometry of light is employed in many precision measurement devices. The Mach-Zehnder interferometer produces interference between two beams traversing two distinct paths, one of which passes through a test chamber containing, for instance, a dilute gas (see Figure 6.1); this setup was originally used to measure the

refraction index of the gas in the chamber. Fabry-Perot interferometer recombines a series of beams, where the  $n$ 'th beam traverses the optical path between two mirrors or through a loop  $n$  times. The narrowness of the resulting interference peaks allows a precise measurement of a light beam's wave length, and is commonly used to measure the Zeeman splitting of an atom in a magnetic field. The most sensitive of all interference constructs, however, is the Sagnac interference[120]. In this setup, a light (or matter [121]) beam is split into two beams, which traverse the interferometer's loop both clock wise and counter clock wise, before being recombined. In this case, the interference fringes arise due to an absolute rotation, and provide the most accurate measure of the angular velocity of the device. This was used by Michelson to measure the absolute rotation of the Earth. More recently, the Sagnac interference effect was cleverly used to measure time reversal symmetry breaking in superconductors [122].

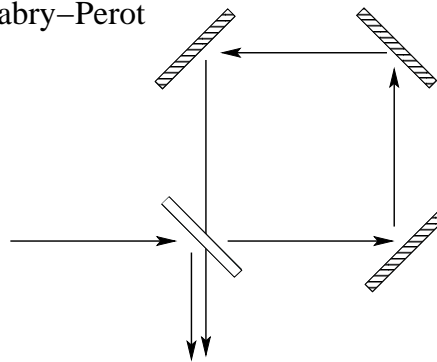
Quantum mechanics opened the way for matter-wave interferometry. Electron interferometry is a powerful probe of interaction effects on low-energy phases of quantum matter, as demonstrated by numerous examples. Mach-Zehnder interferometers reveal Aharonov-Bohm oscillations and quantum hall effect edge channels[123, 124, 125, 126, 127], and can probe exotic fractional quantum Hall states[128, 58, 129]. Similarly, two-path Mach-Zehnder interferometers can probe correlated states of quantum dots[130, 131]. Of particular interest to us are metallic carbon nanotubes. The Luttinger liquid behavior in these systems[132, 133, 134] was partially verified through the observation of Fabry-Perot interference in finite sections of the nanotube [135]. The Fabry-Perot interference should, in principle, allow the observation of spin-charge separation and determination of the interaction parameters of the Luttinger liquid [136]. But the similar energy scales of the spin and charge modes' interference patterns has made such experimental observation challenging.

The most sensitive interferometer of all, however, the Sagnac interferometer, has not been seriously explored yet in the context of interacting electronic systems. In Ref. [119] we proposed that this interference naturally occurs in metallic armchair nanotube loops (Figure 6.2). Instead of rotation, the Sagnac interference arises due to the band velocity difference between right- and left-moving electrons about each

a. Mach–Zehnder



b. Fabry–Perot



c. Sagnac

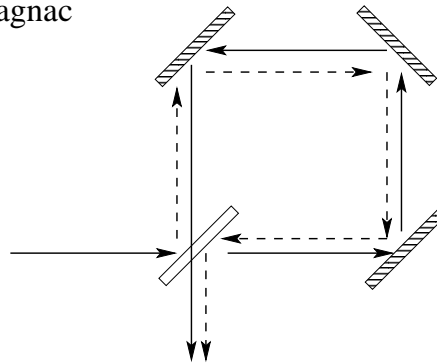


Figure 6.1: (a) In a Mach-Zehnder interferometer the input beam is split into two beams which traverse independent paths before being recombined. (b) In a Fabry-Perot interferometer a beam is split into a deflected ray, which is recombined at the output with a ray that traverses a loop. (c) The Sagnac interferometer splits the beam into a two beams which traverse the loop in two opposite orientations, and get recombined at the output. This allows a very sensitive measurement of the angular velocity of the interferometer, as it results in a different relative speed in the clockwise and counterclockwise rays. Clear rectangles represent beam-splitters, and patterned rectangles represent mirrors.

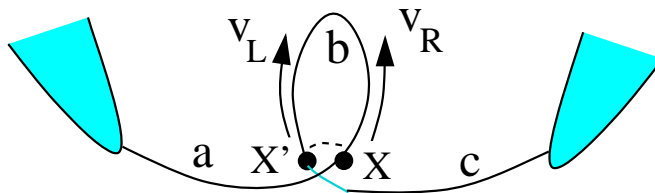


Figure 6.2: Schematic of a nanotube loop reported in Ref. [119]. This geometry allows electrons to tunnel from the point  $X$  on the loop to a distant point  $X'$  on the other end of the loop, and vice versa. We refer to this process as cross-loop tunneling. An electron entering from the left can traverse the loop moving right with velocity  $v_R$ , without scattering, or tunnel from  $X$  to  $X'$  and traverse the loop moving left with velocity  $v_L$ .

Dirac node [137]. This velocity difference is present whenever the electronic Fermi surface is tuned away from the Dirac points at half-filling, as shown in Figure 6.3(a). The operating principle of the electronic Sagnac effect has the same origin as the universal conductance fluctuations, and weak-localization effects in disordered two-dimensional electron gases [138, 139, 140]. In nanotubes, it can also appear due to band-scattering in a pair of impurities [141].

Because the Sagnac effect involves electrons traversing the same path in two different directions, rather than repeating the same path as in Fabry-Perot interference, the phase accumulation is extremely small. Therefore Sagnac interference exhibits large-period conductance fluctuations as a function of gate- and source-drain voltages, and is expected to persist to high temperatures in comparison to Fabry-Perot interference, which is more sensitive to thermal dephasing. This interference mode should thus be able to reveal much more precise information about the unique state of interacting electrons in thin quantum wires.

Our goal in this manuscript is to thoroughly explore the range and robustness of the Sagnac interference mode, concentrating on armchair Carbon nanotubes. The questions we will ask concern the amplitude of this interference mode as a function of the temperature, gate and source-drain voltage, and Luttinger parameter of the nanotube.

This chapter is organized as follows. In section 6.2, as a warm-up, we analyze

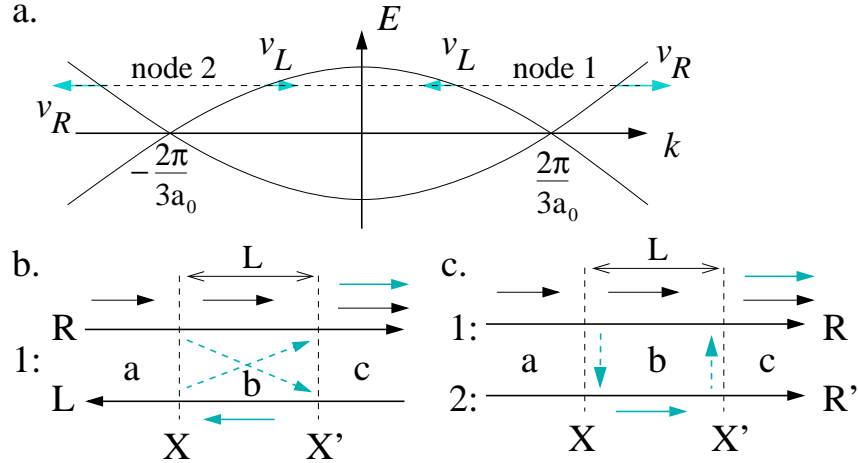


Figure 6.3: (a) The energy spectrum of an armchair nanotube. When the chemical potential is tuned away from the degeneracy points by a gate voltage, the left and right movers in each node will have different velocities, which leads to the Sagnac interference in the loop geometry. (b) This figure shows right and left moving electrons in node 1. The loop was unraveled in this figure, so the tunneling appears to be non-local, from point  $X$  to point  $X'$ , the two ends of the loop. The scattering shown in figure is from a right moving electron from a given node at point  $X$  to a left moving electron, of the same node, at point  $X'$ , and vice versa. This scattering gives rise to the Sagnac interference. (c) Sagnac interference can also arise without the loop geometry through inter-node tunneling, since right movers at node 2 have the same velocity as left movers at node 1.

the simpler case of Sagnac interference in a single channel of right- and left-moving electrons. In subsection 6.2.1 we introduce the model of a single channel with a linearized spectrum, and the cross-loop tunneling which will give rise to the Sagnac interference. In subsection 6.2.2 and subsection 6.2.3 we set up the non-equilibrium perturbative calculation of the conductance in the presence of cross-loop tunneling, and in subsection 6.2.4 and subsection 6.2.5 we analyze the behavior of the oscillating conductance as a function of gate and bias voltages and temperature. In Section section 6.3 we repeat the above steps for the physically relevant case of Carbon nanotubes, including spin and node degeneracies in the calculation, and remark on the similarities and differences from the single channel case. Finally we conclude with a discussion of the experimental implications of our calculations.

## 6.2 Sagnac interference in a single channel

As discussed in the introduction, the Sagnac interference in the loop geometry is due to the asymmetry between the velocities of the left and right moving electrons. To demonstrate this in the simplest form, we first study in this section a single channel with a single type of left and right movers. In a carbon nanotube, there will be four such channels due to spin and node degeneracies.

### 6.2.1 The Model

We start with a single one dimensional channel of electrons and a linearized spectrum, with different left and right mover velocities, and a density-density interaction. The Hamiltonian density for this system is:

$$\begin{aligned} \mathcal{H}_{1ch} = & -i\hbar v_R \psi_R^\dagger \partial_x \psi_R + i\hbar v_L \psi_L^\dagger \partial_x \psi_L \\ & + \lambda \left( \psi_R^\dagger \psi_R + \psi_L^\dagger \psi_L \right)^2 \end{aligned} \quad (6.1)$$

where the operator  $\psi_{R/L}^\dagger$  creates a right/left moving electron, with the velocity:

$$v_{R/L} = v_F \pm u. \quad (6.2)$$

The scattering we are interested in is the one which takes a right moving electron at one side of the loop, point  $X$  in Figure 6.2, and scatters it to a left moving electron at the other side of the loop, point  $X'$ , and vice versa. This process has been dubbed Cross-Loop scattering in Ref. [[119]]. If we choose our coordinate along the loop such that the point  $X$  corresponds to  $x = 0$  and the point  $X'$  corresponds to  $x = L$ , then this scattering process is described by the Hamiltonian:

$$\begin{aligned} H_{bs} = & \Gamma_1 \psi_R^\dagger(0) \psi_L(L) + h.c. \\ & + \Gamma_2 \psi_L^\dagger(0) \psi_R(L) + h.c. \end{aligned} \quad (6.3)$$

In the presence of the quartic density-density interactions in the Hamiltonian, Equation 6.1, it is useful to use the standard bosonization procedure, since the Hamiltonian is quadratic in terms of the bosonic fields. The electron fields are bosonized as follows:

$$\psi_{R/L} \sim e^{i(\phi \pm \theta)} \quad (6.4)$$

where  $\theta$  and  $\phi$  are bosonic fields that satisfy the commutation relations  $[\theta(x), \phi(x')] = i(\pi/2)\text{sgn}(x - x')$ ; also, the total density and the current density are given by  $\frac{1}{\pi}\nabla\theta = \rho_R + \rho_L$ , and  $\frac{1}{\pi}\nabla\phi = \rho_R - \rho_L$ , respectively. The Hamiltonian in terms of the bosonic fields becomes:

$$H_{1ch} = \frac{\hbar v}{2\pi} \int dx \left[ \frac{1}{g}(\nabla\theta)^2 + g(\nabla\phi)^2 + 2\frac{u}{v}\nabla\theta\nabla\phi \right] \quad (6.5)$$

where  $g = \left(1 + \frac{2\lambda}{\pi\hbar v_F}\right)^{-1/2}$  is the Luttinger interaction parameter and  $v = v_F/g$ . This is the familiar Hamiltonian of a 1D interacting electron system, with the addition of the  $u$  term which gives left and right moving particles different velocities. Indeed, this Hamiltonian can be easily diagonalized and the left and right velocities turn out to be for a general value of the interaction parameter  $g$ :

$$v_{R/L} = v \pm u = \frac{v_F}{g} \pm u. \quad (6.6)$$

Our goal is to calculate the effects of the Sagnac interference as seen in the conductance as a function of the applied bias and gate voltages, and as a function of temperature. Due to the applied voltages the system is not in equilibrium, and we must turn to the Keldysh non-equilibrium formalism [142, 143]. Below we carry out this analysis first for the simplified electron gas with the scattering Hamiltonian  $H_{bs}$ , Equation 6.3, as a perturbation.

### 6.2.2 Non-Equilibrium correlation functions and conductance

The response of the loop to a bias source-drain voltage can be analyzed using the non-equilibrium Keldysh formalism. Following Ref.[136], we assume that in the distant past, before turning on the backscattering, the left and right moving electrons separately had well defined thermal distributions set by separate chemical potentials. The density matrix corresponding to this initial distribution at temperature  $T = 1/\beta$  is:

$$\hat{\rho}_V = \frac{1}{Z_V} e^{-\beta \hat{H}_V}, \quad (6.7)$$

with  $Z_V = Tr[e^{-\beta \hat{H}_V}]$  and the Hamiltonian which takes into account the applied voltages is:

$$\begin{aligned} H_V &= H_{1ch} - e \frac{V_{sd}}{2} (N_R - N_L) - \alpha e V_g (N_R + N_L) \\ &= H_{1ch} - e \frac{V_{sd}}{2} \int dx \frac{\nabla \phi}{\pi} - \alpha e V_g \int dx \frac{\nabla \theta}{\pi} \end{aligned} \quad (6.8)$$

The gate voltage,  $V_g$ , simply couples to the total charge density, with  $\alpha$  being a geometrical factor of the system, while the source-drain voltage,  $V_{sd}$ , induces the imbalance in the chemical potentials of the left and right movers.

As explained in Ref. [136], both  $V_{sd}$  and  $V_g$  can be eliminated from the unperturbed action by an appropriate unitary transformation, which is equivalent to shifting the bosonic fields by a function of space and time; this is easy to see if one writes down the Lagrangian including the voltages[119]. The equivalent shifts for the case at hand are:

$$\begin{aligned} \theta &\rightarrow \theta + \frac{\alpha g^2 e V_g}{\hbar v_F} \frac{1}{1 - g^2 u^2 / v_F^2} x - \frac{e V_{sd}}{2 \hbar} t, \\ \phi &\rightarrow \phi - \frac{\alpha g^2 e V_g}{\hbar v_F} \frac{u / v_F}{1 - g^2 u^2 / v_F^2} x, \end{aligned} \quad (6.9)$$

These shifts remove the voltages from the Hamiltonian  $H_V$  and therefore all the correlations to appear in the calculation will be equilibrium correlation functions with respect to  $H_{1ch}$ . The dependence on the applied voltages now appears in the

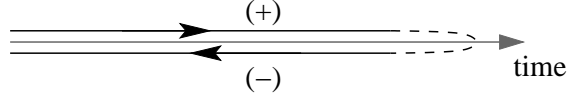


Figure 6.4: The Keldysh contour used in the non-equilibrium calculation. The Keldysh time ordering operator  $T_K$  orders operators along the contour, so fields on the (+) branch is always at an earlier time than fields on the (-) branch.

scattering Hamiltonian,  $H_{bs}$ , due to the shifted bosonic fields.

Let us now focus our attention at the charge current, which in the bosonic language is  $\hat{I} = (e/\pi)\partial_t\theta$ . After performing the unitary transformation described above we can write the formal expression for the expectation value of the current in the usual interaction picture [136]:

$$\langle I \rangle = I_0 + \frac{1}{Z_{V=0}} \text{Tr} \left( e^{-\beta H_{1ch}} \hat{T}_K \left\{ \hat{I}_K(x, t) e^{-i \int_C dt' H'_{bs}(t')} \right\} \right) \quad (6.10)$$

$\hat{T}_K$  is the time ordering operator along the Keldysh contour shown in Figure 6.4, and  $\hat{I}_K(x, t)$  is the symmetrized current operator with respect to the two branches of the contour. The current  $I_0 = e^2 V_{sd}/h$  is the ideal current that would flow in the absence of backscattering in a completely transmitting channel, and it explicitly appears due to the shift of the  $\theta$  field. The Hamiltonian  $H'_{bs}$  denotes the scattering Hamiltonian  $H_{bs}$  with the properly shifted bosonic fields. The expression for the current can be expanded in powers of  $H'_{bs}$ , and all the correlation functions to appear in this expansion are equilibrium correlation functions at temperature  $1/\beta$ . If we denote by  $\theta^+$  and  $\theta^-$  the fields on the forward branch and backward branch of the Keldysh contour respectively, then time ordering along the contour means that  $\theta^+\theta^+$  correlations have the usual time ordering,  $\theta^-\theta^-$  are anti-time ordered, and  $\theta^+(t)$  is always earlier in time than  $\theta^-(t')$ . The same applies for all the fields.

It is useful to apply a Keldysh rotation to the fields,  $\theta^\pm = \theta \pm \frac{i}{2}\tilde{\theta}$ , and similarly for  $\phi$ . The correlation function  $\langle T_K \tilde{\theta}(t)\tilde{\theta}(t') \rangle$  vanishes by construction, and we define

:

$$\begin{aligned}
C^{\theta}(x, t; x', t') &= \langle T_K \theta(x, t) \theta(x', t') \rangle \\
&= \frac{1}{2} \langle \{ \hat{\theta}(x, t), \hat{\theta}(x', t') \} \rangle \\
R^{\theta}(x, t; x', t') &= \langle T_K \theta(x, t) \tilde{\theta}(x', t') \rangle \\
&= -i\Theta(t - t') \langle [ \hat{\theta}(x, t), \hat{\theta}(x', t') ] \rangle
\end{aligned} \tag{6.11}$$

and similarly for the  $\phi_j$  fields, and for the mixed correlations:

$$\begin{aligned}
C^{\theta\phi}(x, t; x', t') &= \langle T_K \theta(x, t) \phi(x', t') \rangle \\
&= \frac{1}{2} \langle \{ \hat{\theta}(x, t), \hat{\phi}(x', t') \} \rangle \\
R^{\theta\phi}(x, t; x', t') &= \langle T_K \theta(x, t) \tilde{\phi}(x', t') \rangle \\
&= -i\Theta(t - t') \langle [ \hat{\theta}(x, t), \hat{\phi}(x', t') ] \rangle
\end{aligned} \tag{6.12}$$

where operators with a hat are simply the time dependent operators with no time ordering. As explained above, these correlation function are to be evaluated in equilibrium, and therefore are easily explicitly calculated (section 6.B). Due to translational invariance in time and space, these correlations are functions of  $x - x'$  and  $t - t'$ , for example:

$$\begin{aligned}
C^{\theta\phi}(x, t) &\equiv C^{\theta\phi}(x, t; 0, 0) = \\
&\frac{1}{4} \left[ \log \left( v_R \sinh \left( \frac{(v_R t - x)\pi}{\beta v_R} \right) \right) \right. \\
&\left. - \log \left( v_L \sinh \left( \frac{(v_L t + x)\pi}{\beta v_L} \right) \right) \right].
\end{aligned} \tag{6.13}$$

### 6.2.3 Perturbation Theory

The Sagnac interference fringes occur already with weak backscattering at the base of the loop, and can be deduced from a perturbation analysis of the tunneling Hamiltonian, Equation 6.3. As outlined above, to calculate the current,  $I_{1ch} = \langle \frac{e}{\pi} \partial_t \theta \rangle$ ,

we absorb the gate and bias voltages,  $V_g$  and  $V_{sd}$  respectively, in the shifts in Equation 6.9, which allow us to move the voltages from the unperturbed Hamiltonian  $H_{1ch}$  to the backscattering perturbation,  $H_{bs}$ . Then, we expand the formal expression we found for the current using the Keldysh technique, Equation 6.10, in powers of  $H_{bs}$ , and use Wick's theorem to evaluate the resulting contributions.

To lowest nontrivial order, which is second order in  $H_{bs}$ , we obtain after a lengthy calculation:

$$I_{1ch} = \frac{e^2 V_{sd}}{h} + I_{co} + I_{inco} \quad (6.14)$$

The first term is simply the current that would flow through the system in the absence of backscattering. The coherent current,  $I_{co}$ , oscillates with the gate voltages  $V_g$ , and is given by:

$$I_{co} = c \Gamma_1 \Gamma_2 \cos \left( \frac{2ug^2 L \alpha}{\hbar^2 v_F^2 (1 - g^2 u^2 / v_F^2)} V_g \right) \times \int dt \sin \left( \frac{eV_{sd}}{\hbar} t \right) e^{-C_{co}(L,t)} \sin(R_{co}(L,t)) \quad (6.15)$$

where  $c$  is a constant of order unity, and we assume that  $\Gamma_i$  are real for simplicity. The incoherent current,  $I_{inco}$ , is independent of the gate voltage, and is given by:

$$I_{inco} = c \left( \Gamma_1^2 \sum_{\eta=\pm} \int dt \sin \left( \frac{eV_{sd}}{\hbar} t \right) e^{-C_{inco}^\eta(L,t)} \sin(R_{inco}(L,t)) \right) + c (\Gamma_1 \rightarrow \Gamma_2, L \rightarrow -L) \quad (6.16)$$

The functions  $C_{co}$ ,  $C_{inco}^\pm$ ,  $R_{co}$  and  $R_{inco}$  are complicated combinations of the correlation functions defined in subsection 6.2.2 and are given explicitly in section 6.B. These functions do not simplify, partly due to the fact that the correlation functions in this problem are not symmetric under  $x \rightarrow -x$  since left and right movers have different velocities.

### 6.2.4 Voltage dependence of the single-mode Sagnac interference

The voltage current characteristics given in Equation 6.14 - Equation 6.16 can be evaluated numerically to obtain the voltage and temperature dependence of the single-mode Sagnac interference. The period of the interference as a function of the gate voltage ( $I_{co}$ ) are easily observed to be (for small  $u/v_F$ ):

$$\Delta V_g^{Sagnac} \approx \frac{v_F}{u} \frac{\pi \hbar^2 v_F}{\alpha g^2 L} = \frac{v_F}{u} \Delta V_g^{FP} \quad (6.17)$$

where  $\Delta V_g^{FP}$  is the period in gate voltage for Fabry-Perot interference. Fabry-Perot interference occurs whenever part of the wave's trajectory can be repeated. Since the Sagnac interference involves traversing the same path in two different directions, the phase difference accumulated in the process is much smaller than the difference incurred by repeating part of the path, and therefore the period of the Sagnac interference is much larger than the period of the Fabry-Perot interference. Such large period oscillations have been experimentally observed in Carbon nanotubes, in the loop geometry, as reported in Ref.[119], in addition to the shorter period Fabry-Perot oscillations.

For a given gate voltage, both the coherent and incoherent parts of the current oscillate with the bias voltage  $V_{sd}$ . This oscillation is due to the fact that in the presence of bias voltage, the Fermi energy of the left- and right- moving electrons are different by  $V_{sd}$ , and hence their Fermi wavevectors are different also and they would acquire different phases traversing the loop. This oscillation will be present even for no velocity detuning,  $u = 0$ . When the detuning is finite,  $u \neq 0$ , the differential conductance  $G_{1ch} = \partial I_{1ch} / \partial V_{sd}$  will show a beating pattern due to the two different left and right moving excitation velocities. Here we are only considering the Sagnac oscillations arising from the cross-loop tunneling, Equation 6.3. Figure 6.5 shows the oscillations of the differential conductance at a fixed gate voltage. For non-interacting electrons, the beating pattern corresponds to the addition of two harmonics with

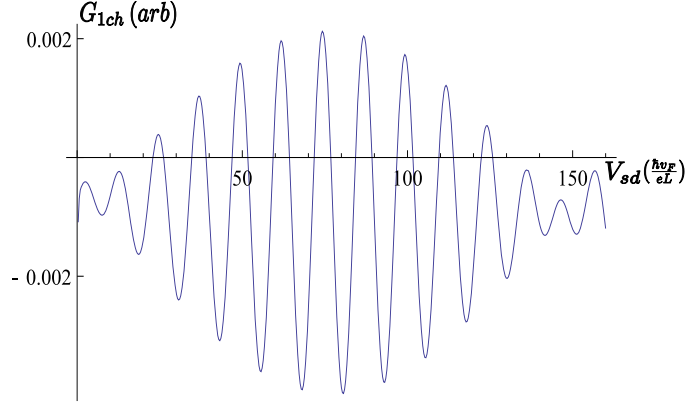


Figure 6.5: Differential conductance oscillations of a single channel of fermions, as a function of bias voltage  $V_{sd}$ , for velocity detuning  $u/v_F = 0.1$  and interaction strength  $g = 0.5$ . The beating is due to the only two voltage oscillation frequencies in the problem,  $\Omega_1 = \frac{eL}{\hbar(v+u)}$  and  $\Omega_2 = \frac{eL}{\hbar(v-u)}$ , where  $v = v_F/g$ . The voltage is in units of  $\hbar v_F/eL$ . The shorter voltage oscillation periods is  $\Delta V_{sd} = 2\pi \left(\frac{\Omega_1 + \Omega_2}{2}\right)^{-1} \approx 12.5 \hbar v_F/eL$ , and the large oscillation period is  $\Delta V_{sd} = 2\pi \left(\frac{\Omega_1 - \Omega_2}{2}\right)^{-1} \approx 250 \hbar v_F/eL$ .

two different frequencies in voltage,  $\sin(\Omega_R V_{sd})$  and  $\sin(\Omega_L V_{sd})$ , with  $\Omega_{R/L} = \frac{eL}{\hbar v_{R/L}}$  and  $v_{R/L} = v_F \pm u$ . The beating pattern will then display fast oscillations with voltage period  $\Delta V_{sd}^{fast} = 2\pi \left(\frac{|\Omega_R + \Omega_L|}{2}\right)^{-1}$ , and slow voltage oscillations with period  $\Delta V_{sd}^{slow} = 2\pi \left(\frac{\Omega_R - \Omega_L}{2}\right)^{-1}$ . For interacting fermions,  $g \neq 1$ , the oscillations will not be simple harmonic oscillations. Still, the periods will be evident and will have the same functional form, in terms of  $v_{R/L}$ , as the frequencies in the non-interacting case. The periods  $\Delta V_{sd}^{fast}$  and  $\Delta V_{sd}^{slow}$  do depend on  $g$  through velocities  $v_L$  and  $v_R$ ,  $v_{R/L} = \frac{v_F}{g} \pm u$  (Equation 6.6).

These oscillation, generally, lie atop a powerlaw behavior of the differential conductance as a function of  $V_{sd}$ , as expected from the known behavior of the conductance in the presence of impurity backscattering [144]. For backscattering from an impurity in a Luttinger liquid, the backscattered current, for low temperature, behaves as  $I \propto V_{sd}^{2g-1}$ . We chose to plot the Sagnac oscillations as a function of  $V_{sd}$  (Figure 6.5) for the interaction parameter  $g = 0.5$  since for that value the corresponding power law would be  $I \propto V_{sd}^0$ , and the contribution of such a powerlaw to the *differential* conductance would vanish, making the oscillation atop this powerlaw more visible.

### 6.2.5 Temperature dependence of the single-mode Sagnac interference

Next we consider the temperature dependence of the gate-voltage driven oscillations in the coherent part of the current. As argued in Ref. [119], the large period Sagnac oscillations are expected to be observed at much higher temperature than the shorter period Fabry-Perot oscillations. This difference in temperature behavior can be easily understood by examining the phase giving rise to the interference in both cases. In the Fabry-Perot case for a loop, the lowest order interference is between a beam of electrons which is not scattered, and a beam of electrons which, due to scattering at the base of the loop, does a roundtrip between the two scattering points. The phase difference between these two beams at energy  $E$  is  $\Delta\phi_{FP} = k_R L = \frac{1}{v_R} L \frac{E}{\hbar}$ . Finite temperature effectively causes uncertainty of order  $T$  in the energy  $E$ , and the interference pattern will be washed out when the uncertainty of the phase  $\Delta\phi_{FP}$  is of order  $2\pi$ , which happens at a temperature  $T_{FP} = \frac{2\pi\hbar}{L} v_R$ .

In the Sagnac case, the interference is between a beam that traverses the loop moving left and one which traverses the loop moving right. The phase difference between these two beams at energy  $E$  is  $\Delta\phi_{SAG} = k_L L - k_R L = \left(\frac{1}{v_L} - \frac{1}{v_R}\right) L \frac{E}{\hbar}$ , and this interference will be washed out at temperature  $T_{SAG} = \frac{2\pi\hbar}{L} \left(\frac{1}{v_L} - \frac{1}{v_R}\right)^{-1}$ . For non-interacting electrons the right and left moving velocities are  $v_{R/L} = v_F \pm u$ . Thus to lowest order in  $u/v_F$ , the highest temperatures for observing interference according to the argument above are:

$$T_{FP} \approx \frac{\pi\hbar v_F}{L}; \quad T_{SAG} \approx \frac{\pi\hbar v_F}{L} \frac{v_F}{u} = T_{FP} \cdot \frac{v_F}{u} \quad (6.18)$$

For non-interacting electrons, we expect the Sagnac interference to survive to a temperature higher by a factor of  $v_F/u$  than the corresponding Fabry-Perot temperature. We will show through explicit calculation that this is indeed true for the non-interacting case. For interacting electrons, we will see that  $T_{SAG}$  will still be considerably larger than  $T_{FP}$ , but their ratio is less than the dramatic  $v_F/u$  ratio.

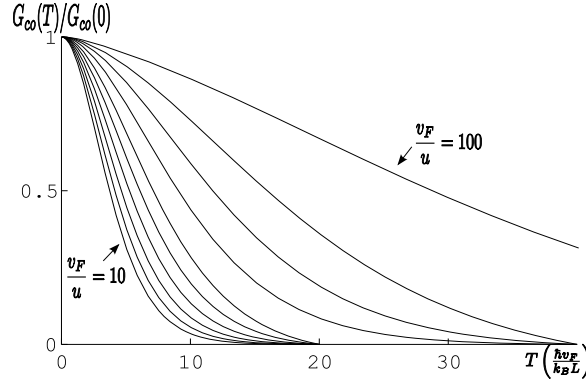


Figure 6.6: Coherent Sagnac oscillation amplitude vs. temperature for different values of  $(v_F/u)$ , for noninteracting electrons ( $g = 1$ ). The slowest decaying plot corresponds to  $v_F/u = 100$ , and the fastest decaying plot corresponds to  $v_F/u=10$ . Temperature is given in units of  $\hbar v_F/k_B L$ .

To explore the Sagnac temperature range, we evaluate the amplitude of the coherent oscillations (the oscillations in  $V_g$ ) as a function of temperature, for different interaction parameters  $g$  and different ratios of  $u/v_F$ . For non-interacting electrons,  $g = 1$ , we find that the Sagnac oscillations indeed survive up to a high temperature, which is a factor of  $v_F/u$  higher than the corresponding Fabry-Perot oscillations. Figure 6.6 plots the oscillation amplitude as a function of temperature, normalized by its zero-temperature value, and for different values of  $u/v_F$ . The functional dependence on temperature is given approximately by:

$$\frac{G_{co}(T)}{G_{co}(T=0)} = \left( \frac{2\pi k_B L T}{\hbar v_F} \right) \left( \frac{u}{v_F} \right) \frac{1}{\sinh(2\pi k_B T \frac{L}{\hbar v_F} \frac{u}{v_F})} \quad (6.19)$$

This result is similar to the exact form of the temperature dependence of the Fabry-Perot interference amplitude [145], with the only difference being the factor of  $u/v_F$ . Therefore, the Sagnac oscillations of non-interacting electrons indeed survive up to a temperatures which are a factor of  $v_F/u$  larger than the Fabry-Perot oscillations.

For interacting electrons,  $g \neq 1$ , the Sagnac interference still survives up to temperatures significantly higher than the corresponding Fabry-Perot temperature scales, but the enhancement is suppressed compared to that of non-interacting electrons. Figure 6.7 shows the Sagnac temperature scale  $T^*$  vs.  $u/v_F$  for three different values

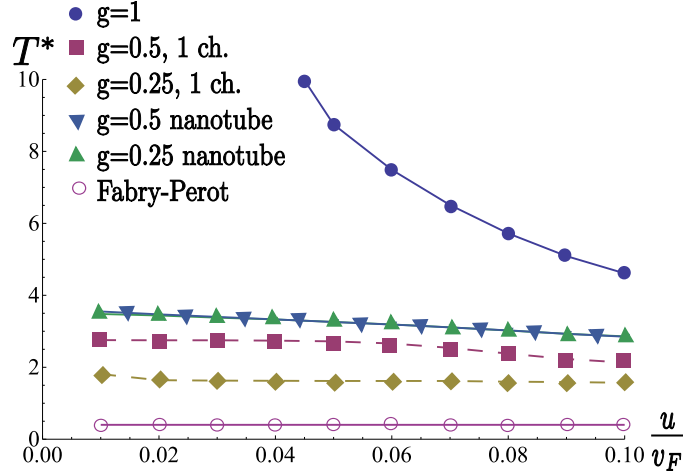


Figure 6.7:  $T^*$  vs.  $u/v_F$ , where  $T^*$  is the temperature at which the coherent differential conductance (the part of the conductance which oscillates with gate voltage) reaches  $e^{-1}$  of its zero temperature value. For a non-interacting system,  $g = 1$ , the single channel case gives the same temperature dependence as the case with spin and node degeneracies,  $T^* \propto v_F/u$ . The single channel temperature dependence is given for  $g = 0.5$  (squares, dashed), and  $g = 0.25$  (diamonds, dashed). The Carbon nanotube temperature dependence is given for  $g = 0.5$  (triangles), and  $g = 0.25$  (inverted triangles). Temperature is given in units of  $\hbar v_F/k_B L$ . For reference, the  $T^*$  corresponding to the  $g = 1$  Fabry-Perot oscillations is also plotted.

of the interaction parameter  $g$ , where we define  $T^*$  to be the temperature at which the amplitude of the oscillations reaches  $e^{-1}$  of its amplitude at zero temperature. For non-interacting electrons  $T^*$  is strongly dependent on the ratio  $u/v_F$  as discussed above. For the interaction parameter values  $g = 0.5$  and  $g = 0.25$  (Dashed lines), the temperature  $T^*$  is only weakly dependent on the ratio  $u/v_F$ . As an example for the resulting enhancement of the Sagnac compared to the Fabry Perot interference, consider  $g = 0.25$ , where the  $T^*$  temperature scale for the Sagnac oscillations is roughly  $1.6 \hbar v_F/k_B L$ , a factor of 4 enhancement over  $T^*$  of the non-interacting Fabry-Perot oscillations which is  $0.42 \hbar v_F/k_B L$ , despite the suppression of the Sagnac  $T^*$  due to interactions. As can be seen in the figure, for  $g = 0.5$  the enhancement is about 7. While it is difficult to extract the analytic dependence of the temperature on the interaction parameter, one can repeat our calculation for any value of  $g$ .

## 6.3 Interference in Nanotubes

Equipped with our understanding of the single-channel Sagnac interference, we can now consider the likely physical system where it may be observed: a metallic Carbon nanotube with four different Dirac nodes. We now add the spin and node degeneracies of a Carbon nanotube, and examine their effect on the Sagnac interference pattern voltage and temperature dependence.

### 6.3.1 The Model

The energy spectrum of a Carbon nanotube is shown in Figure 6.3 a. This spectrum is usually linearized around the Fermi surface, which yields four chiral modes, two left moving and two right moving (not including spin), with linear dispersion. These modes can be bosonized and treated within the Luttinger Liquid theory framework, as we have done in the single channel case in the previous sections. All these modes are usually assumed to have the same velocity, the Fermi velocity  $v_F$ . For the purposes of this chapter, it is important to notice that when the Fermi surface is away from the degeneracy points where the upper and lower bands meet, linearizing the spectrum actually gives two different velocities which we shall note  $v_{\pm} = v_F \pm u$ . The linearized Hamiltonian density is, then:

$$\begin{aligned} \mathcal{H}_{Ach} = & i \sum_{a=1}^2 \sum_{\sigma=\uparrow,\downarrow} \left( v_{Ra} \psi_{Ra\sigma}^{\dagger} \partial_x \psi_{Ra\sigma} - v_{La} \psi_{La\sigma}^{\dagger} \partial_x \psi_{La\sigma} \right) \\ & + \lambda \left[ \sum_{a=1}^2 \sum_{\sigma=\uparrow,\downarrow} \left( \psi_{Ra\sigma}^{\dagger} \psi_{Ra\sigma} + \psi_{La\sigma}^{\dagger} \psi_{La\sigma} \right) \right]^2 \end{aligned} \quad (6.20)$$

where  $\psi_{R/La\sigma}$  stands for a right/left moving electron at node  $a$  with spin  $\sigma$ , and we added a total charge density interaction term. The velocities that appear in the

Hamiltonian are:

$$\begin{aligned} v_{R/L1\sigma} &= v_F \pm u = v_{\pm} \\ v_{R/L2\sigma} &= v_F \mp u = v_{\mp}. \end{aligned} \quad (6.21)$$

Thus for  $u > 0$ , at node 1 right movers are faster than left movers, while at node 2 the opposite is true. Now, the nonlinearity of the electronic spectrum in a Carbon nanotube needs to be taken into account when considering the velocity difference,  $u$ ; it depends on the detuning of the chemical potential away from the degeneracy points.

The scattering process we are interested in is very similar to the one we had in the single channel case. We need to consider a term that scatters a right mover at one end of the loop to a left mover at the other end of the loop, conserving spin and node quantum numbers,

$$\begin{aligned} H_{bs} &= \sum_{\sigma,a=1,2} \left[ \Gamma_1 \psi_{Ra\sigma}^\dagger(0) \psi_{La\sigma}(L) + h.c. \right. \\ &\quad \left. + \Gamma_2 \psi_{La\sigma}^\dagger(0) \psi_{Ra\sigma}(L) + h.c. \right]. \end{aligned} \quad (6.22)$$

Next we bosonize the electron field operators in the nanotube. The slowly oscillating parts can be written as:

$$\psi_{R/La\sigma} \sim e^{i(\phi_{a\sigma} \pm \theta_{a\sigma})} \quad (6.23)$$

where  $\theta_{a\sigma}$  and  $\phi_{a\sigma}$  are bosonic fields that satisfy the commutation relations  $[\theta_{a\sigma}(x), \phi_{a'\sigma'}(x')] = i(\pi/2)\delta_{a,a'}\delta_{\sigma,\sigma'}\text{sgn}(x-x')$ . The Hamiltonian in terms of the bosonic fields is [119]:

$$\begin{aligned} H_{4ch} &= \frac{\hbar v_F}{2\pi} \sum_{\sigma,a=1,2} \int dx \left[ (\nabla \theta_{a\sigma})^2 + (\nabla \phi_{a\sigma})^2 \right. \\ &\quad \left. + (-1)^{a+1} 2 \frac{u}{v_F} \nabla \phi_{a\sigma} \nabla \theta_{a\sigma} \right] + \int dx \lambda \left( \sum_{\sigma,a=1,2} \frac{1}{\pi} \nabla \theta_a^\sigma \right)^2. \end{aligned} \quad (6.24)$$

If the velocities of all branches of the spectrum were equal, i.e.  $u = 0$ , then the Hamil-

tonian  $H_B$  would be diagonalized by the spin and node symmetric and antisymmetric combinations of the  $\theta$ 's and  $\phi$ 's [133]. By diagonalizing we mean a linear mapping of the  $\phi$  and  $\theta$  fields such that the Hamiltonian takes the form of four independent channels, each resembling of  $H_{1ch}$ , Equation 6.5. When  $u \neq 0$ , there still exists a local transformation  $\theta_{a\sigma} = \sum_{j=1..4} (A_{a\sigma}^j \theta_j + B_{a\sigma}^j \phi_j)$  that diagonalizes the Hamiltonian, but it is a more complicated combination of the fields that depends on  $u$  and  $\lambda$ , and mixes the *theta* and  $\phi$  fields, which makes the conductance calculation quite cumbersome. While the details of this transformation are given in section 6.A, the diagonal Hamiltonian is:

$$\begin{aligned}
H_{4ch} = & \sum_{j=3,4} \frac{\hbar v_j}{2\pi} \int dx \left[ \frac{1}{g_j} (\nabla \theta_j)^2 + g_j (\nabla \phi_j)^2 \right] \\
& + \sum_{j=1,2} \frac{\hbar v_F}{2\pi} \int dx \left[ (\nabla \theta_j)^2 + (\nabla \phi_j)^2 \right. \\
& \left. + (-1)^{j+1} 2 \frac{u}{v_F} \nabla \phi_j \nabla \theta_j \right]. \tag{6.25}
\end{aligned}$$

The fields  $\theta_{1/2}$  and  $\phi_{1/2}$  are the spin antisymmetric combinations of  $\theta_{1/2\sigma}$  and  $\phi_{1/2\sigma}$  respectively. Since the interaction term in Equation 6.20 involves only the spin symmetric combinations, the spin antisymmetric combinations are untouched and still have the left and right moving velocities as in Equation 6.21. On the other hand, the fields  $\theta_{3/4}$  and  $\phi_{3/4}$  are not simply the remaining symmetric combination and mix the remaining  $\theta$ 's and  $\phi$ 's. These fields have the same left and right moving velocity, which is:

$$v_{3/4} = \frac{v_F}{\sqrt{2}} \sqrt{1 + \frac{1}{g^2} + 2 \frac{u^2}{v_F^2} \pm \sqrt{\left(1 - \frac{1}{g^2}\right)^2 + 8 \frac{u^2}{v_F^2} \left(1 + \frac{1}{g^2}\right)}} \tag{6.26}$$

where  $g = \left(1 + \frac{8\lambda}{\pi \hbar v_F}\right)^{-1/2}$  is the Luttinger parameter.[146]

Fortunately, for the region of parameters which is of interest, namely strong interactions,  $g \leq 0.5$  and  $u/v_F \leq 0.1$ , the exact change of basis required to diagonalize the spin symmetric part of the Hamiltonian is very close to the usual node symmet-

ric/antisymmetric basis. This can be explicitly seen, for example, from the velocities of these modes. For this entire range of parameters, the velocities of the diagonal fields, given by Equation 6.26, are at most 1% different from the values we expect for the left-right symmetric system, which are  $v_F/g$  and  $v_F$ . Due to the strong interactions in this spin symmetric sector, the velocity asymmetry is unimportant, and it is for this reason that we choose to still use the node symmetric-antisymmetric basis and treat these fields as the diagonal ones. In section 6.A we elaborate on and justify this approximation. Note that the velocity asymmetry is still apparent in the non-interacting spin antisymmetric modes labeled by  $j = 1$  and  $j = 2$  in Equation 6.25.

### 6.3.2 Perturbation Theory

Using the diagonal form of the Hamiltonian with the above approximation, we proceed to calculate the current,  $I = (e/\pi)\langle\sum_{a\sigma}\partial_t\theta_{a\sigma}\rangle$ , as in section 6.2. The applied voltages now couple to the total density and total number of left movers and right movers:

$$\begin{aligned} H_V &= H_{4ch} - e\frac{V_{sd}}{2}(N_R - N_L) - \alpha eV_g(N_R + N_L) \\ &= H_{4ch} - e\frac{V_{sd}}{2}\int dx \sum_{\sigma,a} \frac{\nabla\phi_{a\sigma}}{\pi} - eV_g\int dx \sum_{\sigma,a} \frac{\nabla\theta_{a\sigma}}{\pi} \end{aligned} \quad (6.27)$$

The external voltages can be removed from the Hamiltonian by the appropriate shift of the bosonic fields:

$$\begin{aligned} \theta_{a\sigma} &\rightarrow \theta_{a\sigma} + \frac{\alpha g^2 e V_g}{\hbar v_F} \frac{1}{1 - g^2 u^2 / v_F^2} x - \frac{e V_{sd}}{2\hbar} t, \\ \phi_{a\sigma} &\rightarrow \phi_{a\sigma} + (-1)^a \frac{\alpha g^2 e V_g}{\hbar v_F} \frac{u/v_F}{1 - g^2 u^2 / v_F^2} x. \end{aligned} \quad (6.28)$$

Again we use the Keldysh contour to write the formal expression for the current, as in Equation 6.10, and expand it to lowest order in the appropriate  $H'_{bs}$  which contains the voltage dependence due to the shifts of the fields. The approximation we made above, namely that it is the node symmetric/antisymmetric combination which diagonalize the Hamiltonian, allows us to write the current in a very similar

form to the single channel case:

$$I_{4ch} = 4 \frac{e^2 V_{sd}}{h} + \tilde{I}_{co} + \tilde{I}_{inco} \quad (6.29)$$

The first term on the right hand side of Equation 6.29 is the current that would flow in the nanotube in the absence of backscattering. The second term is the coherent current which oscillates with the gate voltage:

$$\begin{aligned} \tilde{I}_{co} = & c \Gamma_1 \Gamma_2 \cos \left( \frac{2ug^2 L \alpha}{\hbar^2 v_F^2 (1 - g^2 u^2 / v_F^2)} V_g \right) \times \\ & \int dt \sin \left( \frac{eV_{sd}}{\hbar} t \right) e^{-\tilde{C}_{co}(L,t)} \sin(\tilde{R}_{co}(L,t)) \end{aligned} \quad (6.30)$$

and the third term is the incoherent current, which is independent of the gate voltage:

$$\begin{aligned} \tilde{I}_{inco} = & \\ & c \left( \Gamma_1^2 \sum_{\eta=\pm} \int dt \sin \left( \frac{eV_{sd}}{\hbar} t \right) e^{-\tilde{C}_{inco}^\eta(L,t)} \sin(\tilde{R}_{inco}(L,t)) \right) + \\ & c (\Gamma_1 \rightarrow \Gamma_2, L \rightarrow -L) \end{aligned} \quad (6.31)$$

The function  $\tilde{C}_{co}$ ,  $\tilde{C}_{inco}^\pm$ ,  $\tilde{R}_{co}$  and  $\tilde{R}_{inco}$  are related to the single channel correlation functions as explained in section 6.B.

### 6.3.3 Temperature and Voltage Dependence in Carbon Nanotubes

As in the single channel case, we find there is a coherent part of the interference current which oscillates as a function of the gate voltage with a large period, much larger than the Fabry-Perot oscillation period, as seen explicitly from the voltage dependence of  $\tilde{I}_{co}$ .

The differential conductance  $\partial I_{4ch} / \partial V_{sd}$ , on the other hand, displays a beating pattern, but a more complicated one than in the single-channel case, since there are four different velocities in the problem now:  $v_F \pm u$ ,  $v_3 \approx v_F$  and  $v_4 \approx v_F/g$ .

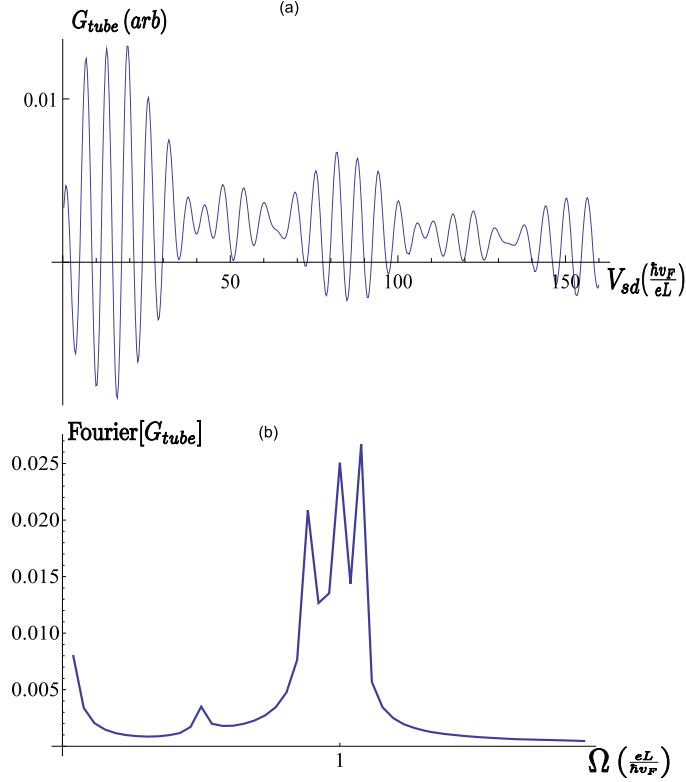


Figure 6.8: (a) Differential conductance oscillations for a nanotube, i.e. including both spins and both nodes in the spectrum, for velocity detuning  $u/v_F = 0.1$ , and interaction strength  $g = 0.5$ . In the nanotube case, the beating is due to the four voltage frequencies in the problem,  $\Omega_i = \frac{eL}{\hbar v_i}$ , where  $v_{1/2} = v_F \pm u$ ,  $v_3 \approx v_F$  and  $v_4 \approx v_F/g$ . (b) The voltage Fourier transform of the oscillations in (a) clearly displays the four dominant frequencies,  $\Omega_{1-4}$ , corresponding to the four velocities in the problem, and encode the nanotube parameters  $v_F$ ,  $g$  and  $u/v_F$ .

Figure 6.8 shows the differential conductance of the nanotube,  $\partial I_{4ch}/\partial V_{sd}$ , and its Fourier transform. From the Fourier analysis we see that clearly there are four dominant frequencies, which correspond to the four different velocities of the collective modes in the nanotube. Thus a careful observation of the large-period, and robust, Sagnac interference allows, in principle, to extract the nanotube parameters, namely the interaction strength  $g$  and the velocity mismatch  $u$  from the Fourier transform of the conductance as a function of bias voltage, up to temperatures much higher than the Fabry-Perot oscillations temperatures.

The temperature dependence of the Sagnac interference in the nanotube case is

qualitatively similar to the single channel case. In the absence of interactions ( $g = 1$ ), the interference can be observed to the scale  $T^*$  proportional to  $v_F/u$ ; in the presence of strong interactions, however,  $T^*$  becomes only weakly dependent on  $u$ . Unlike the single channel case,  $T^*$  in the nanotube case is also only very weakly dependent on  $g$  in the range  $g \leq 0.5$ . This is due to the fact that only one of the four modes which diagonalize the Hamiltonian are interacting and depend on  $g$ . For the same reason,  $T^*$  is higher in the case of the nanotube than in the single channel case, i.e. the reduction of  $T^*$  due to interactions is not as severe in the nanotube case. The temperature dependence on  $u$  and  $g$  is plotted in Figure 6.7. In the range mentioned above,  $T_{SAG}^* \approx 2.8 \frac{\hbar v_F}{k_B L} \approx 7 T_{FP}^*$ .

## 6.4 Summary and Conclusions

In this work we investigated the conductance oscillations in carbon nanotubes due to Sagnac interference. In addition to theoretical interest in this large-period interference mode, the motivation for our study also comes from a recent experimental realization of carbon nanotube loops [119]. The same effect can also be obtained without the loop geometry by inter-node tunneling [141], since right movers at one node of the nanotube move with the same velocity as left movers at the other node. This inter-node tunneling is shown in Figure 6.3(c).

The source of the Sagnac conductance oscillations is the difference in the velocities of left and right moving excitations in a carbon nanotube when the chemical potential is tuned away from half filling. Compared to the more familiar Fabry-Perot oscillations [135], Sagnac oscillations are expected to have a much larger period in gate voltage, and, as we show, in non-interacting wires survive to a temperature a factor of  $v_F/u$  higher than that required to observe Fabry-Perot oscillations.

In interacting electronic wires, the above temperature estimation for free fermions does not apply. Our results for a single channel Luttinger liquid are that  $T_{SAG}$  becomes only weakly dependent on  $v_F/u$ , although still strongly dependent on  $g$ .

From our  $g = 0.5, 0.25$  results, the enhancement of relative to the FP interference is roughly:  $T_{SAG} \approx 15g T_{FP}$  in the range  $u/v_F < 0.1$ .

For a strongly interacting armchair nanotube,  $g \leq 0.5$ , we find that  $T_{SAG}$  becomes not only weakly dependent on  $v_F/u$ , but also nearly independent of  $g$ . The Sagnac interference is expected to survive upto  $T_{SAG}^* \sim 3 \frac{\hbar v_F}{k_B L} \approx 7 - 8 T_{FP}^*$ . Considering that Fabry-Perot oscillations have been observed in nanotubes up to  $T = 10K$  [135], Sagnac oscillations should be observed up to about  $70K$  in nanotubes, despite the strong interactions.

There is also something to be learnt from examining the behavior of the conductance as a function of the applied voltages. We saw that Sagnac oscillations would have a large period of oscillations in the applied gate voltage  $V_g$ ; this period itself is a function of the gate voltage, through the dependence of the velocity difference  $v_R - v_L = 2u$ . Using typical values of a nanotube parameters (e.g. Ref. [119]),  $v_F = 8 \cdot 10^5 m/s$ ,  $L = 7 \mu m$ ,  $g = 0.3$  and  $\alpha = 1/30$ , the period of oscillation in the gate voltage would be  $\Delta V_g = \frac{2\pi \hbar v_F}{eL} \frac{1}{\alpha g^2} \frac{v_F}{u} \approx 17V$ , consistent with the observed oscillations in Ref. [119].

On the other hand, oscillations of the conductance as a function of the applied bias voltage  $V_{sd}$  depend not only on the bare velocities, but also on the interaction strength. A Fourier transform of the Sagnac oscillations as a function of  $V_{sd}$ , we show, contains four different frequencies corresponding to the four different velocities in the problem, which are roughly  $v_F \pm u, v_F$  and  $v_F/g$ . Using the same parameters as above we get  $\Delta V_{sd} = \frac{2\pi \hbar v_F}{eL} \approx 0.5mV$ . This period is much smaller than the bandwidth of a nanotube which is a few eV, so in principle many oscillation periods can be observed and the longer period oscillations should also be measurable, allowing the slower frequency oscillations to appear in the Fourier transform. Observation of these frequencies would allow us to read off the parameters of the nanotube,  $v_F$ ,  $u$  and  $g$ , at temperatures up to  $T_{SAG}^* \approx 70mK$ , which is higher than the temperatures associated with Fabry-Perot oscillations.

In the single channel case, for non-interacting electrons, we were able to extract an analytic expression for the temperature behavior of the conductance gate voltage

oscillations :

$$\frac{G_{co}(T)}{G_{co}(T=0)} = \left( \frac{2\pi k_B L T}{\hbar v_F} \right) \left( \frac{u}{v_F} \right) \frac{1}{\sinh(2\pi k_B T \frac{L}{\hbar v_F} \frac{u}{v_F})} \quad (6.32)$$

and it is apparent how the ratio  $v_F/u$  directly enters the temperature scale. Unfortunately, we were so far unable to extract analytic expression for  $T_{SAG}$  in terms of  $g$  and  $u/v_F$  for the interacting single channel or interacting nanotube cases, inspite of the progress on the qualitative understanding our numerical results allow. Such an analytical understanding should be the focus of a future effort.

As can be observed in Figure 6.1 and Figure 6.2, the paths giving rise to the Sagnac interference are similar to the paths that give rise to weak localization phenomena in 2d disordered conductors. In this work we also essentially show that even in the presence of strong interactions, the interference survives. It is tempting to extrapolate from our results that weak localization should also survive strong interactions. This, however, is presumably true so long that scattering events are dominated by small momentum transfer. Nevertheless, our results suggest that a Luttinger liquid with charge and spin modes will still exhibit weak-localization effects, but suppressed, and only weakly dependent on the detuning between counter propogating electrons. Therefore the magnetoresistance should also be strongly suppressed at low fields.

## 6.A Diagonalizing the Hamiltonian with Degeneracies

In this appendix we show how to diagonalize the Hamiltonian  $H_{4ch}$  of Equation 6.24, where diagonalizing entails finding the appropriate change of basis that will transform  $H_{4ch}$  to the sum of four Hamiltonians, each having a form resembling the single channel  $H_{1ch}$  of Equation 6.5. We also explain here the approximations we have used in our calculation.

The first step in the diagonalization of  $H_B$  is to change the basis from the spin

up/down to the spin symmetric/antisymmetric basis at each node:

$$\theta_{a\pm} = \frac{\theta_{a\uparrow} \pm \theta_{a\downarrow}}{\sqrt{2}} \quad (6.33)$$

applying the same transformation to the  $\phi$ 's as well. We notice that the density-density interaction term involves only the spin symmetric fields  $\theta_{a+}$ , hence the spin antisymmetric fields decouple and appear as two non-interacting ( $g = 1$ ) copies of the single channel problem, described by the Hamiltonian  $H_{1ch}$ , with right moving velocity of  $v_F \pm u$  and left moving velocities of  $v_F \mp u$ . These are the fields labeled with  $j = 1$  and  $j = 2$  in Equation 6.25.

The Hamiltonian for the spin symmetric fields has a similar form to our starting point Hamiltonian,  $H_{4ch}$ :

$$\begin{aligned} H_+ = & \frac{\hbar v_F}{2\pi} \sum_{a=1,2} \int dx [(\nabla\theta_{a+})^2 + (\nabla\phi_{a+})^2] \\ & + (-1)^{a+1} 2 \frac{u}{v_F} \nabla\phi_{a+} \nabla\theta_{a+} \Big] + \int dx 2\lambda \left( \sum_{a=1,2} \frac{1}{\pi} \nabla\theta_{a+} \right)^2 \end{aligned} \quad (6.34)$$

In the absence of the  $u$  term,  $H_+$  is easily diagonalized by taking the node symmetric and antisymmetric combinations of the fields:

$$\theta_{3/4} = \frac{\theta_{1+} \pm \theta_{2+}}{\sqrt{2}} \quad (6.35)$$

The resulting diagonal Hamiltonian would be:

$$\begin{aligned} H_+|_{u=0} = & \frac{\hbar v_3}{2\pi} \int dx \left[ \frac{1}{g_3} (\nabla\theta_3)^2 + g_3 (\nabla\phi_3)^2 \right] \\ & + \frac{\hbar v_4}{2\pi} \int dx \left[ \frac{1}{g_4} (\nabla\theta_4)^2 + g_4 (\nabla\phi_4)^2 \right] \end{aligned} \quad (6.36)$$

with  $v_3 = v_F$ ,  $v_4 = v_F/g$ ,  $g_3 = 1$  and  $g_4 = g$ .

When we consider  $u \neq 0$ , it is still possible to apply a  $g$  and  $u$  dependent transformation to the fields, that will restore  $H_+$  to the form in Equation 6.36, with velocities

$v_{3/4}$  given by Equation 6.26. The field mixing this transformation entails, however, considerably complicates the book keeping in our perturbative calculation. Fortunately, we can show that a good approximation is to simply set  $u$  to zero in  $H_+$  when the interactions are strong, and simply use the transformation given by Equation 6.35. The first indication that this approximation is valid is that the exact velocities  $v_{3/4}$  differ from the  $u = 0$  velocities by at most 1% in the entire range of parameters we are interested in, which is  $u/v_F \leq 0.1$  and  $g \leq 0.5$

Another indication that this approximation is valid comes from the analysis of the single channel problem in section 6.2. In the single channel case we derived exact expressions for the Sagnac interference, and found that for  $g = 0.5$  and  $g = 0.25$ , the temperature dependence is only weakly dependent on  $u/v_F$ ; furthermore  $u$  only enters directly in the expression for the oscillation period of the conductance as a function of gate voltage, the dependence we have explicitly in our expression for the coherent current  $I_{co}$ , Equation 6.15.

Finally, we can also calculate the exact combination of fields that diagonalizes  $H_+$ , and verify that indeed they are very close to the node symmetric/antisymmetric combinations for the range of  $g$  and  $u$  of interest. As an example, the explicit change of basis from the node symmetric/antisymmetric basis to the diagonalizing basis for  $g = 1/2$ , to second order in  $u/v_F$ , is:

$$\mathbb{I}_{4x4} + \begin{pmatrix} -\frac{71}{144}\left(\frac{u}{v_F}\right)^2 & 0 & 0 & \frac{2\sqrt{2}}{3}\left(\frac{u}{v_F}\right) \\ 0 & -\frac{89}{144}\left(\frac{u}{v_F}\right)^2 & \frac{5}{3\sqrt{2}}\left(\frac{u}{v_F}\right) & 0 \\ 0 & \frac{-2\sqrt{2}}{3}\left(\frac{u}{v_F}\right) & -\frac{29}{36}\left(\frac{u}{v_F}\right)^2 & 0 \\ -\frac{5}{3\sqrt{2}}\left(\frac{u}{v_F}\right) & 0 & 0 & -\frac{11}{36}\left(\frac{u}{v_F}\right)^2 \end{pmatrix} \quad (6.37)$$

We see that the is matrix is close to the identity matrix  $\mathbb{I}_{4x4}$ , since  $\frac{u}{v_F} \ll 1$ . The deviation from the identity becomes even smaller for smaller  $g$ . Note that for  $g \approx 1$  the corresponding change of basis matrix is not close to the identity matrix and our approximation fails. This can be seen immediately for the zero interactions case,  $g = 1$ , since when  $u \neq 0$  the standard symmetric/anti-symmetric combinations of

fields do not diagonalize the Hamiltonian of the system.

We stress that setting  $u$  to zero in  $H_+$  is simply a good numerical approximation which simplifies the calculation, and not equivalent to setting  $u$  to zero in the entire problem, as  $u$  still appears in spin anti-symmetric part of the Hamiltonian (where  $g = 1$ ), and also in the gate voltage dependence.

## 6.B Correlation functions

Let us now connect the explicit expressions for the coherent and incoherent currents given in subsection 6.2.3 and section 6.3, Equation 6.15 and Equation 6.16, using the correlation functions defined in subsection 6.2.2.

It is useful to define the following combination of  $C^\theta$ :

$$\overline{C^\theta(x, t)} = C^\theta(0, 0) - C^\theta(x, t) \quad (6.38)$$

and similarly for  $\overline{C^\phi}$ .

In the single channel case discussed in section 6.2, there are only a single  $\theta$  field and a single  $\phi$  field, with the Hamiltonian given by Equation 6.5. Since the Hamiltonian is quadratic we can easily evaluate all the equilibrium correlation functions at finite temperature, paying attention to the different time orderings that appear as a result of the two branches of the Keldysh contour. The results for finite temperature is:

$$\overline{C^\theta(x, t)} = \frac{g}{4} \left[ \log \left( \frac{\beta v_L}{\pi \delta} \sinh \left( \frac{\pi(x + v_L t - i\delta)}{\beta v_L} \right) \right) + \log \left( \frac{\beta v_R}{\pi \delta} \sinh \left( \frac{\pi(x - v_R t + i\delta)}{\beta v_R} \right) \right) \right] + (x \rightarrow -x) \quad (6.39)$$

$$R^\theta(x, t) = -\frac{\pi}{2} g \left[ \Theta(x) \Theta(t - \frac{x}{v_R}) + \Theta(-x) \Theta(t - \frac{|x|}{v_L}) \right] \quad (6.40)$$

where  $\delta$  is a short distance cutoff,  $v_{R/L} = v_F/g \pm u$ , and  $\Theta(x)$  is the step function. As mentioned in Ref. [145], it is important to remember that the step functions are not infinitely sharp, and have a transition width of order  $a$ , the cutoff. The

functions  $\overline{C^\phi(x, t)}$  and  $R^\phi(x, t)$  are obtained from  $\overline{C^\theta(x, t)}$  and  $R^\theta(x, t)$  by replacing the prefactor  $g$  with  $\frac{1}{g}$ . The function  $C^{\theta\phi}$  is given in Equation 6.12, and:

$$R^{\theta\phi}(x, t) = \tag{6.41}$$

$$- \frac{\pi}{2} \Theta(t) [\Theta(x) \Theta(x - v_R t) - \Theta(-x) \Theta(|x| - v_L t)].$$

The currents are expressed in integrals over complicated combinations of such correlation functions. For example, the coherent part of the current, given by Equation 6.15, involves the following combinations:

$$C_{co}(L, t) = 2C^{\theta\phi}(L, t) - 2C^{\theta\phi}(-L, t) \tag{6.42}$$

$$+ 2\overline{C^\theta(0, t)} - 2\overline{C^\theta(L, 0)} + \overline{C^\theta(L, t)} + \overline{C^\theta(-L, t)}$$

$$+ 2\overline{C^\phi(L, 0)} - 2\overline{C^\phi(0, t)} + \overline{C^\phi(L, t)} + \overline{C^\phi(-L, t)}$$

and

$$R_{co}(L, t) = R^{\theta\phi}(L, t) - R^{\theta\phi}(-L, t) \tag{6.43}$$

$$+ R^\theta(0, t) + \frac{1}{2}R^\theta(L, t) + \frac{1}{2}R^\theta(-L, t)$$

$$- R^\phi(0, t) + \frac{1}{2}R^\phi(L, t) + \frac{1}{2}R^\phi(-L, t)$$

The corresponding functions for the incoherent current are :

$$C_{inco}^\pm(L, t) = \pm (2C^{\theta\phi}(L, t) - 2C^{\theta\phi}(-L, t)) \tag{6.44}$$

$$+ 2\overline{C^\theta(0, t)} - 2\overline{C^\theta(L, 0)} + \overline{C^\theta(L, t)} + \overline{C^\theta(-L, t)}$$

$$+ 2\overline{C^\phi(L, 0)} + 2\overline{C^\phi(0, t)} - \overline{C^\phi(L, t)} - \overline{C^\phi(-L, t)}$$

and

$$\begin{aligned}
R_{inco}(L, t) &= R^\theta(0, t) + \frac{1}{2}R^\theta(L, t) + \frac{1}{2}R^\theta(-L, t) \\
&+ R^\phi(0, t) - \frac{1}{2}R^\phi(L, t) - \frac{1}{2}R^\phi(-L, t).
\end{aligned}$$

In a Carbon nanotube there are four channels, rather than a single one. In the non-interacting case,  $g = 1$ , all these channels are independent and we would recover the results of the single channel. Equation 6.42 and Equation 6.43 still apply for this case. When  $g \neq 1$ , the different channels are coupled through the interaction, and we must find the correct combinations of the fields  $\theta_{i\sigma}$  and  $\phi_{i\sigma}$  which decouple and therefore diagonalize the Hamiltonian. These combinations are discussed in section 6.A. This change of basis is in general a function of  $u/v_F$  and  $g$ , and it mixes the  $\theta$  and  $\phi$  fields, which in turn complicates the functions  $C_{co}$  and  $R_{co}$  further. Luckily, the interactions in Carbon nanotubes are strong,  $g \approx 0.3$ , and in that range, the change of basis is very close to the usual spin/node symmetric/antisymmetric change of basis. If we approximate the diagonalizing fields by these symmetric/antisymmetric combinations, then Equation 6.42 and Equation 6.43 would apply provided we make the following substitutions:

$$\overline{C^\theta(x, t)} \rightarrow \frac{1}{4} \sum_{j=1..4} \overline{C^{\theta_j}(x, t)} \tag{6.45}$$

Where each  $\theta_j$  has a different set of values for  $v_R$ ,  $v_L$  and  $g$  to be used in Equation 6.39. The fields  $\theta_1$  and  $\theta_2$  correspond to the spin asymmetric combinations, which decouple from the interaction, and hence have  $g = 1$ , and velocities  $v_R = v_F \pm u$  and  $v_L = v_F \mp u$ . The fields  $\theta_3$  and  $\theta_4$  both have the same left and right mover velocities,  $v_3$  and  $v_4$  respectively, given by Equation 6.26, and interaction parameters 1 and  $g$ , respectively.

# Bibliography

- [1] S. Forte, Quantum mechanics and field theory with fractional spin and statistics, *Reviews of Modern Physics* 64 (1) (1992) 193–236.
- [2] M. E. Peskin, D. V. Schroeder, *An Introduction to Quantum Field Theory* (Frontiers in Physics), Perseus Books, 2008.
- [3] M. K. Gaillard, P. D. Grannis, F. J. Sciulli, The standard model of particle physics, *Reviews of Modern Physics* 71 (2) (1999) S96.
- [4] F. Wilczek, Magnetic flux, angular momentum, and statistics, *Physical Review Letters* 48 (17) (1982) 1144–1146.
- [5] F. Wilczek, Quantum mechanics of fractional-spin particles, *Physical Review Letters* 49 (14) (1982) 957–959.
- [6] K. v. Klitzing, G. Dorda, M. Pepper, New method for high-accuracy determination of the fine-structure constant based on quantized hall resistance, *Physical Review Letters* 45 (6) (1980) 494–497.
- [7] D. C. Tsui, H. L. Stormer, A. C. Gossard, Two-dimensional magnetotransport in the extreme quantum limit, *Physical Review Letters* 48 (22) (1982) 1559–1562.
- [8] Y. Zhang, Y. Tan, H. L. Stormer, P. Kim, Experimental observation of the quantum hall effect and berry’s phase in graphene, *Nature* 438 (7065) (2005) 201–204.  
URL <http://dx.doi.org/10.1038/nature04235>

- [9] K. S. Novoselov, Z. Jiang, Y. Zhang, S. V. Morozov, H. L. Stormer, U. Zeitler, J. C. Maan, G. S. Boebinger, P. Kim, A. K. Geim, Room-Temperature Quantum Hall Effect in Graphene, *Science* (2007) 1137201.  
URL <http://www.sciencemag.org/cgi/content/abstract/1137201v1>
- [10] Z. Hadzibabic, P. Kruger, M. Cheneau, B. Battelier, J. Dalibard, Berezinskii-kosterlitz-thouless crossover in a trapped atomic gas, *Nature* 441 (7097) (2006) 1118–1121.  
URL <http://dx.doi.org/10.1038/nature04851>
- [11] I. B. Spielman, W. D. Phillips, J. V. Porto, Mott-insulator transition in a two-dimensional atomic bose gas, *Physical Review Letters* 98 (8) (2007) 080404.  
URL <http://link.aps.org/abstract/PRL/v98/e080404>
- [12] J. Leinaas, J. Myrheim, On the theory of identical particles, *Il Nuovo Cimento B* (1971-1996) 37 (1) (1977) 1–23.
- [13] Y.-S. Wu, General theory for quantum statistics in two dimensions, *Physical Review Letters* 52 (24) (1984) 2103–2106.
- [14] R. P. Feynman, Space-time approach to non-relativistic quantum mechanics, *Reviews of Modern Physics* 20 (2) (1948) 367–387.
- [15] M. G. G. Laidlaw, C. M. DeWitt, Feynman functional integrals for systems of indistinguishable particles, *Physical Review D* 3 (6) (1971) 1375–1378.
- [16] H. S. Green, A generalized method of field quantization, *Physical Review* 90 (2) (1953) 270–273.
- [17] K. Drühl, R. Haag, J. E. Roberts, On parastatistics, *Communications in Mathematical Physics* 18 (3) (1970) 204–226.  
URL <http://dx.doi.org/10.1007/BF01649433>
- [18] E. Artin, Theorie der Zöpfe, *Abh. math. Sem. Hamburg* 4 (1926) 47–72.

- [19] G. A. Goldin, R. Menikoff, D. H. Sharp, Comments on "general theory for quantum statistics in two dimensions", *Physical Review Letters* 54 (6) (1985) 603.
- [20] R. B. Laughlin, Anomalous quantum hall effect: An incompressible quantum fluid with fractionally charged excitations, *Physical Review Letters* 50 (18) (1983) 1395–1398.
- [21] D. Arovas, J. R. Schrieffer, F. Wilczek, Fractional statistics and the quantum hall effect, *Physical Review Letters* 53 (7) (1984) 722–723.
- [22] E. H. Hall, On a new action of the magnet on electric currents, *American Journal of Mathematics* 2 (3) (1879) 287–292.  
URL <http://www.jstor.org/stable/2369245>
- [23] J. P. Eisenstein, H. L. Stormer, The Fractional Quantum Hall Effect, *Science* 248 (4962) (1990) 1510–1516,  
<http://www.sciencemag.org/cgi/reprint/248/4962/1510.pdf>.  
URL <http://www.sciencemag.org/cgi/content/abstract/248/4962/1510>
- [24] H. L. Stormer, D. C. Tsui, A. C. Gossard, The fractional quantum hall effect, *Reviews of Modern Physics* 71 (2) (1999) S298–S305.
- [25] S. M. Girvin, The quantum hall effect: Novel excitations and broken symmetriescond-mat/9907002.
- [26] B. Huckestein, Scaling theory of the integer quantum hall effect, *Reviews of Modern Physics* 67 (2) (1995) 357–396.
- [27] R. B. Laughlin, Quantized hall conductivity in two dimensions, *Physical Review B* 23 (10) (1981) 5632–5633.
- [28] A. Karlhede, S. Kivelson, S. Sondhi, The quantum Hall effect: the article, in: V. Emery (Ed.), *Jerusalem Winter School for Theoretical Physics: Correlated*

Electron Systems. Vol.9, World Scientific, Singapore, Singapore, 1993, pp. 242–347, Correlated Electron Systems. Proceedings of the 9th Jerusalem Winter School for Theoretical Physics, 30 Dec. 1991–8 Jan. 1992, Jerusalem, Israel.

- [29] F. D. M. Haldane, Fractional quantization of the hall effect: A hierarchy of incompressible quantum fluid states, *Physical Review Letters* 51 (7) (1983) 605–608.
- [30] V. J. Goldman, B. Su, Resonant Tunneling in the Quantum Hall Regime: Measurement of Fractional Charge, *Science* 267 (5200) (1995) 1010–1012, <http://www.sciencemag.org/cgi/reprint/267/5200/1010.pdf>.  
URL <http://www.sciencemag.org/cgi/content/abstract/267/5200/1010>
- [31] B. I. Halperin, Statistics of quasiparticles and the hierarchy of fractional quantized hall states, *Physical Review Letters* 52 (18) (1984) 1583–1586.
- [32] J. K. Jain, Composite-fermion approach for the fractional quantum hall effect, *Physical Review Letters* 63 (2) (1989) 199–202.
- [33] R. Willett, J. P. Eisenstein, H. L. Störmer, D. C. Tsui, A. C. Gossard, J. H. English, Observation of an even-denominator quantum number in the fractional quantum hall effect, *Physical Review Letters* 59 (15) (1987) 1776–1779.
- [34] G. Moore, N. Read, Nonabelions in the fractional quantum hall effect, *Nuclear Physics B* 360 (2-3) (1991) 362 – 396.  
URL <http://www.sciencedirect.com/science/article/B6TVC-470F3HY-33/2/ef73fb19aab9b3fae91e168344fc142d>
- [35] C. Nayak, F. Wilczek, 2n-quasihole states realize 2n-1-dimensional spinor braiding statistics in paired quantum hall states, *Nuclear Physics B* 479 (3) (1996) 529 – 553.  
URL <http://www.sciencedirect.com/science/article/B6TVC-3VPSF6F-1Y/2/b37b7cc53c15b29ad101f9c5e6f52fc2>

- [36] N. Read, Non-abelian adiabatic statistics and hall viscosity in quantum hall states and  $p_x + ip_y$  paired superfluids, *Physical Review B* 79 (4) (2009) 045308.  
URL <http://link.aps.org/abstract/PRB/v79/e045308>
- [37] N. Read, E. Rezayi, Beyond paired quantum hall states: Parafermions and incompressible states in the first excited landau level, *Physical Review B* 59 (12) (1999) 8084–8092.
- [38] J. S. Xia, W. Pan, C. L. Vicente, E. D. Adams, N. S. Sullivan, H. L. Stormer, D. C. Tsui, L. N. Pfeiffer, K. W. Baldwin, K. W. West, Electron correlation in the second landau level: A competition between many nearly degenerate quantum phases, *Physical Review Letters* 93 (17) (2004) 176809.
- [39] R. H. Morf, Transition from quantum hall to compressible states in the second landau level: New light on the  $\nu = 5/2$  enigma, *Physical Review Letters* 80 (7) (1998) 1505–1508.
- [40] E. H. Rezayi, F. D. M. Haldane, Incompressible paired hall state, stripe order, and the composite fermion liquid phase in half-filled landau levels, *Physical Review Letters* 84 (20) (2000) 4685–4688.
- [41] X. Wan, Z.-X. Hu, E. H. Rezayi, K. Yang, Fractional quantum hall effect at  $\nu = 5/2$ : Ground states, non-abelian quasiholes, and edge modes in a microscopic model, *Physical Review B* 77 (16) (2008) 165316.  
URL <http://link.aps.org/abstract/PRB/v77/e165316>
- [42] M. R. Peterson, K. Park, S. D. Sarma, Spontaneous particle-hole symmetry breaking in the  $\nu = 5/2$  fractional quantum hall effect, *Physical Review Letters* 101 (15) (2008) 156803.  
URL <http://link.aps.org/abstract/PRL/v101/e156803>
- [43] E. H. Rezayi, N. Read, Non-abelian quantized hall states of electrons at filling factors  $12/5$  and  $13/5$  in the first excited landau level, *Physical Review B* 79 (7)

(2009) 075306.

URL <http://link.aps.org/abstract/PRB/v79/e075306>

- [44] M. Dolev, M. Heiblum, V. Umansky, A. Stern, D. Mahalu, Observation of a quarter of an electron charge at the  $\nu = 5/2$  quantum hall state, *Nature* 452 (7189) (2008) 829–834, 10.1038/nature06855.

URL <http://dx.doi.org/10.1038/nature06855>

- [45] I. P. Radu, J. B. Miller, C. M. Marcus, M. A. Kastner, L. N. Pfeiffer, K. W. West, Quasi-Particle Properties from Tunneling in the Formula Fractional Quantum Hall State, *Science* 320 (5878) (2008) 899–902, <http://www.sciencemag.org/cgi/reprint/320/5878/899.pdf>.

URL <http://www.sciencemag.org/cgi/content/abstract/320/5878/899>

- [46] W. E. Chickering, J. P. Eisenstein, J. L. Reno, A hot electron thermocouple and the diffusion thermopower of two-dimensional electrons in gaas (2009), 0903.0835.

- [47] R. Willett, L. Pfeiffer, K. West, Measurement of filling factor  $5/2$  quasiparticle interference: observation of charge  $e/4$  and  $e/2$  period oscillations (2008), arXiv:0807.0221.

- [48] B. I. Halperin, Quantized hall conductance, current-carrying edge states, and the existence of extended states in a two-dimensional disordered potential, *Physical Review B* 25 (4) (1982) 2185–2190.

- [49] X. Wen, Theory of the edge states in fractional quantum hall effects, *International Journal of Modern Physics B* 6 (10) (1992) 1711–1762.

- [50] C. Nayak, S. H. Simon, A. Stern, M. Freedman, S. D. Sarma, Non-abelian anyons and topological quantum computation, *Reviews of Modern Physics* 80 (3) (2008) 1083.

URL <http://link.aps.org/abstract/RMP/v80/p1083>

- [51] M. Milovanović, N. Read, Edge excitations of paired fractional quantum hall states, *Physical Review B* 53 (20) (1996) 13559–13582.
- [52] J. K. Jain, S. A. Kivelson, D. J. Thouless, Proposed measurement of an effective flux quantum in the fractional quantum hall effect, *Physical Review Letters* 71 (18) (1993) 3003–3006.
- [53] C. de C. Chamon, D. E. Freed, S. A. Kivelson, S. L. Sondhi, X. G. Wen, Two point-contact interferometer for quantum hall systems, *Physical Review B* 55 (4) (1997) 2331–2343.
- [54] C. L. Kane, Telegraph noise and fractional statistics in the quantum hall effect, *Physical Review Letters* 90 (22) (2003) 226802.
- [55] E.-A. Kim, M. Lawler, S. Vishveshwara, E. Fradkin, Signatures of fractional statistics in noise experiments in quantum hall fluids, *Physical Review Letters* 95 (17) (2005) 176402.
- [56] S. Das Sarma, M. Freedman, C. Nayak, Topologically protected qubits from a possible non-abelian fractional quantum hall state, *Physical Review Letters* 94 (16) (2005) 166802.
- [57] P. Bonderson, A. Kitaev, K. Shtengel, Detecting non-abelian statistics in the  $\nu = 5/2$  fractional quantum hall state, *Physical Review Letters* 96 (1) (2006) 016803.  
URL <http://link.aps.org/abstract/PRL/v96/e016803>
- [58] A. Stern, B. I. Halperin, Proposed experiments to probe the non-abelian  $\nu = 5/2$  quantum hall state, *Physical Review Letters* 96 (1) (2006) 016802.  
URL <http://link.aps.org/abstract/PRL/v96/e016802>
- [59] C. Bena, C. Nayak, Effects of non-abelian statistics on two-terminal shot noise in a quantum hall liquid in the pfaffian state, *Physical Review B* 73 (15) (2006) 155335.  
URL <http://link.aps.org/abstract/PRB/v73/e155335>

- [60] S.-S. Lee, S. Ryu, C. Nayak, M. P. A. Fisher, Particle-hole symmetry and the  $\nu = (5/2)$  quantum hall state, *Physical Review Letters* 99 (23) (2007) 236807.  
URL <http://link.aps.org/abstract/PRL/v99/e236807>
- [61] B. Halperin, Theory of the quantized Hall conductance, *Helvetica Physica Acta* 56 (1-3) (1983) 75–102.
- [62] A. E. Feiguin, E. Rezayi, C. Nayak, S. D. Sarma, Density matrix renormalization group study of incompressible fractional quantum hall states, *Physical Review Letters* 100 (16) (2008) 166803.  
URL <http://link.aps.org/abstract/PRL/v100/e166803>
- [63] M. J. Manfra, R. de Picciotto, Z. Jiang, S. H. Simon, L. N. Pfeiffer, K. W. West, A. M. Sergent, Impact of spin-orbit coupling on quantum hall nematic phases, *Physical Review Letters* 98 (20) (2007) 206804.  
URL <http://link.aps.org/abstract/PRL/v98/e206804>
- [64] M. Levin, B. I. Halperin, B. Rosenow, Particle-hole symmetry and the pfaffian state, *Physical Review Letters* 99 (23) (2007) 236806.  
URL <http://link.aps.org/abstract/PRL/v99/e236806>
- [65] A. MacDonald, Introduction to the physics of the quantum Hall regime, in: E. Akkermans, G. Montambaux, J.-L. Pichard, J. Zinn-Justin (Eds.), *Les Houches. Session LXI. Mesoscopic Quantum Physics*, Elsevier, Amsterdam, Netherlands, 1995, pp. 659–720, *Proceedings of the Les Houches Summer School on Mesoscopic Quantum Physics*, 28-29 June 1994, Les Houches, France.
- [66] S. H. Simon, E. H. Rezayi, N. R. Cooper, Pseudopotentials for multiparticle interactions in the quantum hall regime, *Physical Review B* 75 (19) (2007) 195306.  
URL <http://link.aps.org/abstract/PRB/v75/e195306>
- [67] R. Shankar, Renormalization-group approach to interacting fermions, *Reviews of Modern Physics* 66 (1) (1994) 129–192.

- [68] M. Greiter, X. G. Wen, F. Wilczek, Paired hall states, Nuclear Physics B 374 (3) (1992) 567 – 614.  
URL <http://www.sciencedirect.com/science/article/B6TVC-4719KFV-120/2/a811e2d4f44787c5d5db61e167a354d4>
- [69] W. Bishara, C. Nayak, Edge states and interferometers in the pfaffian and anti-pfaffian states of the  $\nu = (5/2)$  quantum hall system, Physical Review B 77 (16) (2008) 165302.  
URL <http://link.aps.org/abstract/PRB/v77/e165302>
- [70] R. de Picciotto, M. Reznikov, M. Heiblum, V. Umansky, G. Bunin, D. Mahalu, Direct observation of a fractional charge, Nature 389 (6647) (1997) 162–164, 10.1038/38241.  
URL <http://dx.doi.org/10.1038/38241>
- [71] L. Saminadayar, D. C. Glatthli, Y. Jin, B. Etienne, Observation of the  $e/3$  fractionally charged laughlin quasiparticle, Physical Review Letters 79 (13) (1997) 2526–2529.
- [72] F. E. Camino, W. Zhou, V. J. Goldman, Realization of a laughlin quasiparticle interferometer: Observation of fractional statistics, Physical Review B 72 (7) (2005) 075342.
- [73] J. P. Eisenstein, K. B. Cooper, L. N. Pfeiffer, K. W. West, Insulating and fractional quantum hall states in the first excited landau level, Physical Review Letters 88 (7) (2002) 076801.
- [74] N. Read, E. Rezayi, Quasiholes and fermionic zero modes of paired fractional quantum hall states: The mechanism for non-abelian statistics, Physical Review B 54 (23) (1996) 16864–16887.
- [75] E. Fradkin, C. Nayak, A. Tsvelik, F. Wilczek, A chern-simons effective field theory for the pfaffian quantum hall state, Nuclear Physics B 516 (3) (1998) 704 – 718.

URL <http://www.sciencedirect.com/science/article/B6TVC-3T2HB89-9/2/82b4da27c036f7d266cd726915bbf294>

- [76] N. Read, D. Green, Paired states of fermions in two dimensions with breaking of parity and time-reversal symmetries and the fractional quantum hall effect, *Physical Review B* 61 (15) (2000) 10267–10297.
- [77] D. A. Ivanov, Non-abelian statistics of half-quantum vortices in *p*-wave superconductors, *Physical Review Letters* 86 (2) (2001) 268–271.
- [78] E. Ardonne, E.-A. Kim, Non-abelian statistics in the interference noise of the moore&ndash;read quantum hall state, *Journal of Statistical Mechanics: Theory and Experiment* 2008 (04) (2008) L04001 (8pp).  
URL <http://stacks.iop.org/1742-5468/2008/L04001>
- [79] L. Fidkowski, Double point contact in the  $k=3$  read-rezayi state (Apr. 2007), 0704.3291.
- [80] B. J. Overbosch, X.-G. Wen, Dynamical and scaling properties of  $\nu=5/2$  interferometer (Jun. 2007), 0706.4339.
- [81] B. Rosenow, B. I. Halperin, S. H. Simon, A. Stern, Bulk-edge coupling in the non-abelian  $\nu = 5/2$  quantum hall interferometer, *Physical Review Letters* 100 (22) (2008) 226803.  
URL <http://link.aps.org/abstract/PRL/v100/e226803>
- [82] P. Fendley, M. P. A. Fisher, C. Nayak, Dynamical disentanglement across a point contact in a non-abelian quantum hall state, *Physical Review Letters* 97 (3) (2006) 036801.  
URL <http://link.aps.org/abstract/PRL/v97/e036801>
- [83] P. Fendley, M. P. A. Fisher, C. Nayak, Edge states and tunneling of non-abelian quasiparticles in the  $\nu = 5/2$  quantum hall state and  $p + ip$  superconductors, *Physical Review B* 75 (4) (2007) 045317.  
URL <http://link.aps.org/abstract/PRB/v75/e045317>

- [84] K. Le Hur, Electron fractionalization-induced dephasing in luttinger liquids, *Physical Review B* 65 (23) (2002) 233314.
- [85] K. L. Hur, Dephasing of mesoscopic interferences from electron fractionalization, *Physical Review Letters* 95 (7) (2005) 076801.  
URL <http://link.aps.org/abstract/PRL/v95/e076801>
- [86] K. L. Hur, Electron lifetime in luttinger liquids, *Physical Review B* 74 (16) (2006) 165104.  
URL <http://link.aps.org/abstract/PRB/v74/e165104>
- [87] X. Wan, K. Yang, E. H. Rezayi, Edge excitations and non-abelian statistics in the moore-read state: A numerical study in the presence of coulomb interaction and edge confinement, *Physical Review Letters* 97 (25) (2006) 256804.  
URL <http://link.aps.org/abstract/PRL/v97/e256804>
- [88] M. Freedman, C. Nayak, K. Walker, Towards universal topological quantum computation in the  $\nu = (5/2)$  fractional quantum hall state, *Physical Review B* 73 (24) (2006) 245307.  
URL <http://link.aps.org/abstract/PRB/v73/e245307>
- [89] W. Bishara, P. Bonderson, C. Nayak, K. Shtengel, J. K. Slingerland, The non-abelian interferometer (Mar. 2009), 0903.3108.
- [90] R. Ilan, E. Grosfeld, A. Stern, Coulomb blockade as a probe for non-abelian statistics in read-rezayi states, *Physical Review Letters* 100 (8) (2008) 086803.  
URL <http://link.aps.org/abstract/PRL/v100/e086803>
- [91] W. Bishara, G. A. Fiete, C. Nayak, Quantum hall states at  $\nu = (2/(k + 2))$ : Analysis of the particle-hole conjugates of the general level-k read-rezayi states, *Physical Review B* 77 (24) (2008) 241306.  
URL <http://link.aps.org/abstract/PRB/v77/e241306>
- [92] W. Pan, J.-S. Xia, V. Shvarts, D. E. Adams, H. L. Stormer, D. C. Tsui, L. N. Pfeiffer, K. W. Baldwin, K. W. West, Exact quantization of the even-

- denominator fractional quantum hall state at  $\nu = 5/2$  landau level filling factor, Physical Review Letters 83 (17) (1999) 3530–3533.
- [93] N. Read, Excitation structure of the hierarchy scheme in the fractional quantum hall effect, Physical Review Letters 65 (1990) 1502–1505.
- [94] H. C. Choi, W. Kang, S. D. Sarma, L. N. Pfeiffer, K. W. West, Activation gaps of fractional quantum hall effect in the second landau level, Physical Review B 77 (8) (2008) 081301.
- [95] M. H. Freedman, M. J. Larsen, Z. Wang, A modular functor which is universal for quantum computation, Communications in Mathematical Physics 227 (2002) 605–622, quant-ph/0001108.
- [96] P. Bonderson, J. K. Slingerland, Fractional quantum hall hierarchy and the second landau level, Physical Review B 78 (12) (2008) 125323.  
URL <http://link.aps.org/abstract/PRB/v78/e125323>
- [97] V. A. Fateev, A. B. Zamolodchikov, Parafermionic currents in the two-dimensional conformal quantum field theory and selfdual critical points in  $z(n)$  invariant statistical systems, Soviet Physics JETP-USSR 62 (1985) 215–225.
- [98] D. Karabali, H. J. Schnitzer, Brst quantization of the gauged wzw action and coset conformal field theories, Nuclear Physics B329 (1990) 649.
- [99] E. Witten, Nonabelian bosonization in two dimensions, Communications in Mathematical Physics 92 (1984) 455–472.
- [100] C. L. Kane, M. P. A. Fisher, J. Polchinski, Randomness at the edge: Theory of quantum hall transport at filling  $\nu=2/3$ , Physical Review Letters 72 (1994) 4129–4132.
- [101] T. Giamarchi, H. J. Schulz, Anderson localization and interactions in one-dimensional metals, Physical Review B 37 (1) (1988) 325–340.

- [102] X.-G. Wen, Topological orders and edge excitations in fqh states, *Advances in Physics* 55 (1995) 405–473.
- [103] S. D. Sarma, M. Freedman, C. Nayak, Topological quantum computation, *Physics Today* 59 (7) (2006) 32–38.  
URL <http://link.aip.org/link/?PT0/59/32/1>
- [104] J. B. Miller, I. P. Radu, D. M. Zumbuehl, E. M. Levenson-Falk, M. A. Kastner, C. M. Marcus, L. N. Pfeiffer, K. W. West, Fractional quantum Hall effect in a quantum point contact at filling fraction  $5/2$ , *Nature Physics* 3 (8) (2007) 561–565.
- [105] G. A. Fiete, W. Bishara, C. Nayak, Multichannel kondo models in non-abelian quantum hall droplets, *Physical Review Letters* 101 (17) (2008) 176801.  
URL <http://link.aps.org/abstract/PRL/v101/e176801>
- [106] K. G. Wilson, The renormalization group: Critical phenomena and the kondo problem, *Reviews of Modern Physics* 47 (4) (1975) 773–840.
- [107] A. O. Gogolin, A. A. Nersesyan, A. M. Tselik, *Bosonization and Strongly Correlated Systems*, Cambridge University Press, 2004.  
URL <http://www.amazon.ca/exec/obidos/redirect?tag=citeulike09-20&path=ASIN/0521617197>
- [108] R. C. Ashoori, H. L. Stormer, J. S. Weiner, L. N. Pfeiffer, S. J. Pearton, K. W. Baldwin, K. W. West, Single-electron capacitance spectroscopy of discrete quantum levels, *Physical Review Letters* 68 (20) (1992) 3088–3091.
- [109] G. A. Fiete, G. Refael, M. P. A. Fisher, Universal periods in quantum hall droplets, *Physical Review Letters* 99 (16) (2007) 166805.  
URL <http://link.aps.org/abstract/PRL/v99/e166805>
- [110] I. Affleck, A. Ludwig, The Kondo Effect, Conformal Field-Theory And Fusion Rules, *Nuclear Physics B* 352 (3) (1991) 849–862.

- [111] A. Furusaki, K. A. Matveev, Occupation of a resonant level coupled to a chiral luttinger liquid, *Physical Review Letters* 88 (22) (2002) 226404.
- [112] K. A. Matveev, Coulomb blockade at almost perfect transmission, *Physical Review B* 51 (3) (1995) 1743–1751.
- [113] V. J. Emery, S. Kivelson, Mapping of the two-channel kondo problem to a resonant-level model, *Physical Review B* 46 (17) (1992) 10812–10817.
- [114] I. Affleck, A current algebra approach to the kondo effect, *Nuclear Physics B* 336 (3) (1990) 517 – 532.  
 URL <http://www.sciencedirect.com/science/article/B6TVC-4719H2B-6T/2/a3e5bffa564a0f68a4b17ea056324411>
- [115] I. Affleck, A. Ludwig, H. Pang, D. Cox, Relevance of anisotropy in the multichannel Kondo effect - comparison of conformal field-theory and numerical renormalization-group results, *Physical Review B* 45 (14) (1992) 7918–7935.
- [116] Y. Oreg, D. Goldhaber-Gordon, Two-channel Kondo effect in a modified single electron transistor, *Physical Review Letters* 90 (13).
- [117] P. Di Francesco, P. Mathieu, D. Senechal, *Conformal Field Theory* (Graduate Texts in Contemporary Physics), Springer, 1999.  
 URL <http://www.amazon.ca/exec/obidos/redirect?tag=citeulike09-20&path=ASIN/038794785X>
- [118] G. Fiete.
- [119] G. Refael, J. Heo, M. Bockrath, Sagnac interference in carbon nanotube loops, *Physical Review Letters* 98 (24) (2007) 246803.  
 URL <http://link.aps.org/abstract/PRL/v98/e246803>
- [120] G. Sagnac, Luminous ether demonstrated by the effect of relative wind of ether in a uniform rotation of an interferometer, *Comptes Rendus Hebdomadaires Des Seances De L Academie Des Sciences* 157 (1913) 708–710.

- [121] Y. Japha, O. Arzouan, Y. Avishai, R. Folman, Using time-reversal symmetry for sensitive incoherent matter-wave sagnac interferometry, *Physical Review Letters* 99 (6) (2007) 060402.  
URL <http://link.aps.org/abstract/PRL/v99/e060402>
- [122] J. Xia, E. Schemm, G. Deutscher, S. A. Kivelson, D. A. Bonn, W. N. Hardy, R. Liang, W. Siemons, G. Koster, M. M. Fejer, A. Kapitulnik, Polar kerr-effect measurements of the high-temperature  $\text{YBa}_2\text{Cu}_3\text{O}_{6+x}$  superconductor: Evidence for broken symmetry near the pseudogap temperature, *Physical Review Letters* 100 (12) (2008) 127002.  
URL <http://link.aps.org/abstract/PRL/v100/e127002>
- [123] H. Förster, S. Pilgram, M. Büttiker, Decoherence and full counting statistics in a mach-zehnder interferometer, *Physical Review B* 72 (7) (2005) 075301.  
URL <http://link.aps.org/abstract/PRB/v72/e075301>
- [124] F. E. Camino, W. Zhou, V. J. Goldman, Aharonov-bohm electron interferometer in the integer quantum hall regime, *Physical Review B* 72 (15) (2005) 155313.  
URL <http://link.aps.org/abstract/PRB/v72/e155313>
- [125] W. G. van der Wiel, Y. V. Nazarov, S. De Franceschi, T. Fujisawa, J. M. Elzerman, E. W. G. M. Huizeling, S. Tarucha, L. P. Kouwenhoven, Electromagnetic aharonov-bohm effect in a two-dimensional electron gas ring, *Physical Review B* 67 (3) (2003) 033307.
- [126] B. J. van Wees, L. P. Kouwenhoven, C. J. P. M. Harmans, J. G. Williamson, C. E. Timmering, M. E. I. Broekaart, C. T. Foxon, J. J. Harris, Observation of zero-dimensional states in a one-dimensional electron interferometer, *Physical Review Letters* 62 (21) (1989) 2523–2526.
- [127] E. Buks, R. Schuster, M. Heiblum, D. Mahalu, V. Umansky, Dephasing in

- electron interference by a ‘which-path’ detector, *NATURE* 391 (6670) (1998) 871–874.
- [128] D. E. Feldman, A. Kitaev, Detecting non-abelian statistics with an electronic mach-zehnder interferometer, *Physical Review Letters* 97 (18) (2006) 186803.  
URL <http://link.aps.org/abstract/PRL/v97/e186803>
- [129] P. Bonderson, K. Shtengel, J. K. Slingerland, Probing non-abelian statistics with quasiparticle interferometry, *Physical Review Letters* 97 (1) (2006) 016401.  
URL <http://link.aps.org/abstract/PRL/v97/e016401>
- [130] M. Sigrist, T. Ihn, K. Ensslin, M. Reinwald, W. Wegscheider, Coherent probing of excited quantum dot states in an interferometer, *Physical Review Letters* 98 (3) (2007) 036805.  
URL <http://link.aps.org/abstract/PRL/v98/e036805>
- [131] A. Yacoby, M. Heiblum, D. Mahalu, H. Shtrikman, Coherence and phase sensitive measurements in a quantum dot, *Physical Review Letters* 74 (20) (1995) 4047–4050.
- [132] M. Bockrath, D. H. Cobden, J. Lu, A. G. Rinzler, R. E. Smalley, L. Balents, P. L. McEuen, Luttinger-liquid behaviour in carbon nanotubes, *Nature* 397 (1999) 598.
- [133] C. Kane, L. Balents, M. P. A. Fisher, Coulomb interactions and mesoscopic effects in carbon nanotubes, *Physical Review Letters* 79 (25) (1997) 5086–5089.
- [134] Z. Yao, H. Postma, L. Balents, C. Dekker, Carbon nanotube intramolecular junctions, *Nature* 402 (6759) (1999) 273–276.
- [135] W. Liang, M. Bockrath, D. Bozovic, J. H. Hafner, M. Tinkham, H. Park, Fabry - perot interference in a nanotube electron waveguide, *Nature* 411 (2001) 665.
- [136] C. S. Peça, L. Balents, K. J. Wiese, Fabry-perot interference and spin filtering in carbon nanotubes, *Physical Review B* 68 (20) (2003) 205423.

- [137] V. I. Fernández, A. Iucci, C. M. Naón, Luttinger liquid with asymmetric dispersion, *The European Physical Journal B - Condensed Matter and Complex Systems* 30 (1) (2002) 53–56.  
URL <http://dx.doi.org/10.1140/epjb/e2002-00357-8>
- [138] E. Abrahams, P. W. Anderson, D. C. Licciardello, T. V. Ramakrishnan, Scaling theory of localization: Absence of quantum diffusion in two dimensions, *Physical Review Letters* 42 (10) (1979) 673–676.
- [139] L. Gorkov, A. Larkin, D. Khmel'nitskii, Particle conductivity in a two-dimensional random potential, *JETP LETTERS* 30 (4) (1979) 228–232.
- [140] B. L. Altshuler, A. G. Aronov, P. A. Lee, Interaction effects in disordered fermi systems in two dimensions, *Physical Review Letters* 44 (19) (1980) 1288–1291.
- [141] J. Jiang, J. Dong, D. Y. Xing, Quantum interference in carbon-nanotube electron resonators, *Physical Review Letters* 91 (5) (2003) 056802.
- [142] L. Keldysh, Diagram technique for nonequilibrium processes, *Soviet Physics JETP-USSR* 20 (4) (1965) 1018–&.
- [143] J. Rammer, H. Smith, Quantum field-theoretical methods in transport theory of metals, *Reviews of Modern Physics* 58 (2) (1986) 323–359.
- [144] C. Kane, M. Fisher, Transmission through barriers and resonant tunneling in an interacting one-dimensional electron-gas, *Physical Review B* 46 (23) (1992) 15233–15262.
- [145] P. Recher, N. Y. Kim, Y. Yamamoto, Tomonaga-luttinger liquid correlations and fabry-perot interference in conductance and finite-frequency shot noise in a single-walled carbon nanotube, *Physical Review B* 74 (23) (2006) 235438.  
URL <http://link.aps.org/abstract/PRB/v74/e235438>
- [146] Y. Oreg, A. M. Finkel'stein, Interedge interaction in the quantum hall effect, *Physical Review Letters* 74 (18) (1995) 3668–3671.